IMPROVED RADIANT HEAT SOURCE

Avco Government Products Group
Space Systems Division
Wilmington, Massachusetts 01887

L. A. CASS

DECEMBER 1968

FOREWORD

This research and development project was performed by the Avcc Corporation, Space Systems Division, Wilmington, Massachusetts, under USAF Contract No. AF33 (615)-5384. The work was supervised and this report was prepared by Dr. L. A. Cass, Project Engineer. The contract was initiated under Project No. 1347, "Structural Testing of Flight Vehicles", Task No. 134704, "Thermal Application and Control". The work described in this document was authorized by and completed under the auspices of the Air Force Flight Dynamics Labcratory, Structures Division, with Mr. Robert A. Noble as Project Engineer.

This report covers work conducted from September 1966 to March 1968.

This manuscript was released by the author in April 1968 for publication as a Technical Report.

This technical report has been reviewed and is approved.

DAVID M. PURDY, 1st Lt., USAF
Acting Chief
Experimental Mechanics Branch
Structures Division

The Avco Document Number is AVSSD-0133-68-RR.

ABSTRACT

The characteristics of the various components of a radiative heat transfer facility are examined to determine how their combination produces a certain heat flux delivered to a sample.

Two radiant heat sources are proposed as potential improvements over the tungsten filament-quartz envelope lamp. The cesium vapor lamp and a graphite rod heater are theoretically detailed and the results of experimental tests are presented.

The conclusions stated are, that an immediate improvement in heat flux capability is possible by use of a graphite heater, and even greater potential for improvement is inherent in the cesium vapor discharge lamp, but materials problems associated with arc containment prevent the present realization of that potential.

This abstract has been approved for public release and sale; its distribution is unlimited.

CONTENTS

ILLUSTRATIONS

ILLUSTRATIONS (Cont'd)

ILLUSTRATIONS (Cont'd)

ILLUSTRATIONS (Concl'd)

I. INTRODUCTION

A. RADIATIVE HEAT TRANSFER

The purpose of the introduction is to examine a simplified radiative heat transfer facility in order to see how the characteristics of the various components (lamps, reflector, sample) combine to produce a certain heat flux delivered to a sample. Figure 1 represents a periodic planar array of lamps*, the extent of which is large when compared to the separations of the lamps, sample and reflector. Further, the assumption is made that there are spaces between the lamps. Let f be the fraction of the total area which would be covered if the lamps were a continuous sheet. Thus, for example, if the lamps are rods of diameter D and are spaced a distance L apart on the centerlines, then $f = D/L$. For simplicity, let the radiators be two dimensional slats.

First the radiation emitted by the lamps which reaches the sample must be determined. If the lamps are at a temperature T_L and have an overall emittance ϵ_L, then, per unit surface area, the lamps radiate a power

$$P_L = \epsilon_L \sigma T_L^4 \tag{1}$$

and, in a test setup of total area A, a total power

$$P_L = fA \epsilon_L \sigma T_L^4 \tag{2}$$

in both directions (toward the sample and toward the reflector). The quantity $fA \epsilon_L \sigma T_L^4$ radiated toward the sample reaches it. Of the quantity $fA \epsilon_L \sigma T_L^4$ radiated toward the reflector, a fraction R is reflected back and a fraction of this, $(1-f)$, passes between the lamps and reaches the sample. Thus, there is absorbed by the sample a quantity

$$P_{abs,\ sample} = \epsilon_S (fA \epsilon_L \sigma T_L^4 + R(1-f) fA \epsilon_L \sigma T_L^4)$$

$$= \epsilon_S fA \epsilon_L \sigma T_L^4 (1 + R - fR) \tag{3}$$

There are other radiation paths which are being neglected. For example, a portion of the radiation not absorbed by the sample is reflected from it, passes between the lamps, is reflected at the reflector, passes between the lamps again, is incident on the sample again, and is partially absorbed. The assumption is made, however, that the contributions of such multiple-reflected paths are small.

Similarly, the sample also radiates heat, the power being given by

$$P_S = \epsilon_S A \sigma T_S^4 \tag{4}$$

*By lamp is meant the primary radiator, which could be an incandescent tungsten filament, a carbon rod or even the plasma column of an arc discharge.

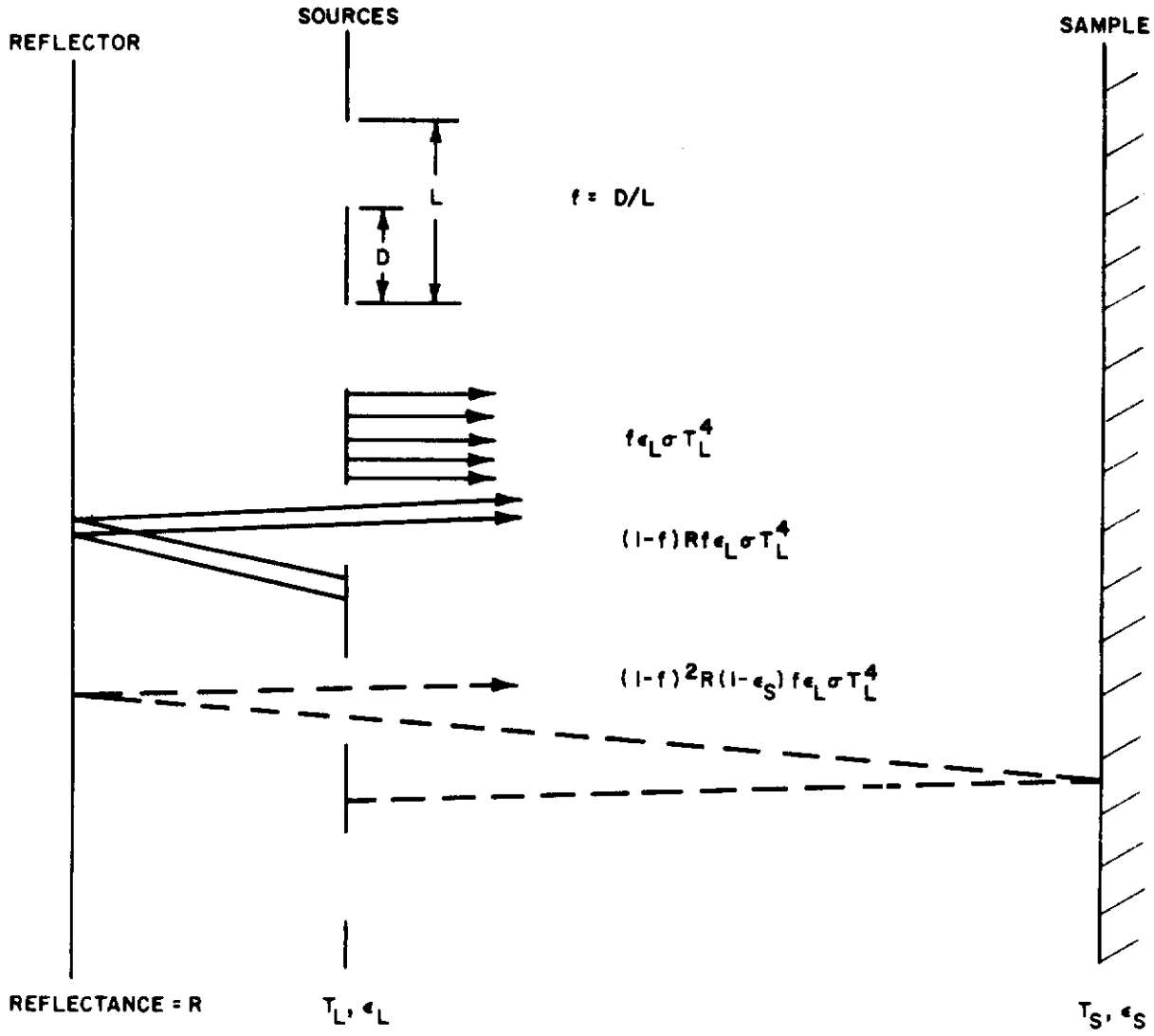

Figure 1 SCHEMATIC OF THERMOSTRUCTURAL TEST FACILITY

Of this, a fraction f is directly incident on the lamps, while a fraction $(1-f)$ passes between the lamps. Of the latter amount, a fraction R is reflected by the mirror and a fraction f of this is incident upon the lamps. Thus, the power originating at the sample and absorbed by the lamps is

$$P_{abs,\,lamp} = fA\,\epsilon_L\,\epsilon_S\,\sigma\,T_S^4\,(1 + R - fR) \tag{5}$$

Again, the radiation originating from the sample which follows more complicated paths to the lamps is neglected and the assumption is made that the reflector is passive in the sense that it does not originate any radiation.

What then is the radiative transfer between the lamps and the sample? If the following definition is made:

$$\dot{Q}_{trans} = \frac{P_{abs,\,sample} - P_{abs,\,lamp}}{A} \tag{6}$$

then, using equations (3) and (5)

$$\dot{Q}_{trans} = f\,(1 + R - fR)\,\epsilon_L\,\epsilon_S\,\sigma\,(T_L^4 - T_S^4) \tag{7}$$

Taking into account the power reflected from the sample to the reflector and then re-reflected back to the sample, equation (7) becomes (See Figure 1.)

$$\dot{Q}_{trans} = f\,[1 + R\,(1-f) + (1-\epsilon_S)\,R\,(1-f)^2]\,\epsilon_L\,\epsilon_S\,\sigma(T_L^4 - T_S^4) \tag{8}$$

The maximum power per unit area that can be transferred from the lamps to the sample occurs when the sample is a perfect absorber (blackbody), i.e., $\epsilon_S = 1$, and the lamps fill all the plane, i.e., $f = 1$. Using either equation (7) or (8) this maximum heat flux is given by

$$(\dot{Q}_{trans})_{max} = \epsilon_L\,\sigma\,T_L^4 \tag{9}$$

Of the quantities in equation (7) or (8), σ is a constant of nature, ϵ_S is a sample property which is not under the control of the structural test laboratory*, and T_S is a parameter dictated by the mission and the sample properties to be simulated. The parameters which can be adjusted are f, R, ϵ_L, and T_L. In the following sections of this discussion these are examined in detail.

B. GEOMETRY AND REFLECTORS

In equation (8), the geometry and reflector terms are not completely uncoupled from the sample properties, i.e., there is some effect due to the term $(1-\epsilon_S)$, the reflectance of the sample material. What is to be demonstrated here is more easily accomplished by assuming the sample material is an imperfect absorber but a perfect non-reflector. This was the assumption used in deriving equation (7).

In equation (7) the heat flux transferred to the sample from the source is linearly dependent upon the term $f[1 + R\,(1-f)]$ where f is the fraction of available projected area filled by lamps and R is the reflectivity of the reflector which

*This result assumes that no geometrical schemes are being used to make an effective emittance higher than the "usual" material emittance. See paragraph IC.

backs the lamps. Thus, both f and R are positive numbers and are less than or equal to unity. Figure 2 shows, for various values of R, the quantity $f(1+R-fR)$ as a function of f. Examination of Figure 2 reveals several interesting features. First, of course, the quantity $f(1+R-fR)$ never exceeds unity, and it attains this value only for $f=1$. Second, while high reflectivities, R, are useful, f is, in general, more important. For a value $f=0.4$, the difference in the parameter $f(1+R-fR)$ between $R=0.2$ (a poor reflector) and $R=0.8$ (a good reflector) is only about 30 percent. To look at it another way, if $f=0.4$ and $R=0$, the parameter $f(1+R-fR)$ has the value 0.4. Increasing R from 0 to 0.8 has only about the same effect as increasing f from 0.4 to 0.6.

Finally, and perhaps most important of all, one should note that if $f=0.5$ and $R=0.6$, the parameter $f(1+R-fR)$ has the value 0.65. No further increase in either f or R over these values can improve the heat transfer parameter by more than about 50 percent. Thus, if an existing system with $f\sim0.5$ and $R\sim0.6$ delivers a heat flux of $\sim120 \times 10^4$ watt/m^2 to a cold sample, no improvement in reflectors and no variation in source packing arrangement can yield more than about 180×10^4 watt/m^2, if the source temperature and emissivity remain the same.

As previously indicated, the above discussion is based on the sample being a non-reflector. For the more realistic case that the sample does reflect some of the incident radiation, the above numerical results will be modified, but will show the same trends with regard to the relative importance of variations in f and R on the radiative heat flux deliverable to a sample.

C. EMITTANCE

The radiative transfer equation (7) or (8) is also linear in the emittance* of the lamps. Thus, since the tungsten heater elements in the tungsten-quartz lamps which form the basis for most present thermo-structural test facilities have an emittance of approximately 0.30-0.35 in the range of temperatures over which they can be usefully operated, and since the theoretical limit on emittance is unity, the theoretical potential exists that, without changing geometry or temperature, an increase in radiation intensity by a factor of ~3 could be achieved if the emittance could be increased to approach the theoretical limit.

Emittance can, in principle, be increased by changing radiator material (that is, using a material with higher emissivity) or by changing the surface characteristics for the given material. A common procedure employed for obtaining slight improvements in emittance is to roughen the surface. Experience at Avco in measuring the emittance of tungsten wires suggests that, at high temperatures, there are mechanisms operating which tend to smooth the finish so that, in a short time, the emittance approaches the emissivity very closely.

By suitable geometrical shaping, the possibility exists of raising the emittance of a radiator arbitrarily close to the blackbody limit of unity, depending on

*The emittance is a property of a particular sample of radiator, and is analogous to the emissivity of a material. Thus, the emissivity of tungsten is a basic property of the material which cannot be altered without changing the material, while the emittance of a particular tungsten wire can be affected by surface finish, etc.

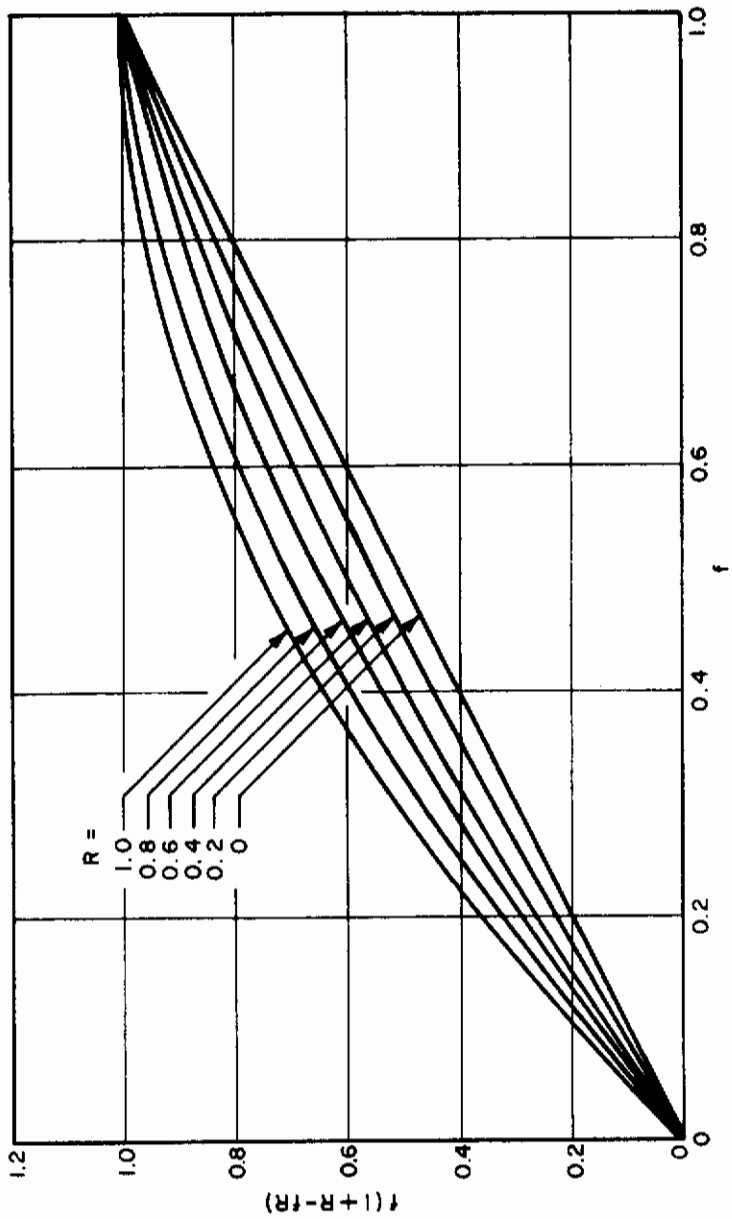

Figure 2 VARIATION OF GEOMETRY-REFLECTOR PARAMETER WITH f AND R

the amount of effort which one is willing to devote towards that end. One way, impractical though it may be, is to use the material in question to build an insulated enclosure with a small hole in the wall leading to the outside. (See Figure 3a.) If the enclosure is brought to equilibrium at a temperature T, then the radiation emanating from the hole is that from a blackbody at the temperature T; that is, the enclosure has an emittance of unity, even though the material out of which the enclosure is made may have an emissivity of 0.1. Another method, which is somewhat more practical, is to increase greatly the effective surface area in such a way that the radiation emitted from an element of area makes many reflections from other surface elements before finally escaping. (See Figure 3b.) Another way is to take building block elements, rods for example, and make a deep stack as indicated in Figure 3c. If each radiator element which has an emittance ϵ is at a temperature T, then as the stack becomes deeper, the radiation from the stack approaches that of a blackbody at the temperature T.

Why, then, can't these ideas be used to increase the effective emittance of present radiator elements. The answer is that all of the schemes lack practicality. The blackbody enclosure method permits only a small area of sample to be irradiated. The scheme involving multiple reflections at the surface (Figure 3b) could in part be accomplished for flat surfaces, but is difficult to achieve for small diameter rods. The stacking scheme in Figure 3c is plausible unless the radiator elements need a protective envelope, such as do the tungsten-quartz lamps. Then the temperature that the envelope would reach as a result of being immersed in this stack of lamps would be the temperature of the radiators, which in general greatly exceeds the melting point of the envelope material.

Though it is possible to increase the effective emittance of a radiator by methods illustrated in Figure 3, when comparing two different radiating materials, all other things being equal, the one with the higher emittance is to be preferred. A material of emittance 0.9 is a better choice than selecting a material of emittance 0.3 and attempting to increase the effective emittance by geometrical shaping schemes such as those illustrated in Figure 3 (which impose further restraints on the design of the lamp system).

In any further discussions involving emittance the assumption will be made, unless otherwise stated, that schemes like those presented in Figure 3 are not involved.

D. TEMPERATURE

The parameter which affects the radiative transfer most sharply is the lamp temperature, which appears raised to the fourth power in equation (7) or (8). Thus, while there are limits on the improvements that can be obtained by improving lamp geometry, reflector design and radiator emittance, there are no theoretical limits imposed on the radiator temperature. For example, if the radiator temperature is increased by only 20 percent, the radiative transfer for fixed lamp geometry, emittance and sample temperature is increased approximately 100 percent, while if the radiator temperature is increased by a factor of 2, the radiative transfer is increased by a factor of 16.

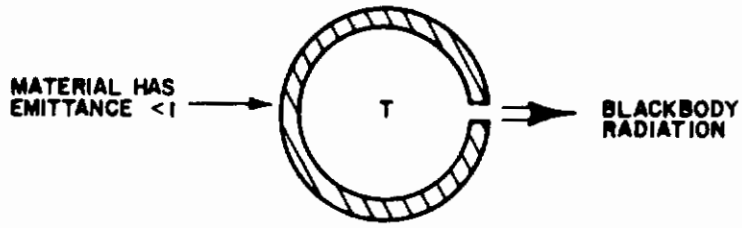

a BLACKBODY ENCLOSURE AT TEMPERATURE T

b INCREASE IN THE EMITTANCE OF SURFACE

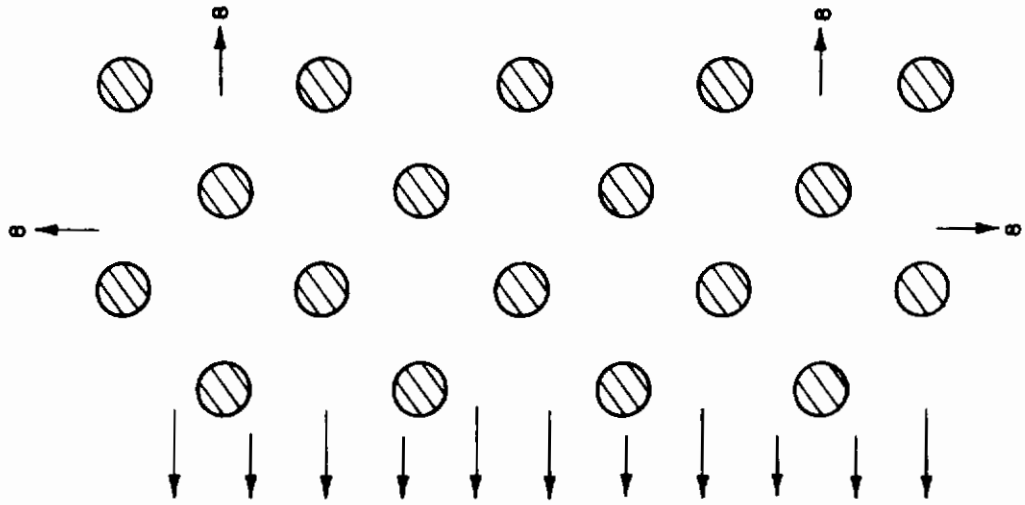

c BLACKBODY RADIATION FROM AN INFINITE STACKED ARRAY OF RODS

Figure 3 VARIOUS SCHEMES FOR INCREASING RADIATION FROM A MATERIAL OF EMITTANCE <1 AND TEMPERATURE T

II. PROPOSED RADIANT HEAT SOURCES

A. HEAT SOURCE REQUIREMENTS

To provide thermostructural test facilities which give useful simulations of the thermal loadings associated with future aerospace developments and missions, a capability of delivering heat fluxes as high as 350 watts/cm^2 to structural members of varied contours, over areas as large as 15 m^2 is desirable. A total of 50 megawatts of electrical power (short duration) is available at AFFDL for this task.[1]

Because the contours of the specimens to be tested may be varying rapidly (as, for example, on a leading edge), the heat sources should be modular in concept. That is, provision of carefully controlled heat fluxes to a large and possibly irregularly-shaped specimen is best accomplished with a large number of small heat sources, rather than with a few large heat sources. Further, since there will be large areas in many specimens where a uniform heat flux is desired, the heat sources should be such that they can be fairly closely packed to avoid flux gradients between sources.

Looking at equations (7) or (8), the radiation characteristics of such a heat source are easily determined. To consider the one-way heat flux to the sample, set $\epsilon_s = 1$, and $T_s = 0$ in equation (7) or (8); i.e., consider the sample to behave as a cold perfect absorber. Assume that $f[1 + R(1-f)]$ has a value of 0.7 (e.g., $R=0.9$ and $f=0.48$) which, though optimistic, is achievable if, for example, two rows of staggered lamps are used. Then for each value of $\dot{Q}_{trans}$, the resulting expression becomes an equation in the two variables ϵ_L and T_L. The relation between these two lamp parameters is shown in Figure 4 for various heat fluxes delivered to a cold absorbing sample. From this figure, one may note that for an emittance of unity, a lamp temperature of 2650°K gives a heat flux of 200 watt/cm^2, while 3050°K is needed for 350 watt/cm^2. For a heat flux of 350 watt/cm^2, note that if the temperature can be raised to 6000°K, then the emittance need only be 0.07, while at 10,000°K an emittance of 0.009 is adequate.

B. TUNGSTEN-QUARTZ LAMP

Among the facilities that deliver heat flux to a sample by means of radiative transfer, the most commonly employed lamp is the T-3 tungsten-quartz unit which consists of tungsten wire wound into a cylindrical coil surrounded by a 3/8-inch quartz tube. The quartz envelope is used to provide an inert gas environment to protect the tungsten filament from oxidation. The resistance characteristics of the T-3 lamps make it easy to run multiple lamps in parallel using standard commercial power sources.

The T-3 lamp suffers failures due to end seal oxidation, high temperature failure of the quartz envelope and tungsten deposition on the quartz due to high filament temperatures.

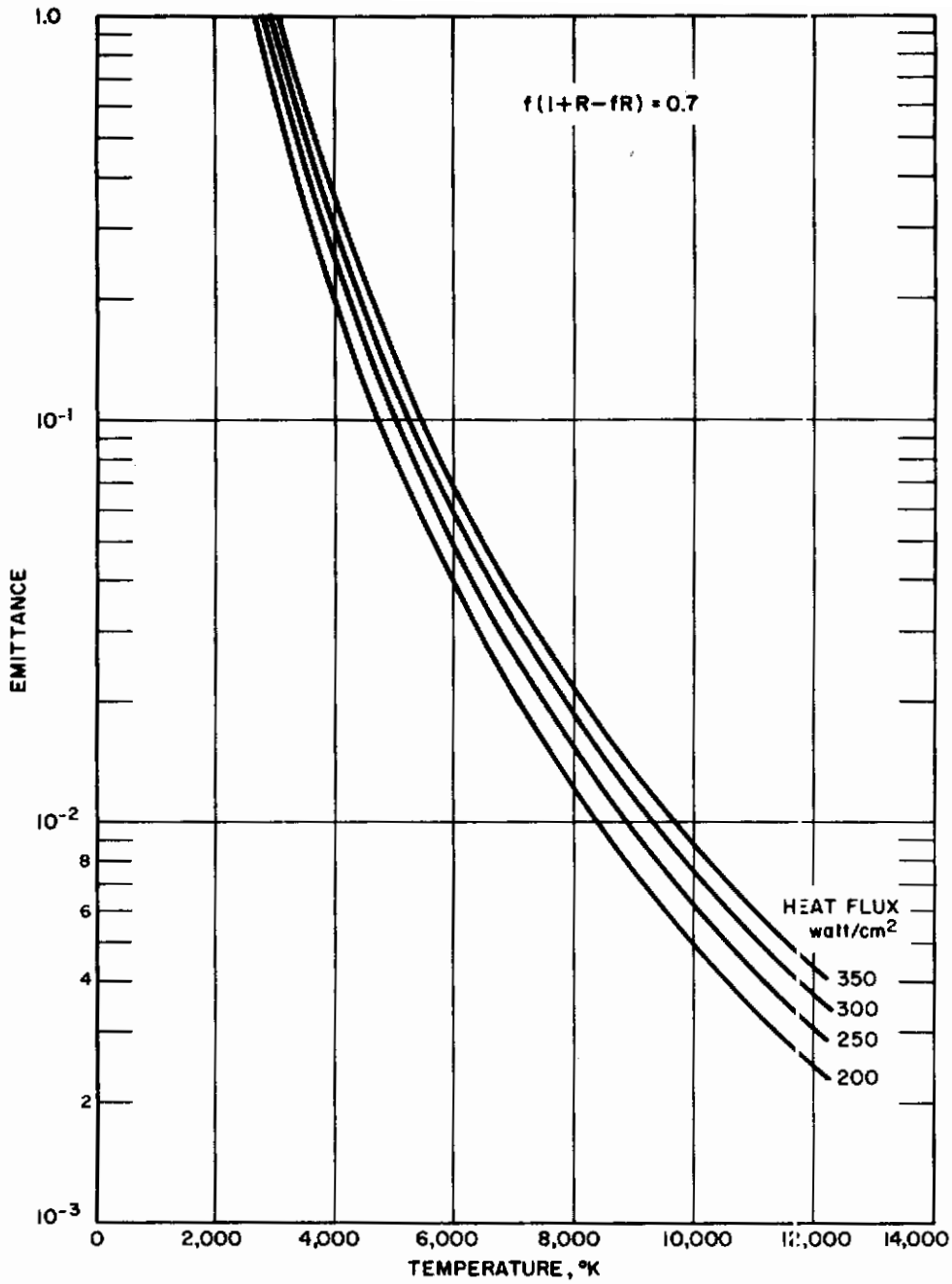

Figure 4 REQUIRED EMITTANCE VERSUS TEMPERATURE FOR VARIOUS HEAT FLUXES DELIVERED TO SAMPLE

Tungsten has a melting temperature of 3655°K. The highest temperature attained by the tungsten filament in the T-3 lamp appears to be 3250°K.[2,3] The emittance of the tungsten filament can be taken to be 0.35 at this temperature.

From Figure 4, one may note that tungsten is inadequate as a radiator material. The temperature required to give a heat flux of 200 watt/cm^2 is 3500°K, and 350 watt/cm^2 necessitates 4000°K, which is in excess of the melting point by more than 300°K. At a temperature of 3250°K (the highest operational filament temperature for the T-3 lamp), the maximum heat flux deliverable to a sample is found from equation (9) to be 220 watt/cm^2 (corresponding to $f=1$; i.e., all of the plane is filled with tungsten).

In practice, $f[1 + R(1 - f)]$ is quite a bit smaller than unity. Where a single row of single filament lamps is used, the f factor* is ~ 0.2. In some cases, a double row of staggered lamps has been used, thereby doubling the f factor, but severe difficulty with inter-lamp heating is then encountered. Thus, in practice, the largest deliverable heat flux to a sample using tungsten-quartz lamps is around 130 watt/cm^2, and maximum values of 100 watt/cm^2 or less are more frequently the case where subsidiary cooling of the end seal and quartz envelope is not provided.

C. PLASMA HEAT SOURCE

For a fixed geometry and reflector, equation (7) or (8) shows that a higher heat flux to a given sample than that obtainable by the tungsten-quartz lamp is accomplished either by increasing the radiator emittance, ϵ_L, or by increasing the radiator temperature T_L. As was indicated, an increase in T_L has a profound effect, while the heat flux increases only linearly with ϵ_L.

A radiator temperature significantly higher than tungsten, of course, is difficult to obtain. The highest known melting point of a solid is about 15 percent higher than tungsten.

If the concept of a radiator is expanded to include gas discharges as well as incandescent solids, then the achievable temperature range is greatly extended. In a gas discharge, the current is carried by electrons produced by ionization of neutral gas atoms and molecules. The gas temperature necessary in a relatively high pressure discharge to yield sufficient ionization for appreciable currents to be carried is related to the ionization potential of the gas in which the discharge burns. As a very crude rule of thumb, the discharge temperature rises 1000°K for every electron-volt increase in ionization potential. Thus, a discharge in argon gas tends to run at a temperature of the order of 16,000°K, while in sodium vapor, a temperature of 6000°K is more appropriate. These temperatures are, of course, large compared to those which are achievable with solids.

Why, then, is it not a simple matter to approach arbitrarily high flux levels in gas discharges? The answer concerns the emittance, which, for most gas discharges, is very low compared with that for almost any solid. As a conse-

*Due to the quartz envelope, if the lamps are arranged in a single row, touching side by side, the f factor is about 1/3.

quence, the radiation from a typical gas discharge at moderate pressure (< 1 atm) retains a great deal of the spectral detail characteristic of the gas, with many wavelength regions in which little radiation is emitted adjacent to other regions in which large amounts of radiation are emitted. If the pressure and current in a gas discharge are increased, however, the spectral character of the emitted radiation changes. Continuum radiation builds up relative to the lines and, at very high pressures and power densities the spectrum is like that of a very high temperature solid, while the emittance may approach unity. An example of this is the xenon flash tube. The FX-47B manufactured by EG&G radiates essentially with an emissivity of one and a temperature of nearly 10,000°K, yielding a flux of approximately 700 x 10^6 watt/m^2 just outside the quartz envelope.[4] However, this level of radiation can be delivered for times only of the order of milliseconds.

Thus it may be seen that the plasma arc source has a potential which greatly exceeds that of solid radiator lamps. Even the carbon radiator, discussed in more detail in the next section, must be operated close to its ultimate limit to deliver a heat flux of 350 watt/cm^2.

Why, then, have plasma radiation sources not found earlier application in the thermostructural test area? Principally because they are inherently more complex devices than the simpler and more reliable tungsten-quartz lamps, and because most thermostructural testing requirements to date have fallen within the capability of properly used tungsten-quartz lamps.

Avco has developed an alkali vapor radiation source. The source configuration consists of a Lucalox* tube with the electrodes mounted coaxially at each end of the tube. The electrode-endcap assembly is joined to the envelope by means of a ceramic-to-metal brazing process. This type of process has received considerable attention recently, and there are a number of empirical techniques described in the literature[5,6,7]. The process which has been employed in this program is quite similar to certain of those described elsewhere. Joints that are leak-tight can be fabricated as a routine matter. These joints have operated well at temperatures in excess of 700°C when exposed to alkali metal atmospheres and have maintained their integrity for periods of operation in excess of 15 hours at the aforementioned temperature.

The tube is loaded with alkali metal and with a gaseous environment of argon at a pressure of approximately 10 torr. The initial discharge is established by means of the low-pressure Paschen phenomenon[8]. An argon arc forms and rapidly brings the internal surfaces of the electrodes and arc tube to a temperature sufficient to vaporize the metal. The lowest liquid-vapor interface temperature determines the vapor pressure of the alkali metal. The spectral properties of the arc after warmup are determined by the alkali vapor because the partial pressure of argon is so low.

Operation of a plasma discharge in an alkali vapor offers two significant advantages. First, the alkali metal improves the starting characteristics. At room temperature, the vapor pressure of an alkali metal is negligible so that

*Lucalox is the trade name of a polycrystalline alumina material developed by the General Electric Company.

a low-pressure (~10 torr) buffer gas such as argon initiates an initial discharge of the low-pressure type, thereby, eliminating the added complexity (RF power or additional starting electrodes) associated with establishing a high-pressure discharge, as the discharge may be initiated with a comparatively low voltage dc power supply. As the tube discharge continues to operate, the envelope and endcaps heat up, raising the vapor pressure of the alkali metal. As the pressure in the discharge increases, so does the emittance and the radiating efficiency.

Second, the low ionization potential of the alkali metal vapors (4-5 volts) insures a lower discharge temperature and, consequently, generates relatively little ultraviolet radiation (at 5000°K only 0.1 percent of the blackbody radiation is at wavelengths below 2000 Å while at 10,000°K, about 10 percent is). This is an important consideration because envelope materials tend to absorb in the ultraviolet.

Two major problem areas are foreseen in the development of the alkali vapor source lamp into a heat lamp capable of high radiant output. One involves the compatibility of the source with the power supplies available at the Air Force Flight Dynamics Laboratory (AFFDL). The initial exploratory work with these sources has been using dc and pulsating dc power, and but limited effort has been made on operation with 60-cycle ac power. Compatibility also includes the modifications required to go from single-lamp to multiple-lamp operation.

The other problem area is the limitation on the total input power per unit length imposed by the thermostructural properties of the envelope and endcap-electrode assembly. The envelope must be able to transfer to the outside the energy (conducted heat and the radiation it does not transmit) it receives from within, without melting and/or cracking due to thermal stress. The endcap and brazes must maintain their structural integrity at high temperatures.

D. CARBON ELEMENT LAMP

If a radiating material can be found that has a higher emittance and it can be operated at close to the same element temperature, then an increase in the heat flux over that of tungsten could be accomplished. Such a material is carbon or graphite.* Carbon has a total emittance of between 0.90-0.95 at high temperatures, depending on surface condition. This is very close to the theoretical (blackbody) limit of unity. Resistor elements can be heated to 3000°K and at least one case of 3600°K is mentioned. Looking at Figure 4, with carbon elements at a temperature of 3200°K, a heat flux of 350 watt/cm^2 appears marginally possible.

The advantages of using carbon are several. It is a simple resistive element and thus presents no problem in multiple lamp operation, and it is compatible with the existing power supply. Current-carrying cross-sections may be kept small so that extremely high currents are not required. The properties of carbon and graphite can be varied by the selection of raw material and fabrication process.

*Carbon and graphite are both essentially pure carbon. The grain structure of carbon is poorly developed and in a disorderly state while graphite is carbon with an orderly crystal form.

The biggest problem area is concerned with the lifetime of the carbon radiator at this elevated temperature. An inert atmosphere is required because of the rapid erosion of carbon in the presence of oxygen. A further complication is that even if the oxidation can be controlled, carbon sublimes to such an extent that the vapor pressure is 10^3 times greater than that of tungsten at 3000°C. This will result in the buildup of material on the cooler window material, which in turn increases the heat loading because of appreciable absorption of the source radiation. This raises the window temperature, resulting eventually in failure.

This phenomenon is one of the failure mechanisms of the tungsten-quartz lamp and should be more severe for carbon. A scheme involving a gas flow to carry the sublimation products away from the vicinity of the window is a possible solution.

III. CESIUM VAPOR SOURCE

A. ANALYTICAL SOLUTIONS OF THE ARC COLUMN

1. Analytical Model of Arc Column

The high pressure* arc discharge can be divided into three regions, one associated with each electrode and the third, termed the arc column, occupying the major portion of the length of the discharge. The extent of the electrode regions is quite small, being of the order of a few mean free paths thick. Each electrode region has associated with it a fixed voltage drop determined by the electrode material and the plasma composition. The arc column itself has a nearly constant voltage gradient. Thus, the discharge voltage is given by

$$V_o = V_A + V_C + L \frac{dV}{dX} \tag{10}$$

where V_A and V_C are the voltage drops associated with the anode and cathode, dV/dX is the arc column voltage gradient and L is the length of the arc column. For discharges for which the length of the discharge is much larger than its diameter,

$$V_o \approx L \frac{dV}{dX} >> V_A + V_C \tag{11}$$

Thus, equation (11) leads to the result that virtually all the input power (IV) is dissipated in the arc column region (I is the arc current). Further, the operating characteristics of the total arc discharge are essentially the same as those of the arc column.

A relatively simple analytical model of the arc column is obtained by assuming that all variables have radial variation but neither azimuthal nor axial dependence. These assumptions lead to the following equation (conservation of energy) for a differential volume element in the arc column:

$$\sigma E^2 = - \frac{1}{r} \frac{d}{dr} \left(rK \frac{dT}{dr} \right) + P_r \tag{12}$$

The left-hand side of equation (12) is the input term due to Joulean heating; σ is the electrical conductivity (mho/cm) and E is the voltage gradient (volt/cm). The right-hand side of equation (12) consists of two energy loss terms. The first is the radial heat conduction term; K is the thermal conductivity in watt/cm-^oK and T is the temperature in ^oK. The second loss term, P_r, is the radiated power per unit volume (watt/cm^3). Here, the reabsorption of radiation is neglected.

*High pressure means that the heavy particle and electron temperatures are approximately the same.

Note that equation (12) is a second order differential equation and can be solved, for a given E, upon specification of two boundary conditions. The transport properties σ, K and P_r are presumed known as functions of pressure and temperature.

One boundary condition is apparent from symmetry, namely, $\left.\frac{dT}{dr}\right|_{r=0} = 0$. The other boundary condition is a specification of the centerline temperature, $T(r = 0) = T_o$. For each pair, E and T_o, a numerical solution of equation (12) determines the radial temperature profile, arc current, arc radius, total radiated power per unit length of arc column, input power per unit length of arc column and radiating efficiency of the arc column. The radiating efficiency is the ratio of the radiated power to the input power.

Under certain conditions, equation (12) can be used in the region between the arc column and the confining wall. This is permissible in those cases where the major heat transfer mechanism is radial heat conduction. Experience has shown that with the cesium arc column, other heat transfer mechanisms are operative outside the arc column. These mechanisms are not completely understood; one possibility is the reabsorption of radiation from the arc column.

2. Transport Properties of Cesium

The solution of equation (12) requires the specification of the transport properties of the plasma. Considerable work, both theoretical and experimental, has been performed by the Avco Space Systems Division (Avco/SSD) in the area of the properties of gases at high temperature. This capability has been utilized in determining the requisite transport properties for cesium vapor. The calculation of the electrical and thermal conductivities are based on the first Chapman-Enskog approximation, using the literature to obtain the most recent values of the required atomic and molecular collision cross sections.

The total continuum radiated power per unit volume is estimated for cesium using Kramers' semi-classical approximation. Molecular band and atomic line radiation have not been included in the total radiation calculation. However, the total radiation calculation does contain an empirical factor to make the calculated value agree as well as possible with the limited experimental data.

The resulting calculated transport properties for cesium are shown in Figures 5 through 7. Figure 8 shows the thermochemical composition of cesium as a function of temperature for pressures of 0.1 and 1.0 atm.

3. Numerical Results

Equation (12) has been programmed for the IBM 7094 computer, and solutions have been obtained for various values of the voltage gradient, E, the central core temperature, T_o, and the pressure. The role of pressure is evidenced by its effect on the transport properties.

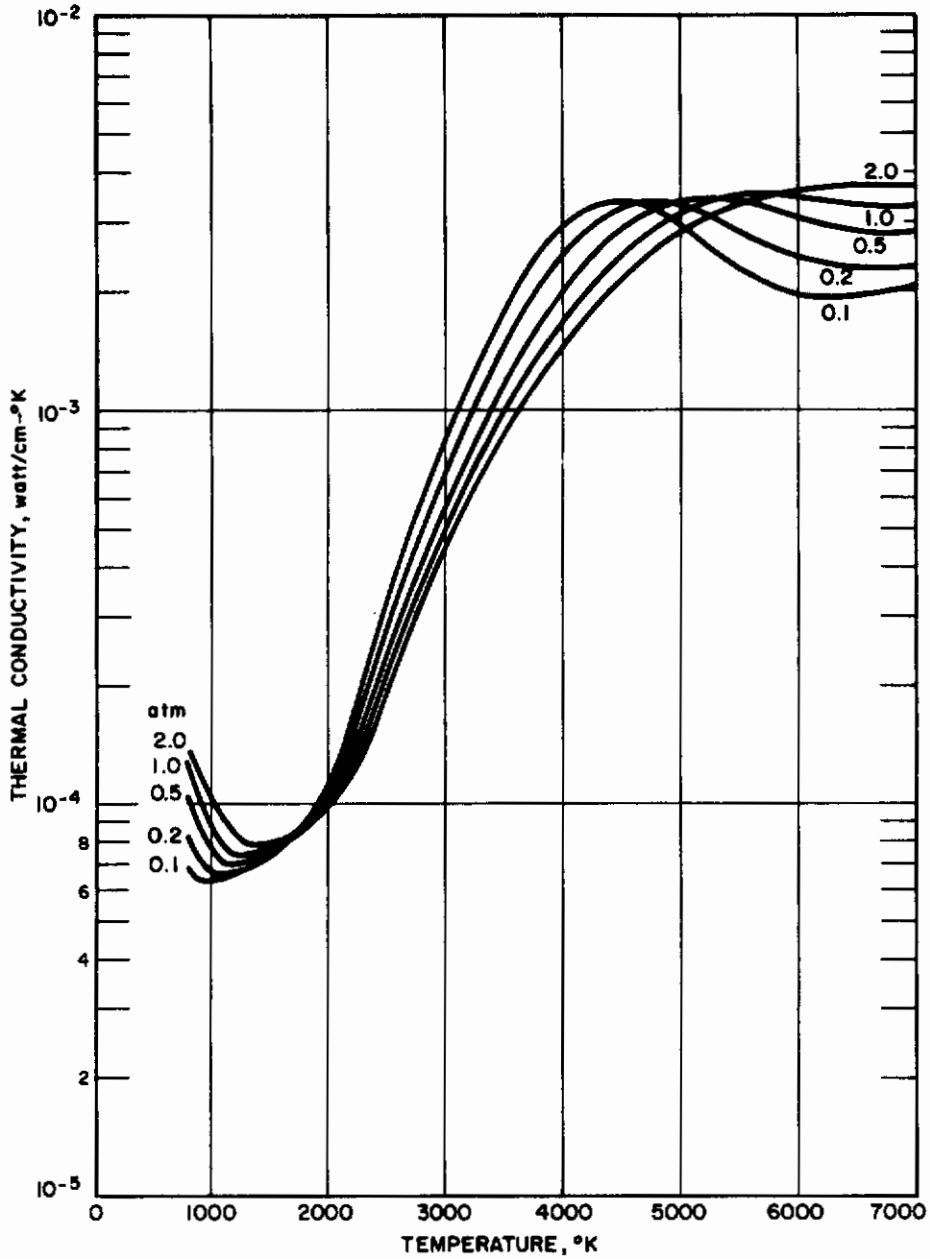

Figure 5 CALCULATED THERMAL CONDUCTIVITY OF CESIUM VAPOR VERSUS TEMPERATURE AT VARIOUS PRESSURES

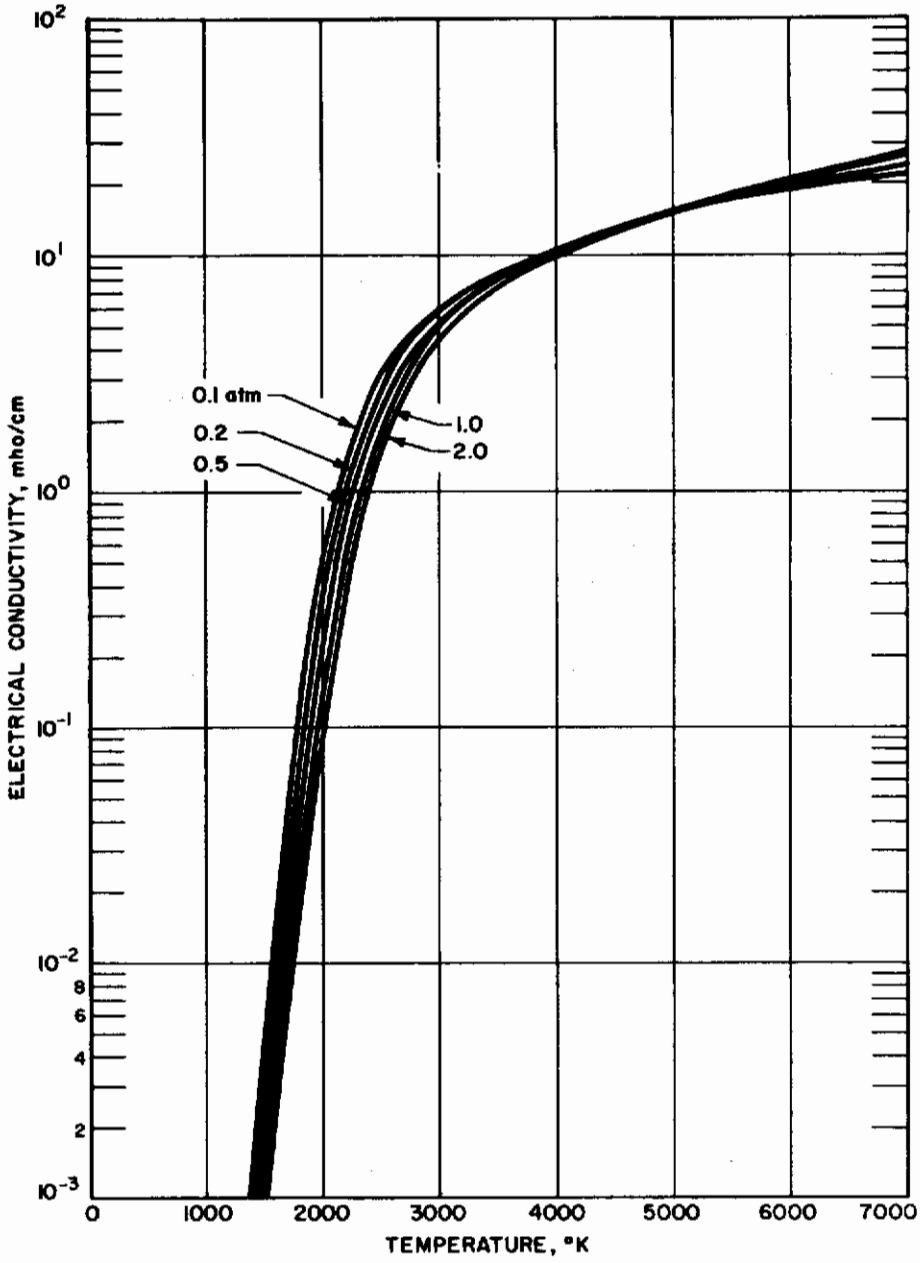

Figure 6 CALCULATED ELECTRICAL CONDUCTIVITY OF CESIUM VAPOR VERSUS TEMPERATURE AT VARIOUS PRESSURES

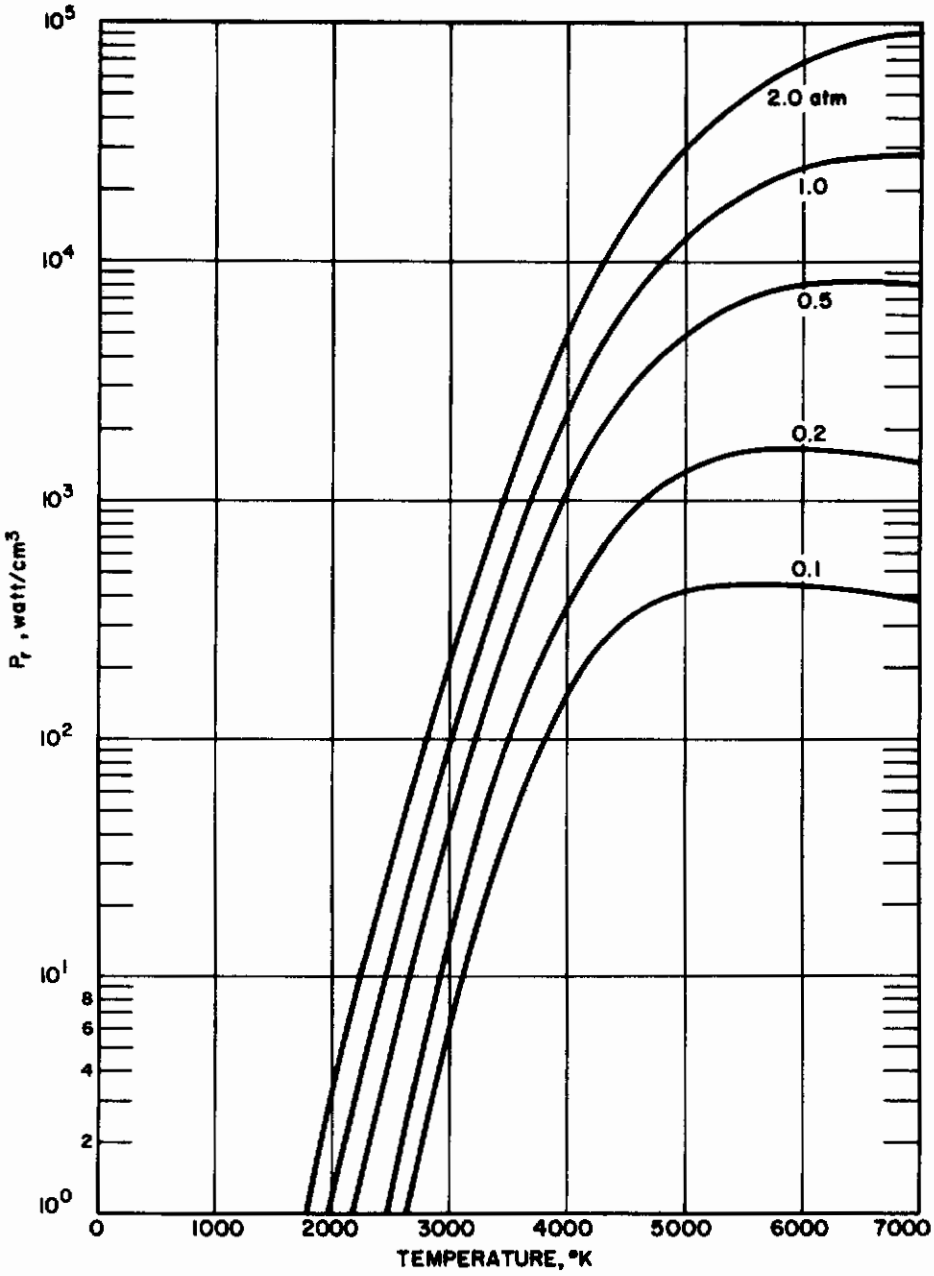

Figure 7 CALCULATED TOTAL RADIATED POWER FROM CESIUM VAPOR VERSUS TEMPERATURE AT VARIOUS PRESSURES

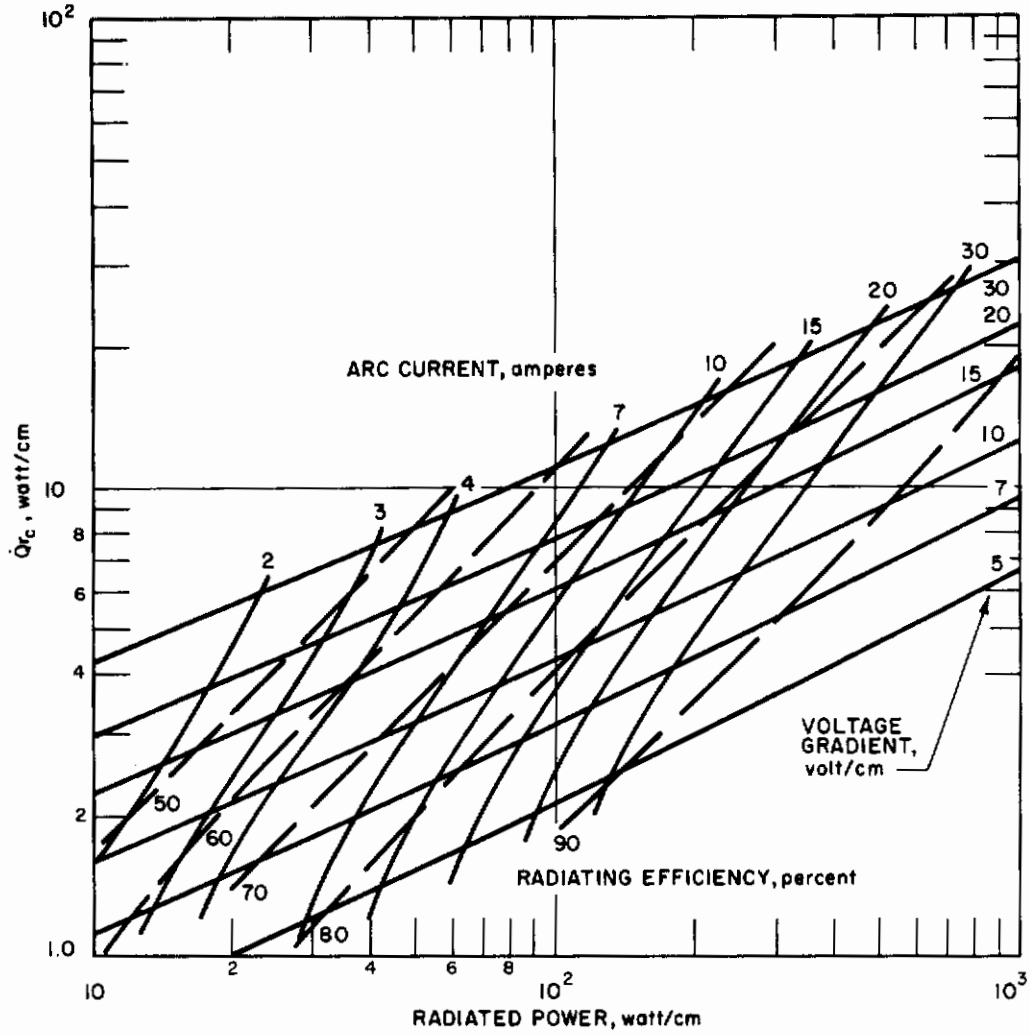

Figure 11 RESULTS FROM ARC COLUMN SOLUTIONS FOR CESIUM PLASMA: PRESSURE = 1.0 ATM

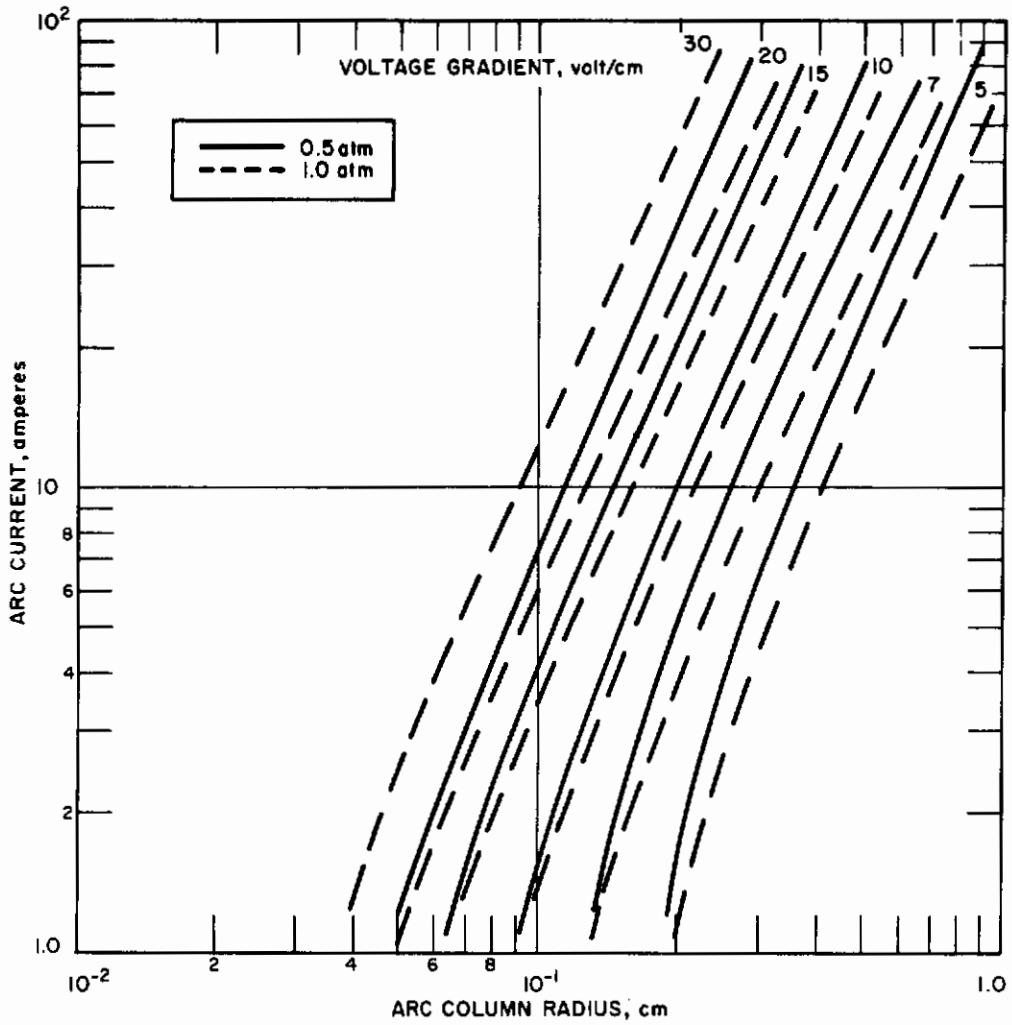

Figure 12 ARC COLUMN CURRENT AS A FUNCTION OF COLUMN RADIUS, VOLTAGE GRADIENT AND PLASMA PRESSURE

A numerical example illustrates how Figures 10 through 12 are used. Consider a lamp operating at a voltage gradient of 30 volts/cm with a plasma pressure of 1 atm. From Figure 11, one can determine that a lamp current of 30 amperes gives rise to a radiated power of 730 watt/cm, a radiating efficiency of slightly higher than 80 percent and a value for $\dot{Q}r_c$ of 26 watt/cm. From Figure 12, one can determine that the arc column radius is 0.15 centimeter, and the corresponding arc surface area per unit length is 0.94 cm^2/cm (2π x 0.15). The radiant flux from the arc column is thus 775 watts per cm^2 of surface area (730/0.94). This is equivalent to a tungsten filament at 4500°K, or a blackbody radiator at 3450°K.

B. THERMAL STRESS DISTRIBUTION IN THE ENVELOPE

1. Introduction

The input power to the plasma arc lamp of some given geometry may be limited by the structural strength of the confining envelope. This factor will be examined by determining the temperature distributions for two modes of cooling for a cylindrical envelope and then analyzing the resulting thermal stresses.

The two different modes of cooling are termed radial cooling and axial cooling. In the radial mode of cooling, the heat conducted to the inner envelope wall from the arc column is considered to pass radially outward through the wall. In the axial mode, the heat conducted to the inner envelope wall is considered to move axially down the tube to the end caps.

2. Temperature Distributions

a. Radial Mode of Cooling

The differential equation governing the flow of heat for the case of steady state with no sinks or sources is

$$\vec{\nabla} \cdot \vec{Q} = 0 \tag{14}$$

where

$$\vec{\underset{\sim}{Q}} = - K \vec{\nabla} T \tag{15}$$

T denotes the temperature and K is the thermal conductivity. Since $\vec{Q}$ is assumed to have only a radial component, then equations (14) and (15) combine to give

$$\frac{1}{r} \frac{d}{dr} \left(r \frac{dT}{dr} \right) = 0 \tag{16}$$

For simplicity, the assumption is made that K is a constant. The solution to equation (16) subject to the boundary conditions

$$\dot{Q}_2 = - K \left. \frac{dT}{dr} \right|_{r = a}$$

and

$$T\,(r = b) = T_L$$

is

$$T - T_L = \frac{\dot{Q}_2\, a}{K} \ln \frac{b}{r} \quad \text{(radial cooling)} \tag{17}$$

The cylinder has inner radius a and outer radius b . In the notation of the arc column solutions,

$$\dot{Q}_2 = \dot{Q} \frac{r_c}{a}$$

b. Axial Mode of Cooling

The axial mode of cooling is not as easily realizable as the radial mode. Since this mode leads to a tractable temperature distribution relative to the stress analysis, it was investigated to see if it offered any advantage in terms of thermal stress.

To calculate the temperature distribution for the axial cooling mode, the following assumptions are made (Figure 13):

1) The power per unit area conducted to the inner wall of the Lucalox tube ($r = a$) is constant, $\dot{Q}_2$, along the tube, consistent with the arc column analysis previously presented.

2) The heat conducted away from the outer wall of the tube ($r = b$) is zero. (If only free convection and radiation act, this is a good assumption).

3) The effect of the endcap is to produce a uniform heat loss per unit area, $\dot{Q}_1$.

4) The heat generated within the tube walls due to absorption of radiation from the arc column is negligible.

Since $\vec{\dot{Q}}$ has both a radial and axial component, equations (14) and (15) combine to give

$$\frac{\partial^2 T}{\partial r^2} + \frac{1}{r}\frac{\partial T}{\partial r} + \frac{\partial^2 T}{\partial z^2} = 0 \tag{18}$$

The boundary conditions are

$$\left.\frac{\partial T}{\partial z}\right|_{z=0} = 0 \quad , \quad \dot{Q}_1 = -K \left.\frac{\partial T}{\partial z}\right|_{z=L/2} \qquad a \leq r \leq b$$

$$\left.\frac{\partial T}{\partial r}\right|_{r=b} = 0 \quad , \quad \dot{Q}_2 = -K \left.\frac{\partial T}{\partial r}\right|_{r=a} \qquad 0 \leq z \leq L/2 \tag{19}$$

The first boundary condition merely expresses the symmetry about the point midway along the tube.

The solution is given by

$$\frac{T(r,z) - T_L}{\frac{\dot{Q}_1 L}{2K}} = \frac{b^2}{L^2}\left[\frac{r^2}{b^2} - 1 + 2\ell_n \frac{b}{r}\right] + \frac{1}{2}\left[1 - \left(\frac{z}{L/2}\right)^2\right] \tag{20}$$

where T_L is the (lowest) temperature at the point $z = L/2$, $r = b$. A condition that must be satisfied is

$$\frac{\dot{Q}_2}{\dot{Q}_1} = \frac{b^2 - a^2}{aL} \tag{21}$$

Combining equations (20) and (21) gives the result

$$T_{max} - T_L = \frac{\dot{Q}_2 a}{2K}\left[f_1(b/a) + (L/b)^2 f_2(b/a)\right] \tag{22}$$

where

$$f_1(b/a) \equiv \frac{b^2}{b^2 - a^2}\left[2\ell_n\, b/a + \frac{a^2}{b^2} - 1\right] \tag{23}$$

$$f_2(b/a) \equiv \frac{b^2}{b^2 - a^2} \tag{24}$$

Plots of f_1 and f_2 are shown in Figure 14. T_{max} is the maximum temperature and occurs at the point $z = 0$, $r = a$. One will note that a large maximum temperature is associated with a large L/b and small b/a. For $L/b = 5$ and $b/a = 2$, T_{max} is $17.5 \frac{\dot{Q}_2 a}{2K}$ above T_L. Finally, Figure 15 is a plot of the isotherms for this case; the isotherm is the non-dimensional quantity $\frac{T(r,z) - T_L}{33.3 \frac{\dot{Q}_2 a}{2K}}$.

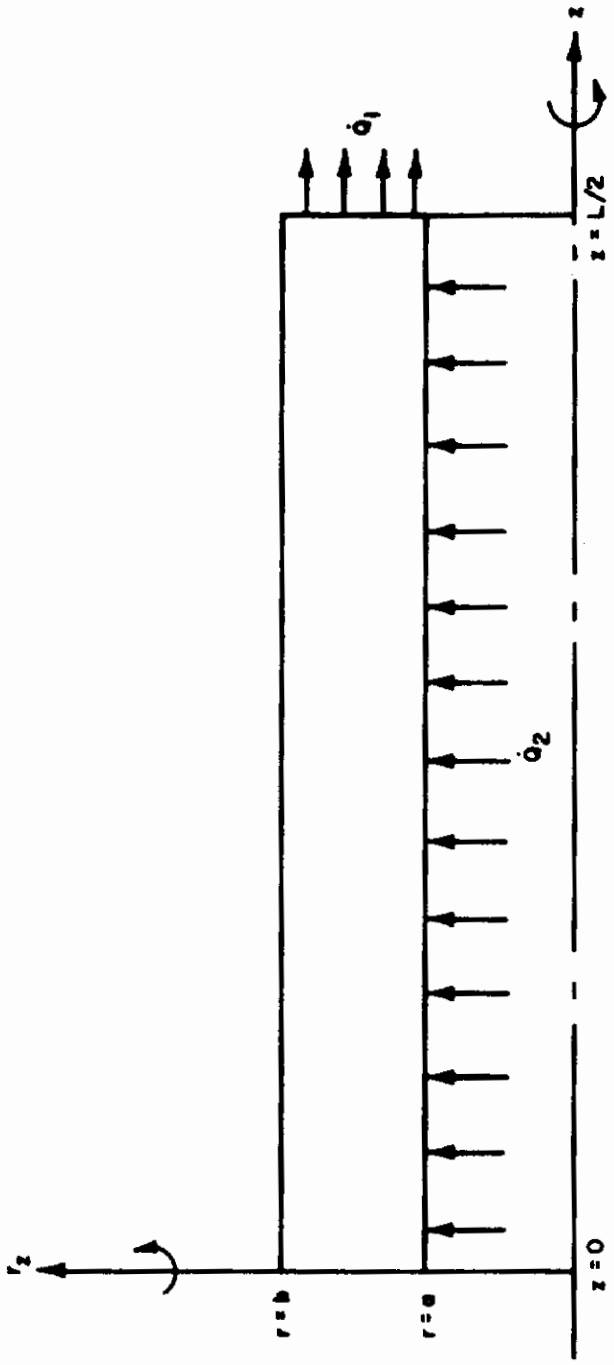

Figure 13 GEOMETRY OF TUBE SHOWING UNIFORM HEAT LOADING

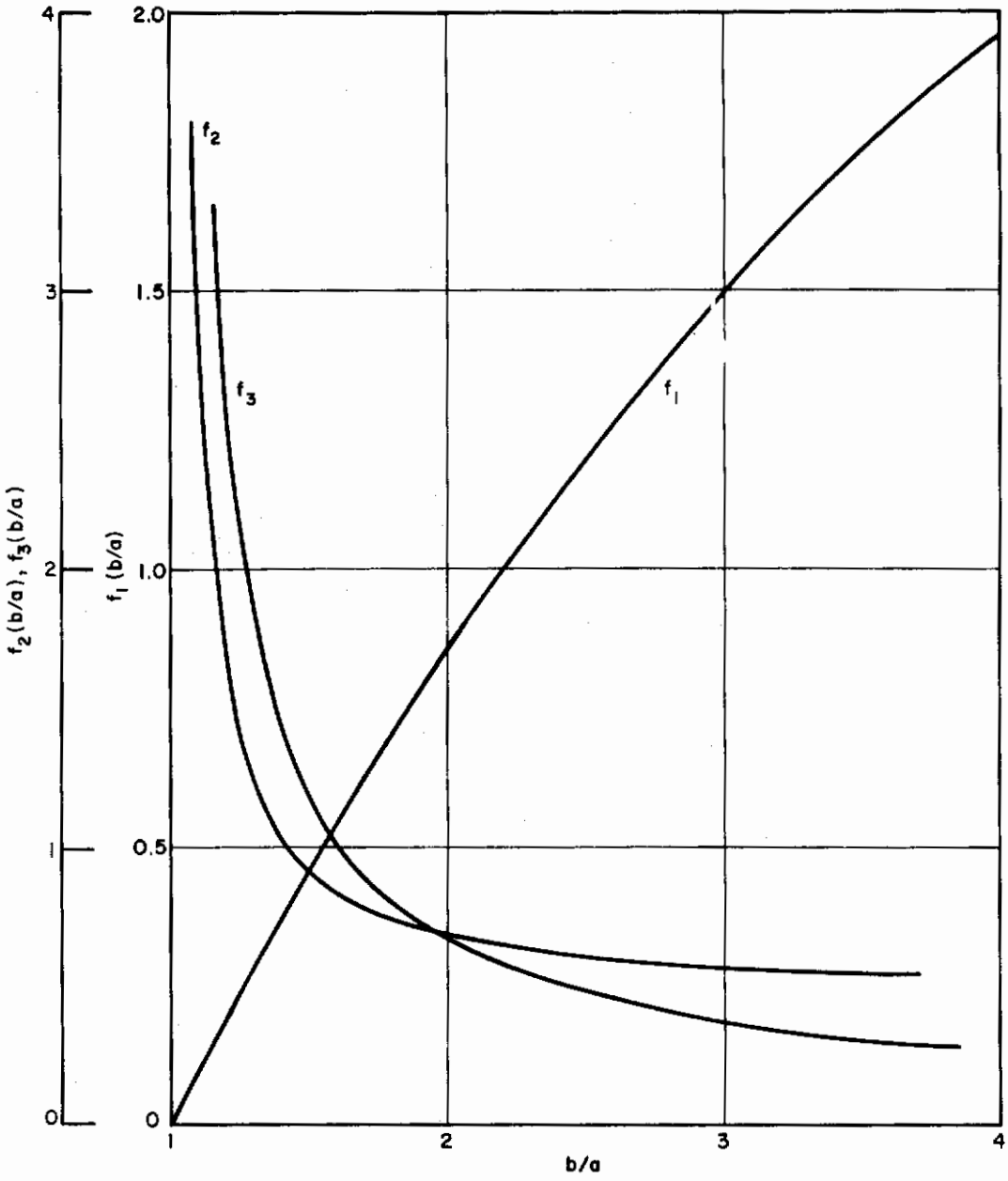

Figure 14 DEPENDENCE OF f_1, f_2 AND f_3 ON RATIO b/a

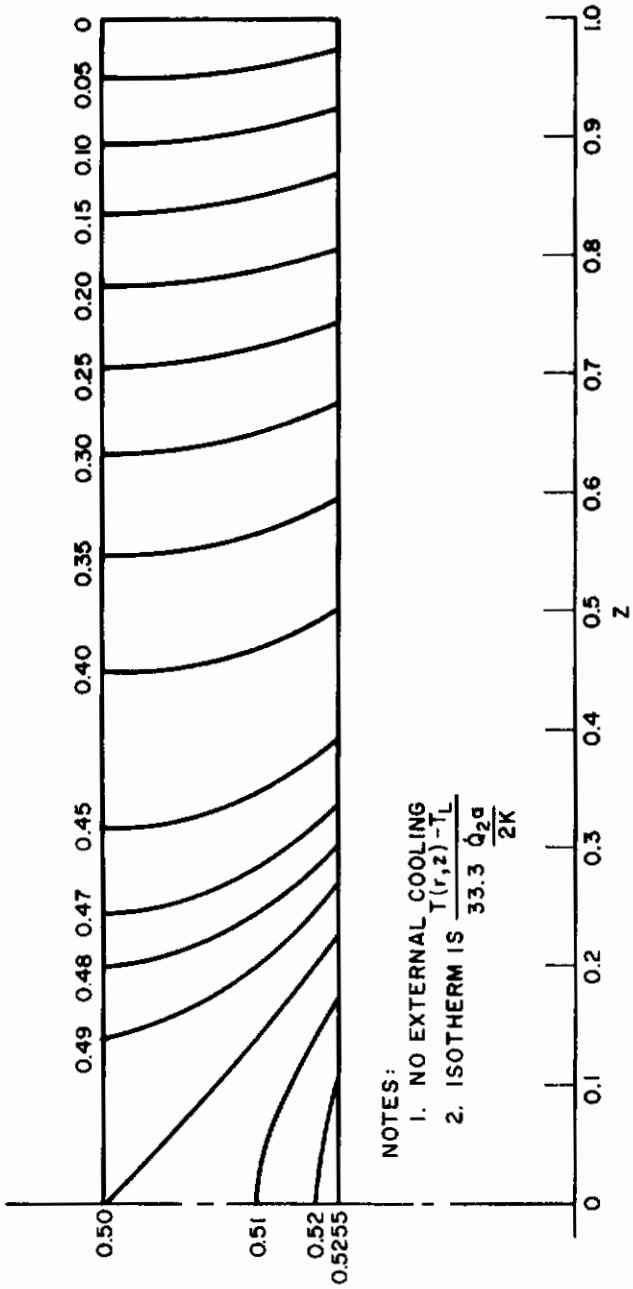

Figure 15 NON-DIMENSIONAL TEMPERATURE DISTRIBUTION IN TUBE FOR WHICH b/a = 2 AND L/b = 5

3. Thermal Stress Distribution

From the foregoing temperature distributions, the thermal stresses can be determined. The analysis is mathematically complicated and the details are found in Appendix A. These analytical stress distributions are inexact in a region of about one outer diameter in extent near the ends of the cylindrical tube.

Solving the appropriate differential equation, expressions are found for the three normal stresses, σ_r , σ_θ , σ_z , where r , θ and z denote the direction along which the stress is directed; a positive (negative) sign indicates tension (compression). Thus a positive σ_z at the outer tube wall indicates a stress tending to open an outer circumferential crack, while a positive σ_θ at the inner tube wall would indicate a stress tending to open an inner longitudinal crack.

a. Axial Cooling Mode

For this cooling mode, the stress components are given by

$$\sigma_r = \frac{-E\alpha\dot{Q}_2 a}{2(1-\nu)K}\left(\frac{r^2-a^2}{b^2-a^2}\right)\left[\frac{1-\nu}{4(1+\nu)}\left(1-\frac{b^2}{r^2}\right)+\frac{b^2}{b^2-a^2}\,\frac{b^2}{r^2}\,\ell n\,\frac{b}{a}\right.$$

$$\left.-\frac{b^2}{r^2-a^2}\,\ell n\,\frac{r}{a}\right] \qquad (25)$$

$$\sigma_\theta = \frac{E\alpha\dot{Q}_2 a}{2(1-\nu)K}\left(\frac{a^2}{b^2-a^2}\right)\left[\frac{-b^2}{b^2-a^2}\,\frac{b^2}{a^2}\,\ell n\,\frac{b}{a}\left(1+\frac{a^2}{r^2}\right)+\frac{(1-\nu)}{4(1+\nu)}\left(1+\frac{b^2}{r^2}\right)\right.$$

$$\left.+\frac{b^2}{a^2}\,\ell n\,\frac{r}{a}+\frac{1}{4(1+\nu)}\left\{3\nu\left(\frac{r^2}{a^2}+\frac{b^2}{a^2}\right)+5\,\frac{b^2}{a^2}-3\,\frac{r^2}{a^2}\right\}\right] \qquad (26)$$

$$\sigma_z = \frac{E\alpha\dot{Q}_2 a}{2(1-\nu)K}\left(\frac{a^2}{b^2-a^2}\right)\left[\frac{(1-\nu)}{2(1+\nu)}\left(2\,\frac{r^2}{a^2}-1\right)+\frac{3\nu+1}{2(1+\nu)}\,\frac{b^2}{a^2}\right.$$

$$\left.+2\,\frac{b^2}{a^2}\,\ell n\,\frac{r}{a}-2\,\frac{b^2}{a^2}\,\frac{b^2}{b^2-a^2}\,\ell n\,\frac{b}{a}\right] \qquad (27)$$

The symbols in equations (25) through (27) and (28) through (30) have the following meaning:

E modulus of elasticity

α coefficient of linear expansion

ν Poisson's ratio

K thermal conductivity of material

$\dot{Q}_2$ power per unit area conducted to inner wall of tube

a inner radius of tube

b outer radius of tube

r radial coordinate ($a \leq r \leq b$)

b. Radial Cooling Mode

For this cooling mode, the stress components are given by

$$\sigma_r = \frac{-E\alpha\dot{Q}_2 a}{2(1-\nu)K}\left[\ell n\ \frac{b}{r} + \frac{a^2}{b^2-a^2}\left(1-\frac{b^2}{r^2}\right)\ell n\ \frac{b}{a}\right] \tag{28}$$

$$\sigma_\theta = \frac{E\alpha\dot{Q}_2 a}{2(1-\nu)K}\left[1-\ell n\ \frac{b}{r} - \frac{a^2}{b^2-a^2}\left(1+\frac{b^2}{r^2}\right)\ell n\ \frac{b}{a}\right] \tag{29}$$

$$\sigma_z = \frac{E\alpha\dot{Q}_2 a}{2(1-\nu)K}\left[1-2\ell n\ \frac{b}{r} - \frac{2a^2}{b^2-a^2}\ell n\ \frac{b}{a}\right] \tag{30}$$

These results are expressed in Figures 16 and 17. Figure 16 shows the behavior of σ_r, σ_θ and σ_z, non-dimensionalized with the quantity $\frac{E\alpha\dot{Q}_2 a}{2(1-\nu)K}$ with $\nu = 0.25$, as a function of r for a tube for which $b/a = 2$, for both cooling modes. The abscissa, also non-dimensional, is defined so as to be zero at $r = a$ (inside wall) and unity at $r = b$ (outside wall). Note that for both cooling modes, the radial stress is wholly compressive while σ_θ and σ_z are compressive near the inside surface and tensile near the outer surface.

Figure 17 shows the maximum thermal stress (σ_z), compressive and tensile, versus b/a for both cooling modes; $\nu = 0.25$. One will note that for a given b/a, the axial cooling mode gives a higher maximum stress, and for small b/a, the radial cooling mode results in a substantially lower stress. Thus, in terms of stress, there is no advantage to be gained by inducing a strong axial cooling mode. This is a fortunate result because the "natural" cooling mode is the radial one.

To evaluate the quantity $\frac{E\alpha\dot{Q}_2 a}{2(1-\nu)K}$, the following physical properties of Lucalox are used:[9,10]

$E = 57 - 50 \times 10^6$ lb/in.^{2} (0-1000° C)

$\alpha = 4.3 - 5 \times 10^6$ in./in. ° F ($550 \leq T \leq 750$° C)

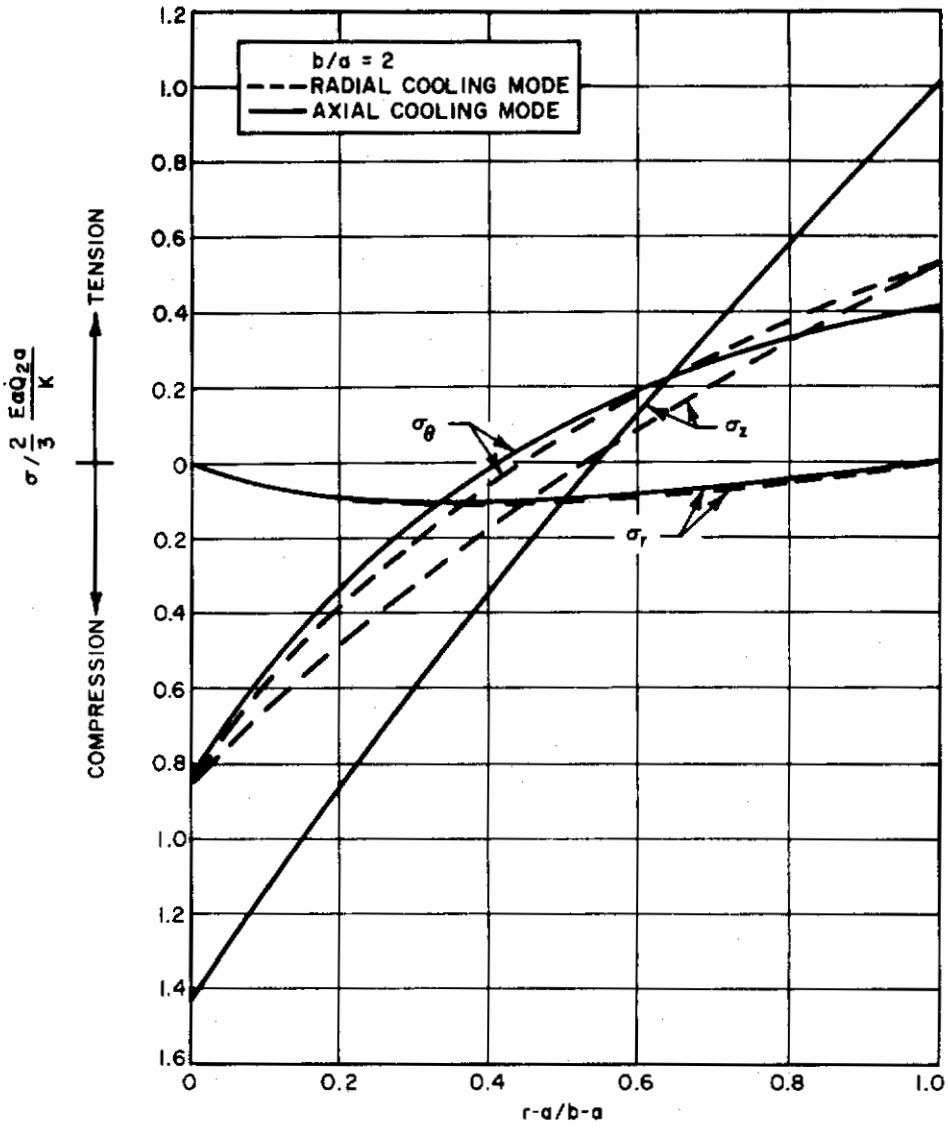

Figure 16 RADIAL DEPENDENCE OF THERMAL STRESS COMPONENTS

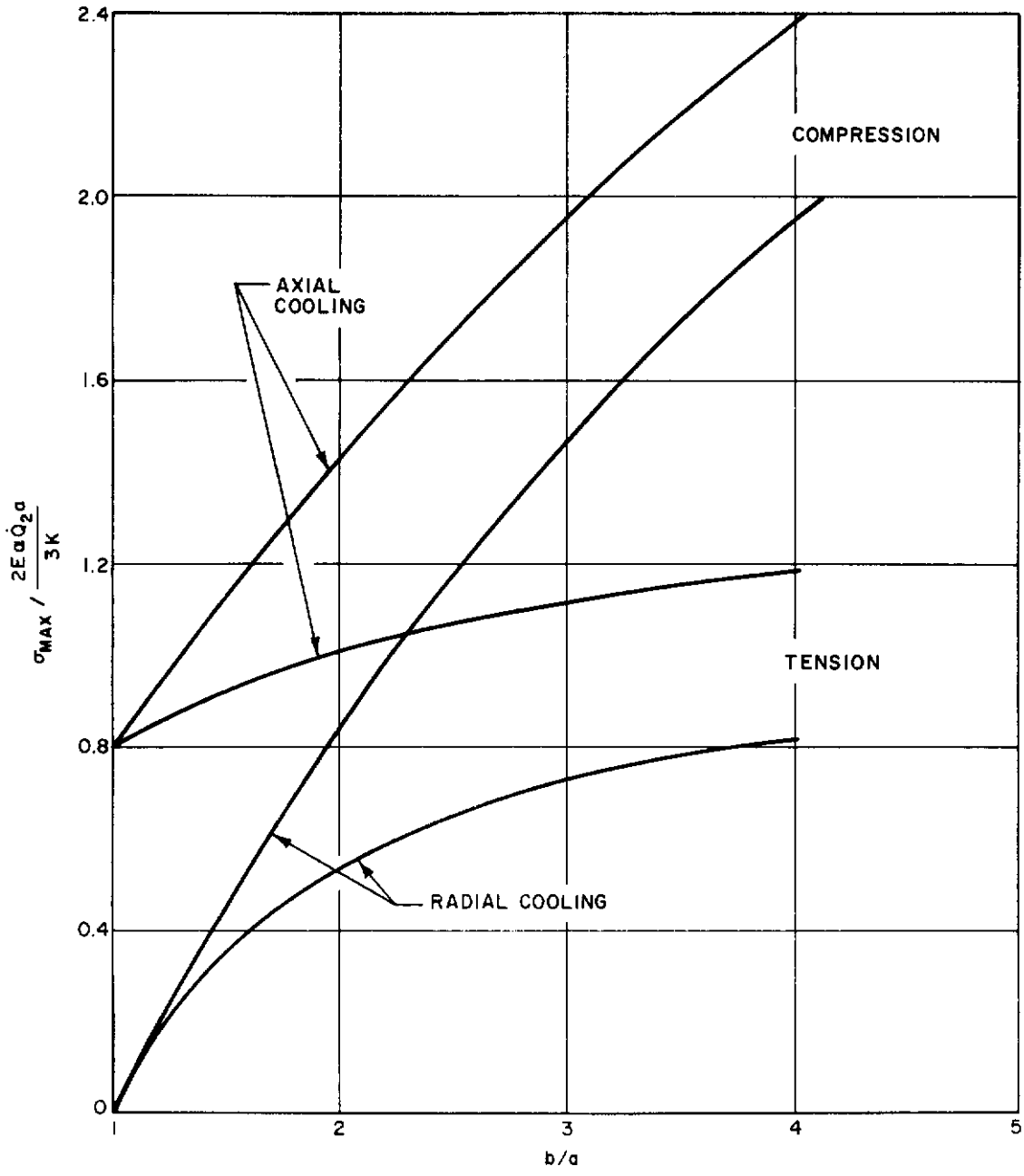

Figure 17 MAXIMUM THERMAL STRESS VERSUS RADIUS RATIO b/a

ν = 0.23 ≈ 0.25

K = See Figure 18.

For an average tube temperature of 600° C, $\frac{E\,a\,\dot{Q}_2{}^a}{2(1-\nu)K}$ becomes 1620 $\dot{Q}_2{}^a$ lb/in.^{2} when $\dot{Q}_2{}^a$ is expressed in watt/cm.

The compressive strength of Lucalox, as indicated in Ref. 10, is greater than 300,000 lb/in.^{2} The tensile strength is difficult to ascertain for it depends on such factors as preparation history, grain size, surface conditions, type of loading and environment. Bending strength measurements indicate that the tensile strength ranges from 70,000 lb/in.^{2} to 35,000 lb/in.^{2}, depending on grain size. Further, the bending strength decreases by about 30 percent at 1000° C.[11]

For a tube for which b/a = 1.33, Figure 17 indicates that $\sigma_{max} \Big/ \frac{2\,E\,\alpha\,\dot{Q}_2{}^a}{3K} = 0.25$

Taking σ_{max} for Lucalox to be 25,000 lb/in.^{2} and the average wall temperature to be 600° C, then the maximum allowable $\dot{Q}_2{}^a$ is 60 watt/cm. If the tube walls have an average temperature of 1200° C, then due to further reduction in the Young's Modulus, tensile strength and thermal conductivity, the estimated allowable $\dot{Q}_2{}^a$ is reduced to about 30 watt/cm. One must note that the values of $\dot{Q}_2{}^a$ in the two examples above may not be consistent with the temperatures assumed for the Lucalox wall.

Assuming that the wall temperatures above are consistent with the implied heat loadings, and thermal stress limits the peak performance, then the maximum radiated power can be determined. Since $\dot{Q}_2{}^a$ is 30 watt/cm, the heat conducted to the inner wall of the envelope is $\dot{Q}_2 2\pi a$ or 188 watt/cm. Table I below gives the input power and radiated power for various values of the radiating efficiency, η, of the arc column. If b/a is decreased from 1.33 to 1.15, then the maximum radiated power (for a given η) is doubled. (See Figure 17.)

TABLE I

CESIUM VAPOR LAMP PERFORMANCE WITH A LUCALOX ENVELOPE ASSUMING THERMAL STRESSES ARE LIMITING

η (percent)	Radiated Power (watt/cm)	Input Power (watt/cm)	Equivalent Blackbody Temperature (° K)
50	190	380	2700
60	280	465	3000
70	440	630	3150
80	750	935	3500
90	1690	1880	3950

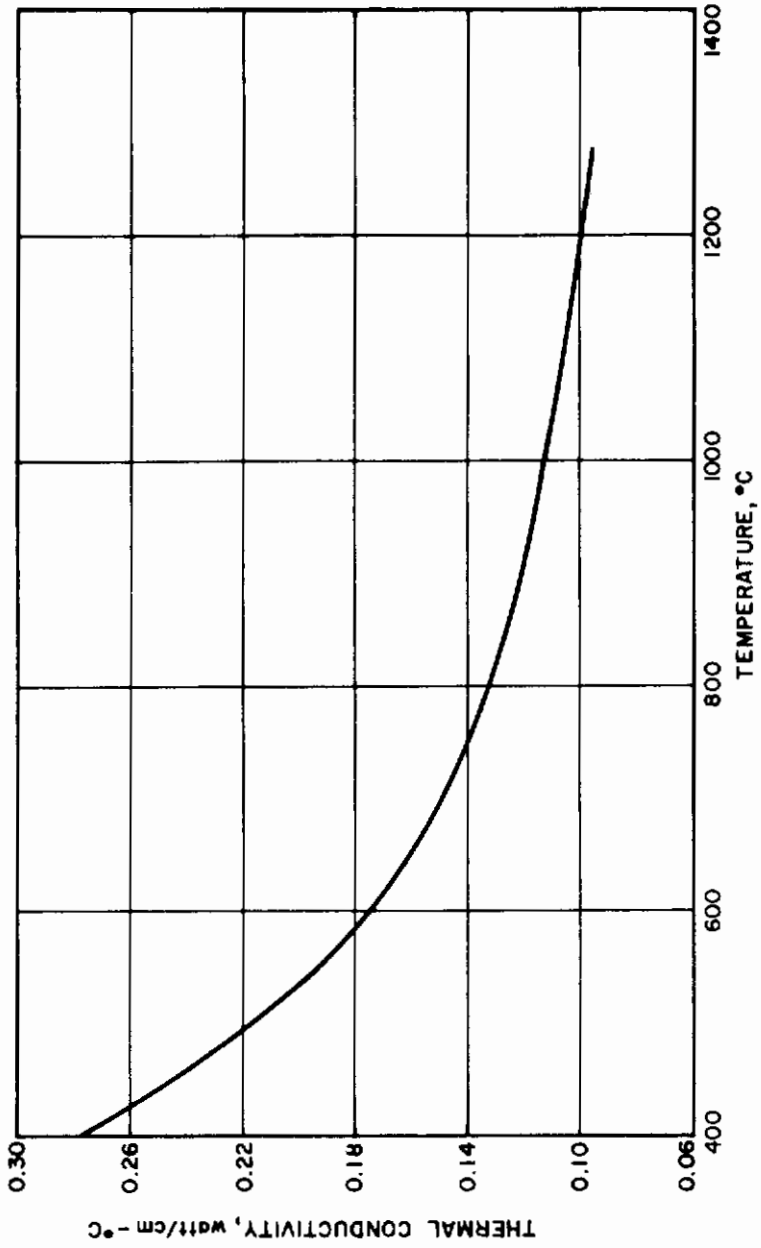

Figure 18 THERMAL CONDUCTIVITY OF LUCALOX VERSUS TEMPERATURE

Also included in Table I is the equivalent blackbody temperature assuming the voltage gradient is 30 volt/cm. Figure 12 is used to determine the arc column radii. Since the radiating efficiency of the arc column can be as high as 90 percent, one will note that if thermal stresses alone are limiting, the potential of the cesium arc discharge radiant source can be realized. At present, however, other factors limit the performance of the source.

C. FACTORS AFFECTING ENVELOPE TEMPERATURE

1. Introduction

Paragraph B indicated that if thermal stresses are the only consideration, the cesium vapor lamp with the Lucalox envelope can provide flux levels at least five times greater than those delivered by the tungsten-quartz lamp. In this section, the factors determining the envelope temperature are examined, and the resulting limitation on input power is considered.

2. Energy Transfer Mechanisms

To determine the envelope temperature, the balance between the energy input to the envelope from the arc column and the means by which the envelope rids itself of this energy must be considered. The details are shown schematically in Figure 19.

A fraction, η , of the input power to the arc discharge leaves the column as radiation. The rest, $(1-\eta)$, is conducted or convected away. A fraction, τ , of the radiated power from the arc column passes through the envelope to the outside. The remainder, $(1-\tau)$, is absorbed. Thus the total power to the envelope is given by

$$\text{Power to envelope} = (1-\eta)\, P_{input} + (1-\tau)\eta\, P_{input} \tag{31}$$

This power input to the envelope causes it to increase in temperature until an equilibrium is attained between the power input and the power lost to the surroundings. The envelope loses energy by two mechanisms, radiation and convective cooling. The power loss by radiation per unit length of the envelope can be expressed as

$$(P_{rad})_{envelope} = 2\pi b\, \epsilon_T\, \sigma\, T^4 \tag{32}$$

where T is the envelope temperature, 2b is the diameter of the envelope and ϵ_T is a quantity similar to emittance. Equation (32) assumes that the lamp is radiating to cold surroundings. For an isolated lamp, that is a reasonable assumption. For a lamp within an array of lamps, equation (32) should be modified to take into account re-radiation back to the envelope from both surrounding lamps and the sample.

The power loss by convection per unit length can be expressed as

$$(P_{conv})_{envelope} = 2\pi b\, h\, \Delta T \tag{33}$$

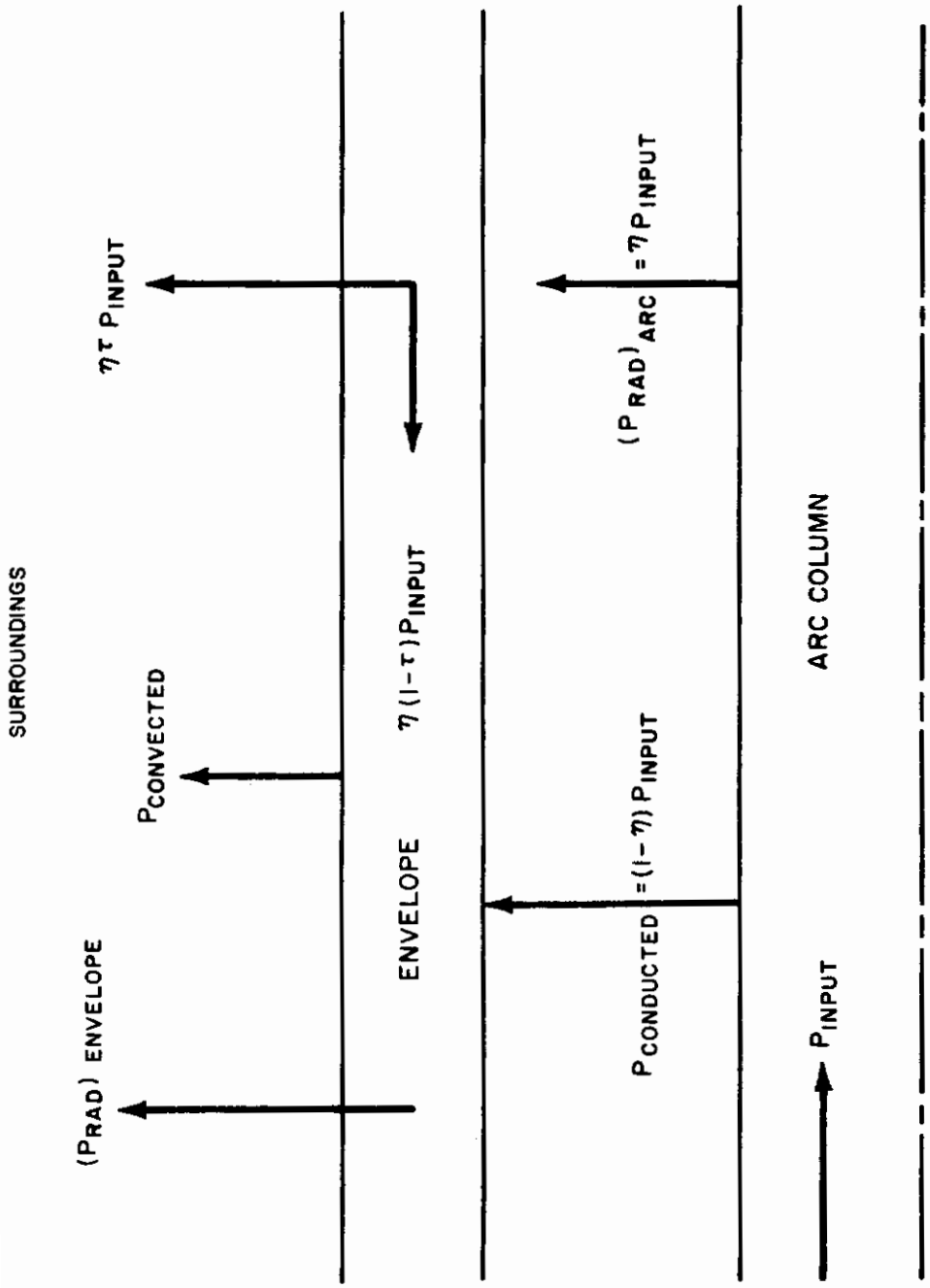

Figure 19 SCHEMATIC REPRESENTATION OF ENERGY TRANSFER BETWEEN ARC COLUMN, ENVELOPE AND SURROUNDINGS

where h is the heat transfer coefficient and ΔT is the difference in temperature between the envelope and the ambient surroundings.

When the envelope is in a steady state condition, the input power must equal the power loss, which leads to the condition

$$P_{input}[1 - \eta\tau] = 2\pi b\,[\epsilon_T\,\sigma T^4 + h\,\Delta T] \tag{34}$$

where P_{input} is the input power per unit length.

The quantity τ is a transmission coefficient. In general, it depends upon the geometry and material of the envelope and on the spectral distribution of the plasma arc radiation. The quantity ϵ_T is not the usual emittance because translucent materials, like Lucalox, are volume emitters rather than just surface emitters. Thus ϵ_T, as defined by equation (32) is a function not only of the material but also of the geometry and surface condition. For a cylinder, it would depend upon the inner and outer radii. Finally, since the volume emission would, in general, be wavelength dependent, the total emission would depend on temperature.

3. Heat Transfer Coefficient for Natural Convection

The heat transfer coefficient for natural or free convection for a horizontal cylinder is given by[11]

$$h_c = 0.27\left(\frac{\Delta T}{2b}\right)^{0.25} \quad (\text{Btu/hr-ft}^2\text{-}^\circ\text{F})$$

$$= 4.16 \times 10^{-4}\left(\frac{\Delta T}{2b}\right)^{0.25} \quad (\text{watt/cm}^2 - {}^\circ\text{C}) \tag{35}$$

Figure 20 is a plot of the power, per unit length, lost to ambient air at 70° F by natural convection for three different envelope diameters.

4. Heat Transfer Coefficient for Forced Convection

The heat transfer coefficient for the cross flow of non-turbulent air over a cylinder is usually expressed as an experimental correlation between the Nusselt number, $\frac{h_m\,2b}{K_f}$, and the Reynolds number, $\frac{2b\rho U}{\mu_f}$, where the symbols have the following meaning:

h_m azimuthally averaged heat transfer coefficient

$2b$ diameter of cylinder

ρ density of free stream

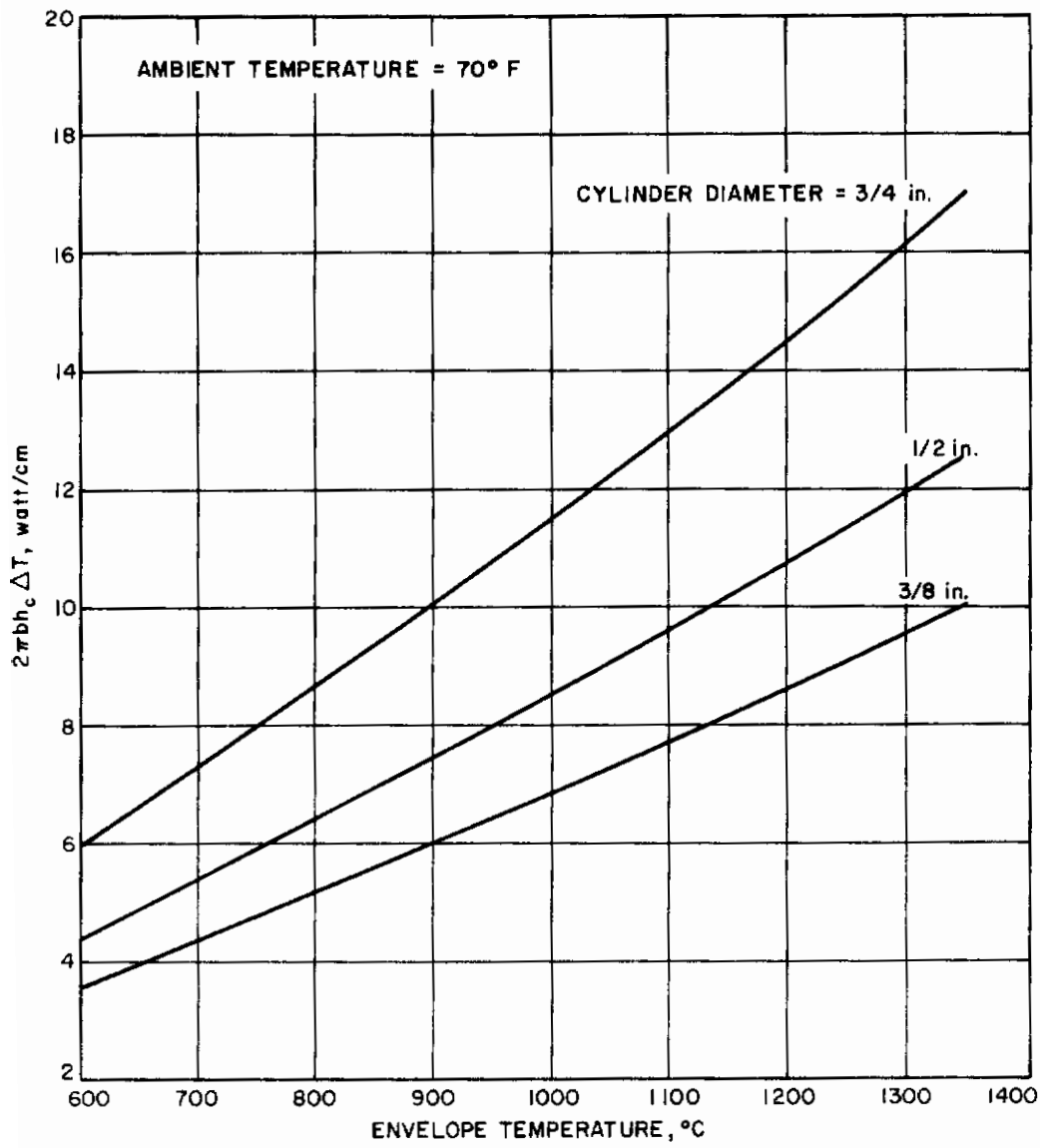

Figure 20 POWER LOSS DUE TO NATURAL CONVECTION FROM A HORIZONTAL CYLINDER AS A FUNCTION OF WALL TEMPERATURE AND CYLINDER DIAMETER

U free stream velocity

μ_f viscosity of film

K_f thermal conductivity of film

The film temperature is taken to be $(T_{wall} + T_a)/2$ where T_{wall} is the temperature of the cylinder surface and T_a is the temperature of the free stream flow.

For $1000 \leq \frac{2b\rho U}{\mu_f} \leq 50{,}000$, the correlation is given by[12]

$$\frac{h_m 2b}{K_f} = 0.24 \left(\frac{2b\rho U}{\mu_f} \right)^{0.6} \tag{36}$$

Figure 21 is a plot of the power loss per unit length due to the cross flow of air at one atmosphere pressure and 70° F over a cylinder with a diameter of 1/2 inch for various free stream velocities and wall temperatures. These results can be used for cylinders of diameter D inches by multiplying by the ratio $\left(\frac{D}{0.5} \right)^{0.6}$.

5. Power Loss by Radiation

The power loss by radiation is given by equation (32). Figure 22 is a plot of $\epsilon_T \sigma T^4$ versus temperature for various values of ϵ_T. Some experiments were undertaken to determine ϵ_T for the Lucalox tubes used as envelopes for the cesium vapor lamps. The procedure consisted of heating the Lucalox tube to some known temperature and comparing the radiation from it to that from a silicon carbide rod of the same diameter and at the same temperature. The arrangement was such that both the Lucalox and the silicon carbide rod were located in the same position relative to the detector. A slit was used to restrict the field of view.

The ratio of the two signals was interpreted to be ϵ_T in equation (32). This makes the assumption that the radiation from both materials has the same angular distribution. Other experiments have indicated that Lucalox is a Lambertian radiator out to angles of 55 deg from the normal. The results of these measurements are represented by the dashed line on Figure 22.

6. Relation Between Input and Envelope Temperature

The right-hand side of equation (34) can be evaluated as a function of envelope temperature for various cooling conditions so that equation (34) can be used to find the input power associated with a given envelope temperature. The term r still must be evaluated. The term $(1 - r)$ represents the fraction of the radiation from the arc column that is absorbed by the Lucalox envelope. Measurements made on a Lucalox envelope (1/2-inch outer diameter with a 1/16-inch wall thickness) indicate that in the spectral range of 1-4 μ, where most of the radiation of the cesium plasma is found, the amount of absorption is 5-10 percent. Thus, r has a value of 0.90-0.95.

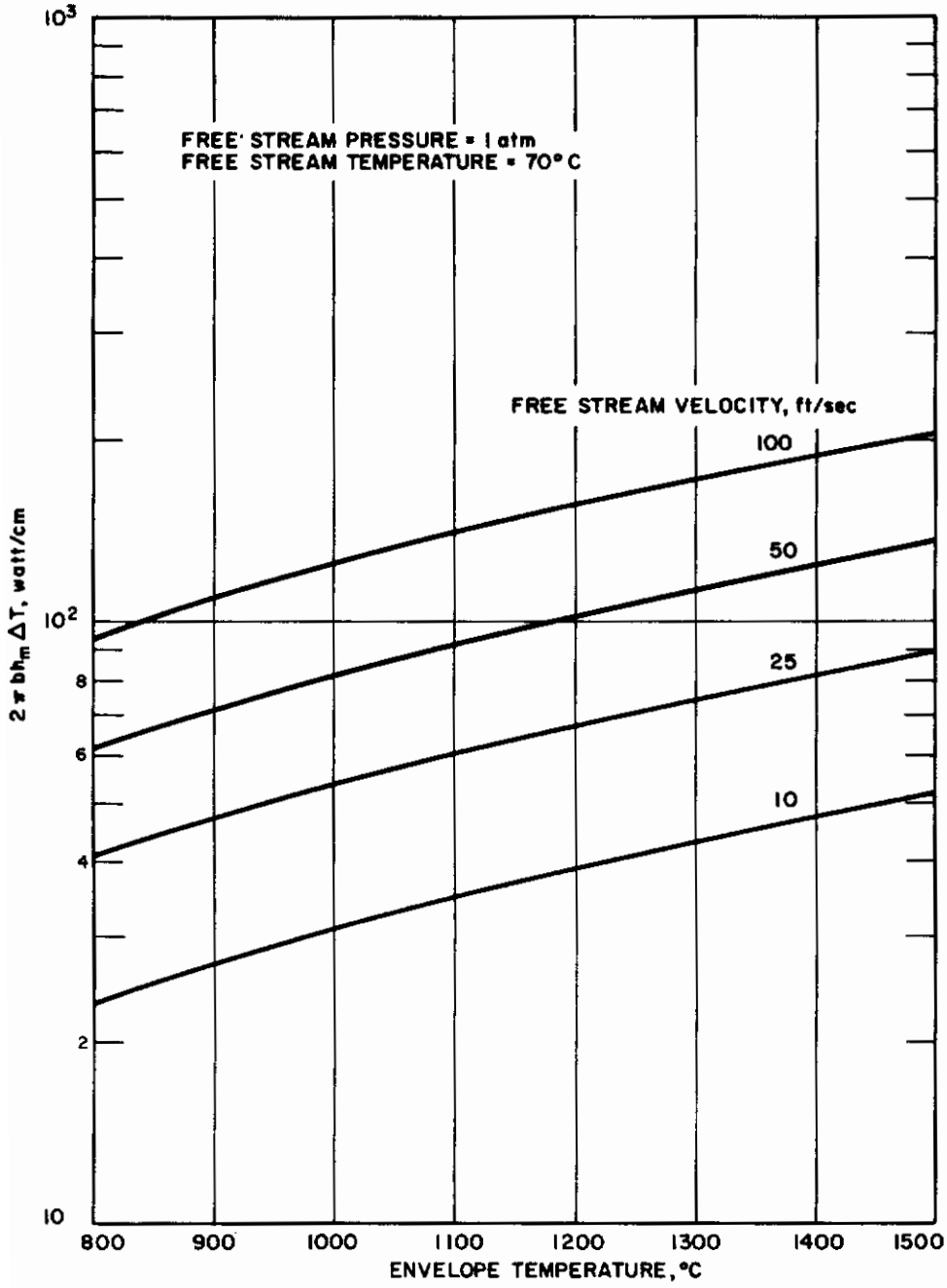

Figure 21 POWER LOSS DUE TO CROSS FLOW OF AIR OVER A 1/2-INCH CYLINDER AS A FUNCTION OF CYLINDER TEMPERATURE AND FREE STREAM VELOCITY

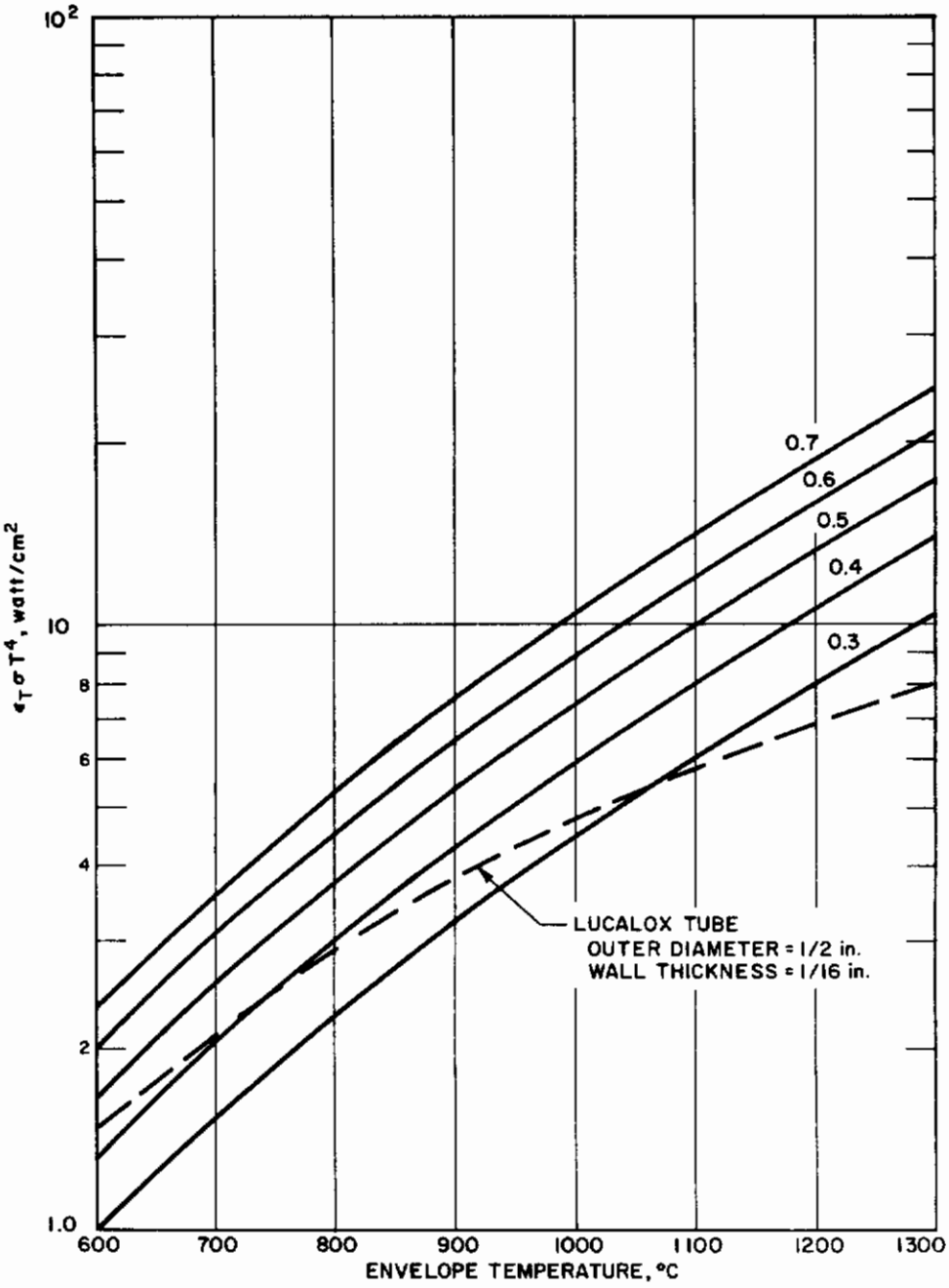

Figure 22 RADIATED POWER FLUX FROM ENVELOPE AS A FUNCTION OF TEMPERATURE AND EMITTANCE

Figure 23, based on Figures 20 and 22 and equation (34), shows the input power versus ηr for a cesium vapor lamp with a 1/2-inch Lucalox tube for various wall temperatures, where the power loss from the tube is due to natural convection and radiation cooling to cold surroundings. Taking $r = 0.95$ and assuming the radiating efficiency of the arc column is 0.9, an input power of 360 watt/cm is possible for a wall temperature of 1500° C. This input power is probably close to the maximum for the cesium vapor lamp in the 1/2-inch Lucalox tube with only natural convection cooling. For an arc column with a radius of 0.1 centimeter, this corresponds to a blackbody temperature of 3100° K. This input power would be reduced considerably if the lamp was in an array where both the natural convection and the radiation cooling would be less. With this cooling arrangement, the potential of the cesium vapor lamp is not realized.

When forced convection is used, the input power can be increased markedly. Figure 24, based on Figures 21 and 22, shows the input power that results when forced convection as well as radiation cooling is employed. The results are shown for three different free stream velocities and two different values of η ; r is taken to be 0.95. For a free stream velocity of 50 ft/sec and an arc radiating efficiency of 90 percent, the input power for a wall temperature of 1500° C is 1175 watt/cm. For a voltage gradient of 30 volt/cm, the current is 39 amperes. From Figure 12, this corresponds to an arc radius of 0.17 centimeter. (From Figure 34, 30 volt/cm corresponds to ~1 atm vapor pressure.) Thus, the arc column is radiating at a rate of 1000 watt/cm^2, which is equivalent to a blackbody temperature of 3700°K. By comparison, the tungsten-quartz lamps are equivalent to a blackbody temperature of 2500° K, which corresponds to radiation output which is four times smaller.

D. LAMP GEOMETRY AND FABRICATION

The plasma arc lamp consists of a cylindrical envelope sealed at both ends by means of endcaps. Attached to the endcaps are the electrodes. Figure 25 is a sketch of the lamp. The envelope is made of Lucalox with one essential advantage over quartz: it is inert with respect to molten alkali metals. It also offers the advantages of a higher operating temperature and greater modulus of rupture. Also, higher temperature metal seals are possible. In addition, Lucalox has a higher transmission than quartz in the 4-6 μ range. The envelope most commonly used in this investigation had a 1/2-inch o.d., a 1/16-inch wall thickness and was 8 inches long.

The endcaps are 0.010-inch thick and are made by cold-forming. The material used is tantalum, though niobium has been employed and rejected because of the lower melting point. The basic requirement is a match to Lucalox in coefficient of thermal expansion, though melting point and ease of forming are secondary considerations. The principal disadvantage to tantalum is its poor resistance to oxidation.

The braze between the Lucalox and the endcap is composed of a sandwich containing layers of titanium, nickel and then titanium. The heating is accomplished by radiation from an inductively heated source. A ductile braze is obtained at a temperature of about 1170° C. Titanium is generally not a good constituent for a braze alloy because of its tendency to form brittle intermetallic compounds, but it does "wet" Lucalox.

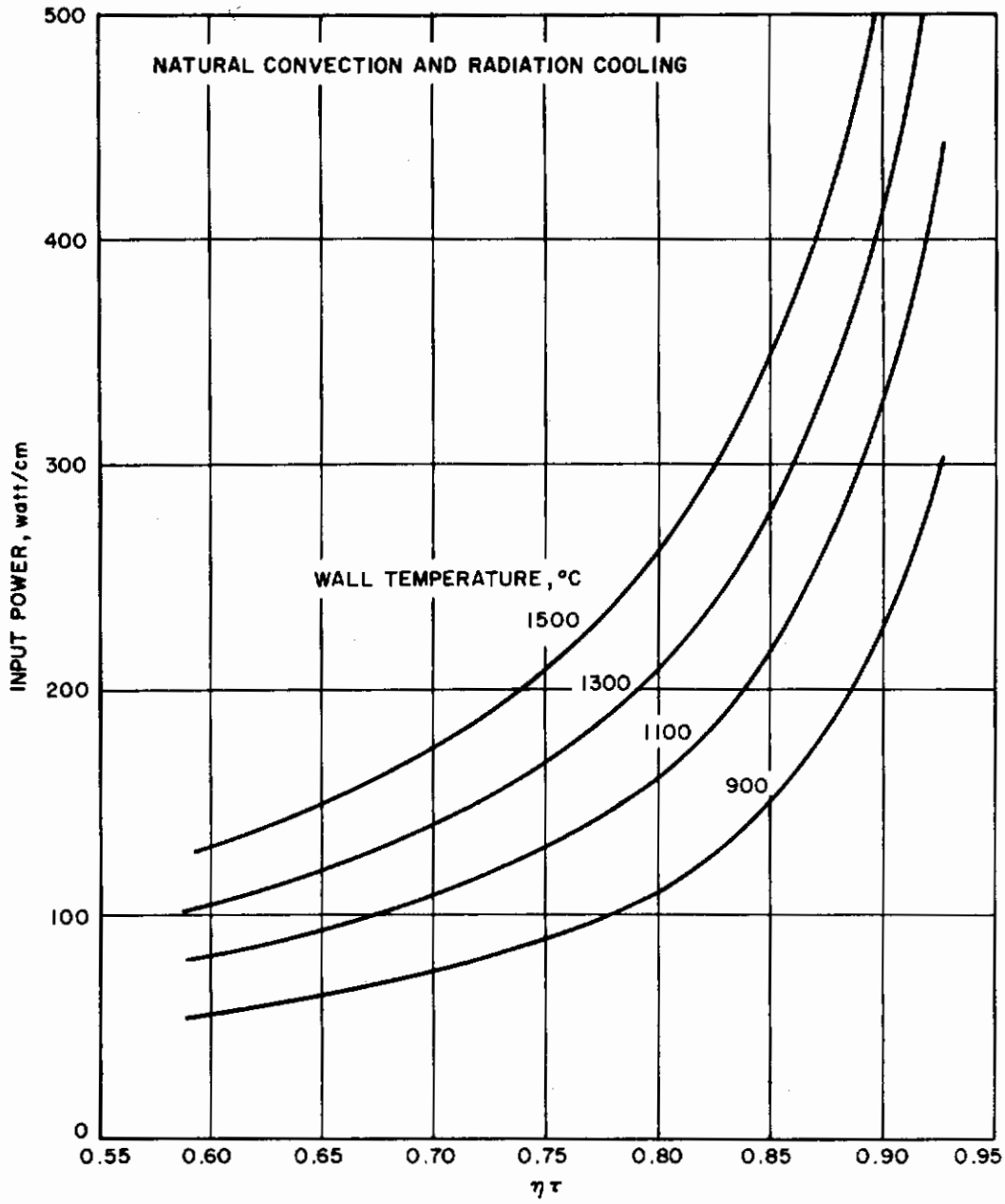

Figure 23 INPUT POWER TO CESIUM VAPOR LAMP WITH 1/2-INCH LUCALOX ENVELOPE AS A FUNCTION OF $\eta\tau$ AND WALL TEMPERATURE

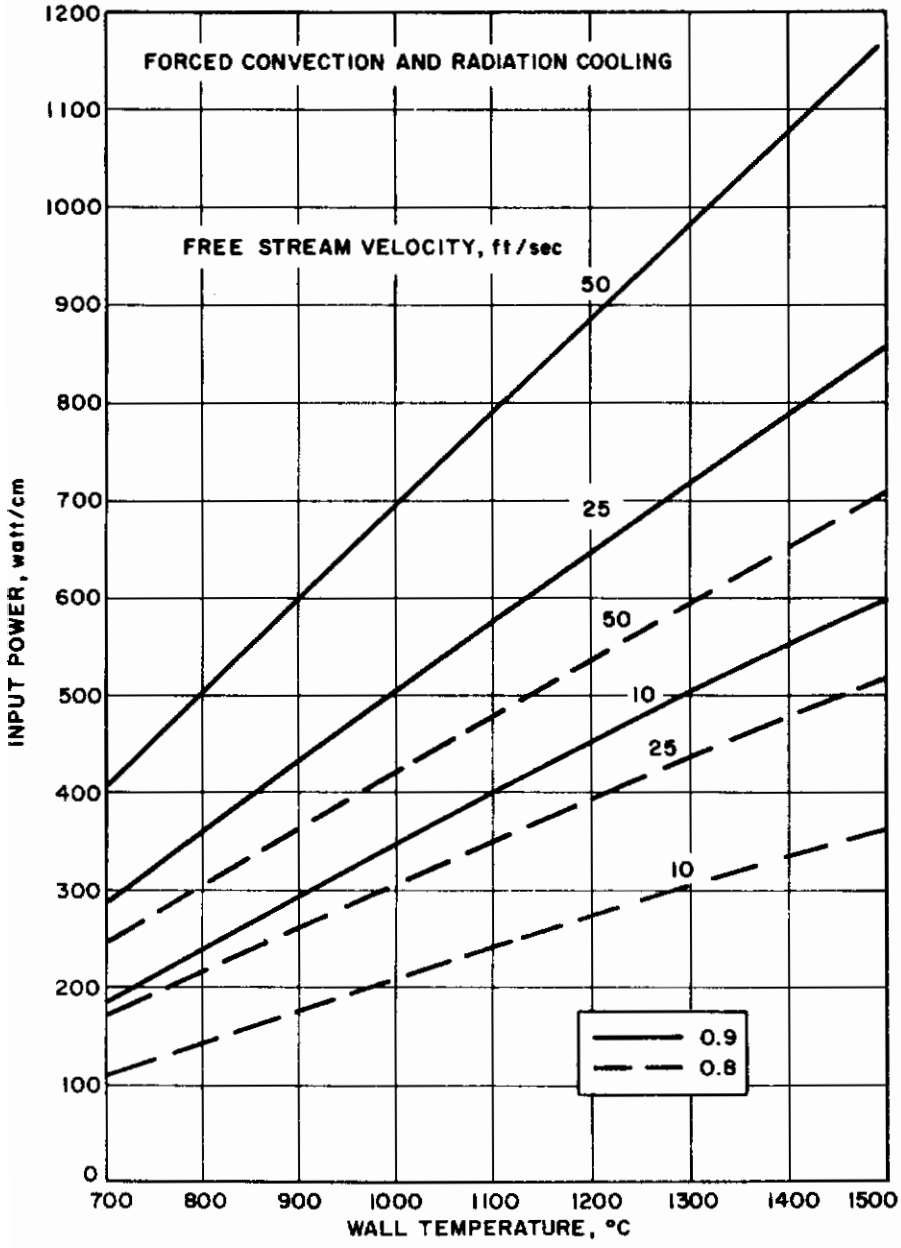

Figure 24 INPUT POWER TO CESIUM VAPOR LAMP WITH 1/2-INCH LUCALOX ENVELOPE AS A FUNCTION OF WALL TEMPERATURE AND FREE STREAM VELOCITY

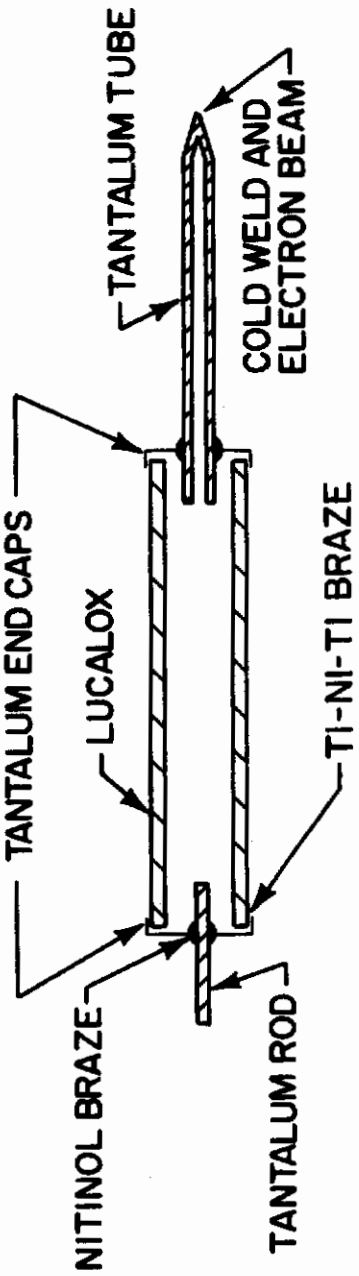

Figure 25 SKETCH OF CESIUM VAPOR LAMP SHOWING CONSTRUCTION DETAILS

As indicated in Figure 25, one electrode is a solid tantalum rod which has a diameter of 0.060-inch. The other electrode is a tantalum tube with a 1/8-inch o.d. and a wall thickness of 0.010 inch. The basic requirements for the electrode materials are resistance to corrosion by alkali metals, a high melting point and enough ductility that it can be cold-welded. The electrodes are inserted through the endcaps and into the envelope about 7/16-inch.

The braze employed to join the electrodes to the endcaps is nitinol (50 percent nickel and 50 percent titanium), which has a melting point of 1300° C. A later development was to replace this braze by an electron beam weld. The basic advantages of this are a higher melting point joint and an improved adherence of the plating (better adherence to tantalum than to the braze material). The resistance to corrosion by the alkali metals of these brazes is not well-established. Experience seems to indicate that the brazes are not wholly satisfactory in this respect.

The fabrication procedure is to braze the electrodes to the endcaps and then braze the endcaps to the envelope. The next step is to introduce cesium into the tube. This is accomplished in a glove box which provides an inert environment, thereby preventing the rapid oxidation of cesium upon exposure to air. The lamp is evacuated and then filled with approximately 100 mg of cesium, which is enough so that there is always some liquid cesium present while the lamp is in operation. Along with the cesium, the lamp is filled with argon to a pressure of approximately 10 torr. The end of the filler tube is then cut off and cold-welded by compression. The lamp is then removed from the glove box and the cold-weld joint is permanently sealed by electron beam welding.

The last step in the fabrication of a lamp is the electroplating of the tantalum surfaces to prevent oxidation. A program to develop tantalum coatings was carried forth in cooperation with the Materials Development Section of Avco/SSD. Various coatings were first evaluated by subjecting test samples to elevated temperatures in a furnace for various periods of time. Coatings that showed promise were then applied to a lamp and evaluated under actual running conditions.

The coating that showed the best performance was one consisting of a layer of nickel followed by a layer of platinum followed by a layer of gold. This coating withstands 1000° C for 10 hours without signs of oxidation.

E. DIRECT CURRENT OPERATION AND PERFORMANCE

1. Starting Characteristics

A self-sustaining electric discharge in the lamp is initiated when the potential across the electrodes reaches a value V_s, called the sparking potential. The sparking potential depends upon the gas, the pressure, p, the electrode separation, d, the electrode geometry and material. If the gas, electrode material and geometry are kept fixed, then it is found that V_s is a function of pd, the product of the gas pressure and electrode separation. This fact is known as Paschen's law.[8] Figure 26 is a plot of V_s versus pd obtained from measurements with argon in an unsealed cesium vapor lamp. The lowest pressure represented on Figure 26 is 1.2 torr.

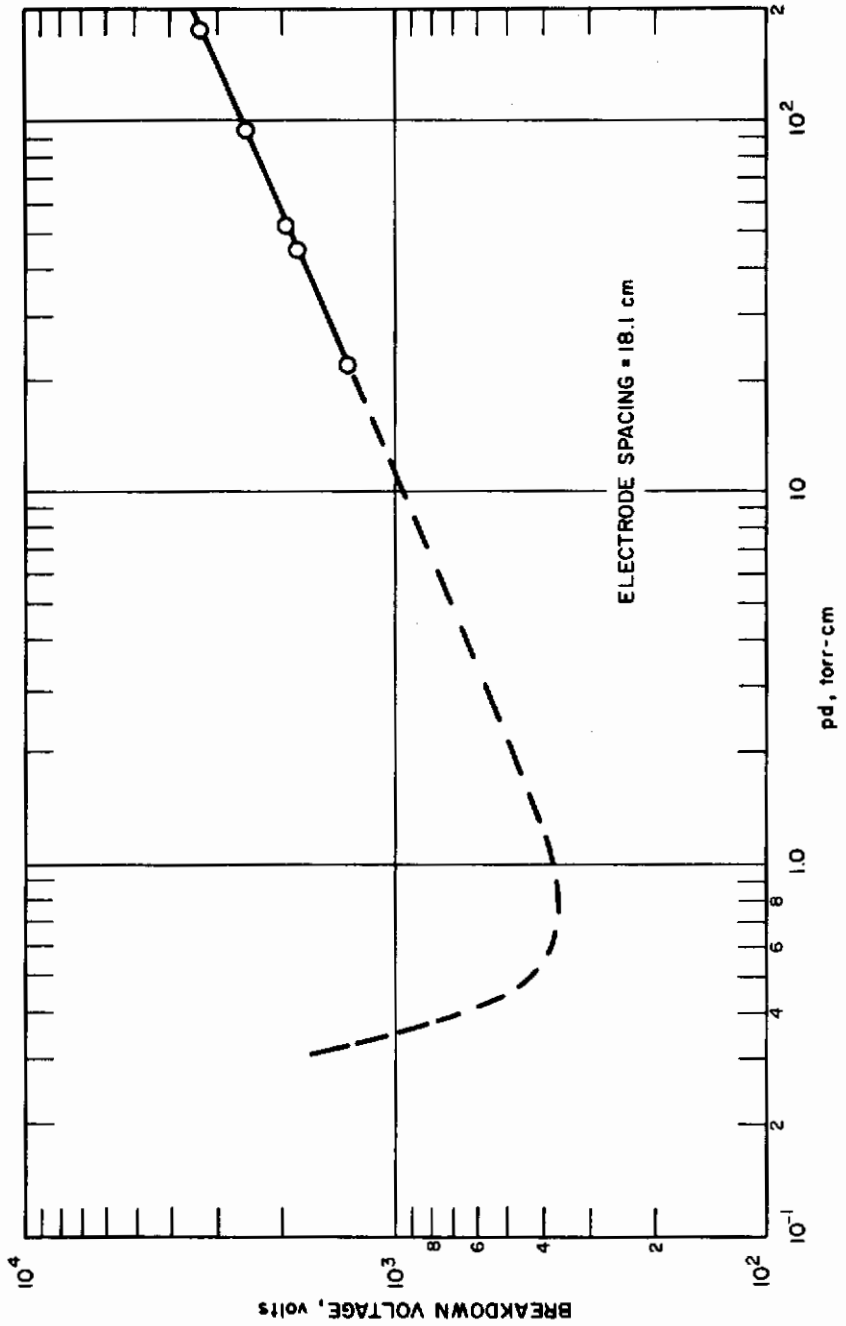

Figure 26 BREAKDOWN VOLTAGE VERSUS pd FOR ARGON IN 1/2-INCH TUBE

If these measurements were carried to lower pressures, the curve would show a minimum as indicated by the dashed line. This minimum occurs at a potential of from 140 to 350 volts and at a pd of approximately 1 torr-cm.[8,13]

Once breakdown is initiated, the nature of the ensuing discharge depends on the characteristics of the circuit and power supply. If the power supply is current-limited, a glow discharge may develop which is characterized by low currents (typically ma) and large cathode fall voltages (typically hundreds of volts) with the result of a high power transfer to the cathode. If the power source can supply currents of the order of amperes, then an arc discharge is established. The arc discharge is characterized by modest anode and cathode fall voltages (typically volts) and an arc column where voltage gradient, radiation and temperature are essentially constant along the column.

Figure 27 shows a plot of lamp voltage versus lamp current for a cesium-filled lamp at an operating temperature that is low enough to represent the characteristics of argon at a pressure of about 10 torr. The portion of Figure 27 where the voltage starts to rise steeply is a transition region between the arc discharge mode and glow discharge mode.

Figure 28 is a plot of lamp voltage versus current for a lamp filled with argon at a pressure of 300 torr. Comparison between Figures 27 and 28 shows that at higher pressure, the position of minimum voltage moves toward higher current.

2. Power Supply

The power supply used in the laboratory evaluation of the dc operation of the cesium-vapor lamp was a dc welding unit. For currents in the range 0-30 amperes, the power supply can be considered to be a 700-volt battery with a resistance of 1 ohm in series. The lamp was connected in series with a 0-200-ohm variable ballast resistor. The circuit is shown in Figure 29.

The 700-volt open-circuit voltage output is not generally sufficient to cause breakdown. Breakdown is accomplished by using an oscillator starter. (See Figure 30.) High voltage is delivered by a 15-kw, 30-ma neon sign transformer. A 12,000-volt capacitor is charged up until a spark is created across an adjustable air gap which consists of two tungsten electrodes. During breakdown, the circuit oscillates (with a low Q) at a frequency (typically kc) depending on the value of the capacitance and inductance in the circuit. These high-voltage, high-frequency pulses are inductively coupled to the circuit containing the lamp. The starter causes breakdown and can drive enough current through the lamp to lower the voltage below 700 volts, where the power supply can take over.

If the power supply contains diodes or other rectification elements, a protective capacitor should be put across the leads of the power supply. Once the lamp is started, the starter has no further effect and the protective capacitor could be removed.

The existence and stability of the arc discharge with a dc voltage source and a pure resistance in series is determined by considering Figure 31.

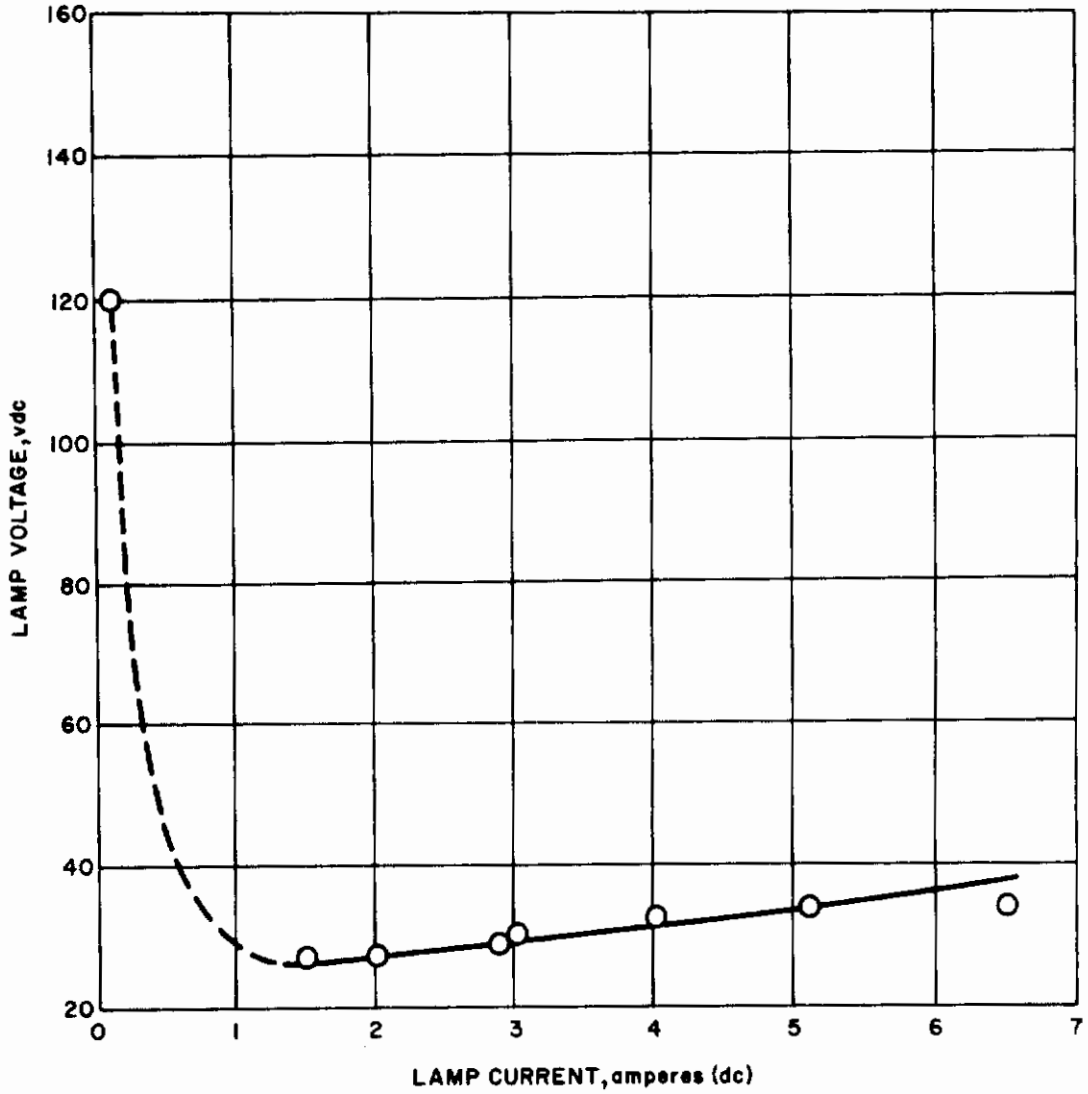

Figure 27 VOLTAGE-CURRENT CHARACTERISTIC OF CESIUM VAPOR LAMP AT IGNITION: ARGON PRESSURE ~10 TORR

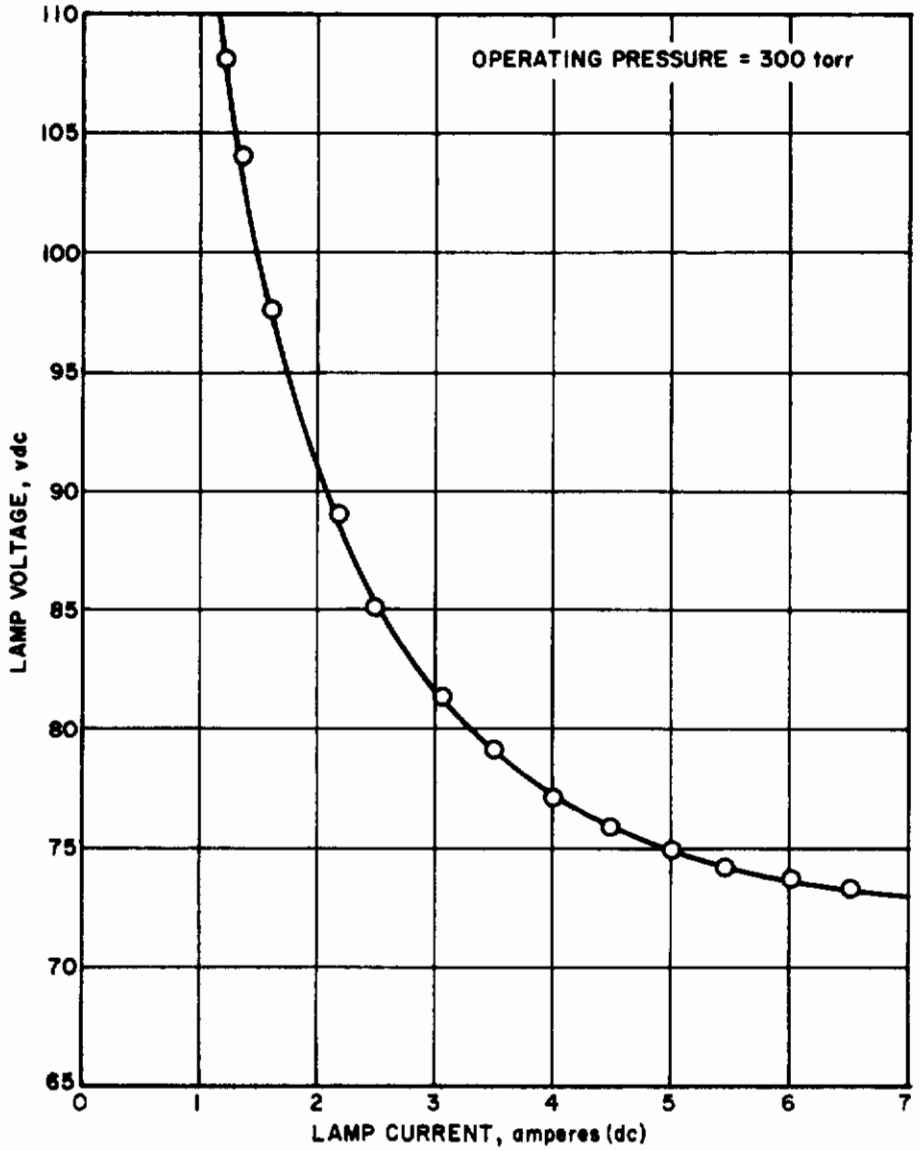

Figure 28 VOLTAGE-CURRENT CHARACTERISTIC FOR LAMP CHARGED WITH ARGON

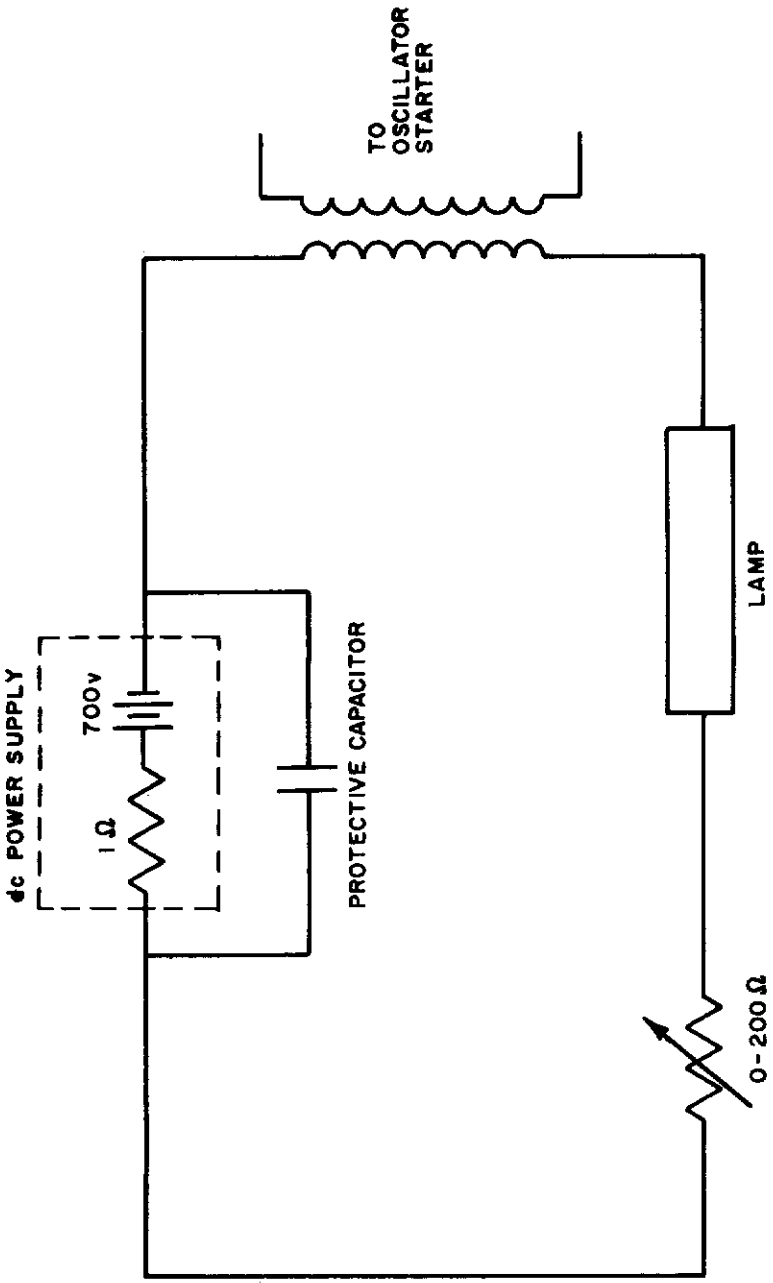

Figure 29 CIRCUIT FOR DC OPERATION OF CESIUM VAPOR LAMP

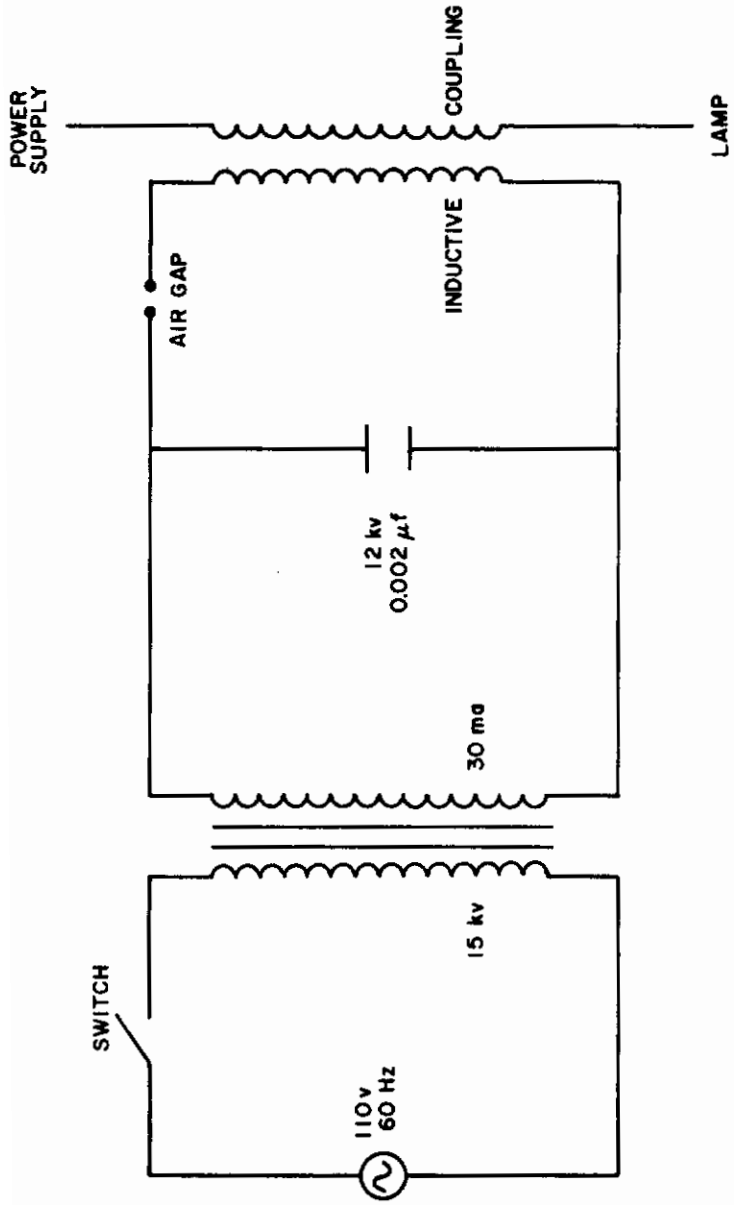

Figure 30 CIRCUIT DIAGRAM OF OSCILLATOR STARTER FOR CESIUM VAPOR LAMP

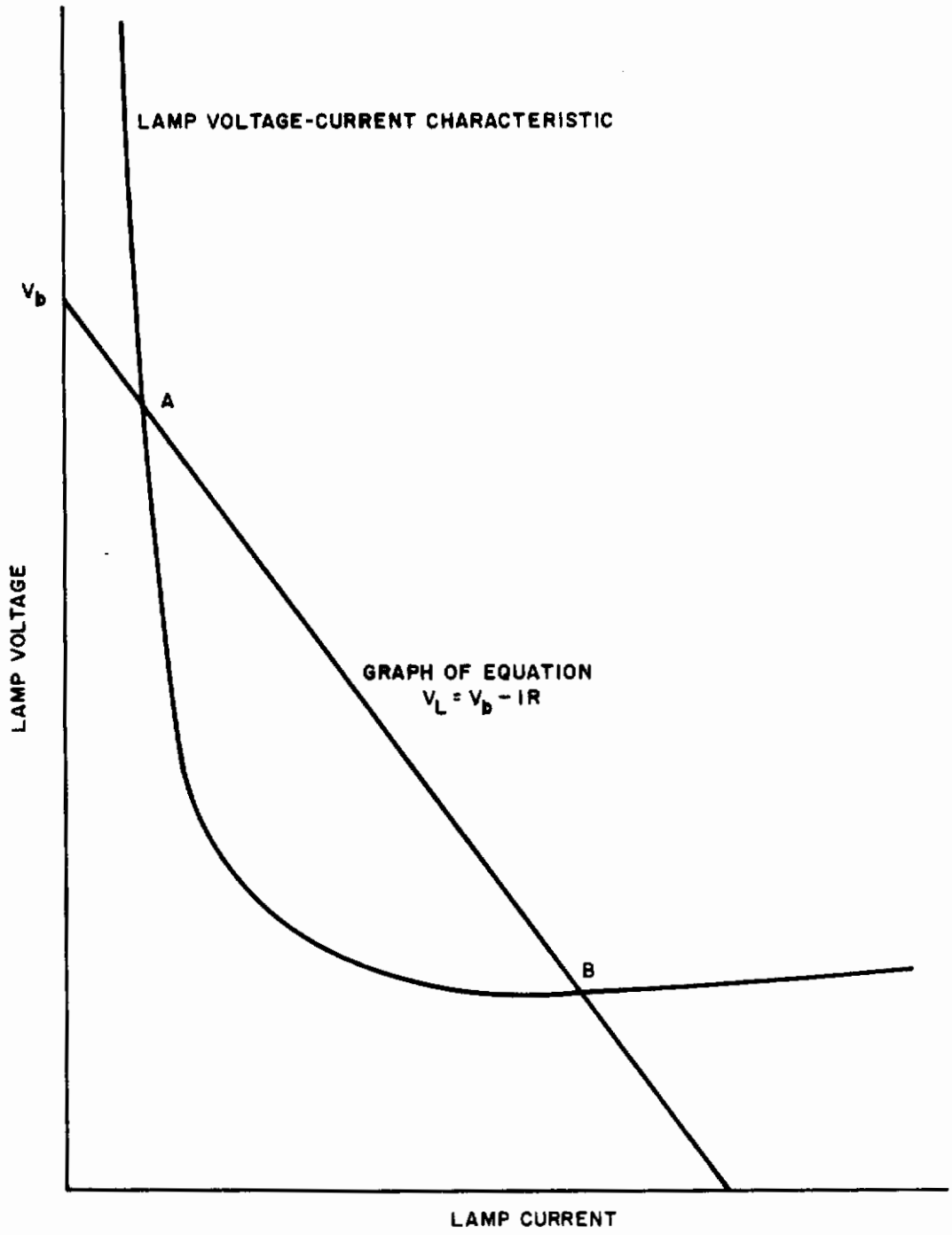

Figure 31 INTERSECTION OF LAMP VOLTAGE-CURRENT CHARACTERISTIC AND RESISTANCE LINE

The curve represents a typical voltage-current characteristic for an arc discharge (e.g., Figures 27 and 28). The straight line is a plot of the relation

$$V_L = V_b - IR \tag{37}$$

which is a consequence of the lamp being in series with a resistor and a battery. V_L is the lamp voltage, V_b is the battery voltage, I is the lamp current and R is the value of the series ballast resistor. Operating point(s) for the arc discharge correspond to the intersection of these two curves. As is indicated in Figure 31, there are two points of intersection. One can show that only one point, A, is stable with regard to small fluctuations in the power supply.[14] The general criterion for stability is

$$\frac{dV}{dI} > -R$$

where $\frac{dV}{dI}$ is the slope of the discharge voltage-current characteristic.

These considerations are useful in determining the lamp current that will result upon initial startup. Returning to Figure 27, one can note that if the startup current is to be 3 amperes and the supply voltage is 160 volts, then a series resistance of 43 ohms is needed. If V_b is 700 volts, a resistance of 223 ohms is required.

3. Plasma Pressure During Lamp Operation

As indicated previously, the filling operation consists of evacuating the lamp, adding approximately 100 mg of cesium and approximately 10 torr of argon, and then sealing off the tube. At room temperature, the vapor pressure of cesium is much less than 1 torr. Thus, upon starting, the lamp radiation has the characteristic bluish-purple color of argon. As the lamp components heat up, the temperature of the cesium liquid-vapor interface increases and hence the cesium pressure increases, with the result that the radiation becomes characteristic of a cesium plasma. Figure 32 shows how the cesium vapor pressure varies with the temperature of the liquid-vapor interface during equilibrium conditions.[15]

Figure 33 is a schematic of the voltage-current characteristics for the lamp for four different plasma pressures. Also included are plots of equation (37) for a fixed battery voltage but different ballast resistors.

Suppose that the lamp is operating at point A corresponding to load line 1 and pressure P_1. Let the ballast resistor be decreased suddenly to a value corresponding to load line 2. Then the lamp operating point moves from A to B, the current and voltage increasing. This increased power causes the cesium liquid-vapor interface temperature to increase to some new steady-state value corresponding to P_2. During this adjustment, the lamp operating point moves along load line 2 from B to C. Two other sudden decreases in ballast resistor are also depicted in Figure 33. In changing from load line 2 to 3, the corresponding change in operating point, C to D, occurs at essentially constant voltage while the voltage decreases with a sudden change from load line 3 to 4. Provided there is sufficient liquid cesium, an increase in current leads to an increase in vapor pressure. This in turn causes an increase

in voltage and an increased input power. If, however, the vapor pressure is kept fixed (by maintaining the liquid-vapor interface temperature by some external means), an increase in current has little effect on lamp voltage. This is a consequence of the small (positive) slope of the arc voltage-current characteristic. Thus, high input power is associated with high pressure and concomitantly high voltage gradient.

The previous discussion implies a direct relation between vapor pressure and voltage gradient. Theoretical considerations suggest this result also.[16] A series of experiments was made with a lamp instrumented with a thermocouple situated so as to measure the cesium liquid-vapor interface temperature at various lamp voltages. Using the vapor pressure curve of Figure 32, a correspondence between vapor pressure and voltage gradient was achieved. The result is shown plotted on Figure 34.

The approximately linear relation seen on the logarithmic plot implies a relation of the form

$$E = k P^m \tag{38}$$

where E is the voltage gradient (volt/cm) and P is the pressure in torr. From Figure 34, m and k are found to have approximate values of 0.4 and 2, respectively.

4. Spectral Distribution and Total Radiation

The total radiation from the lamp was measured by means of a thermocouple detector. The dc signal from the detector is chopped, amplified and then rectified to give a dc signal in the 1 to 10-mv range. The detector contains a CsI window which passes radiation in the band from 0.5 to 30 - 40 μ. The detector system is calibrated using a globar source.

The physical arrangement obscures all but a one-centimeter section of the lamp by using a slit. The detector is typically 20 to 30 inches away from the lamp. Assuming a Lambertian radiator, as discussed previously, and measuring the radiation intensity at the detector, the radiated power per unit length of the lamp can be calculated. This measurement can be checked by subtracting the power loss from the envelope by free convection (equation (35) from the input power. This result is generally 10 to 15 percent higher than is inferred from the direct radiation measurement. This difference may be accounted for partially by end effects and by a combination of effects due to volume radiation from the plasma column and the non-zero in-line transmission of the Lucalox envelope.

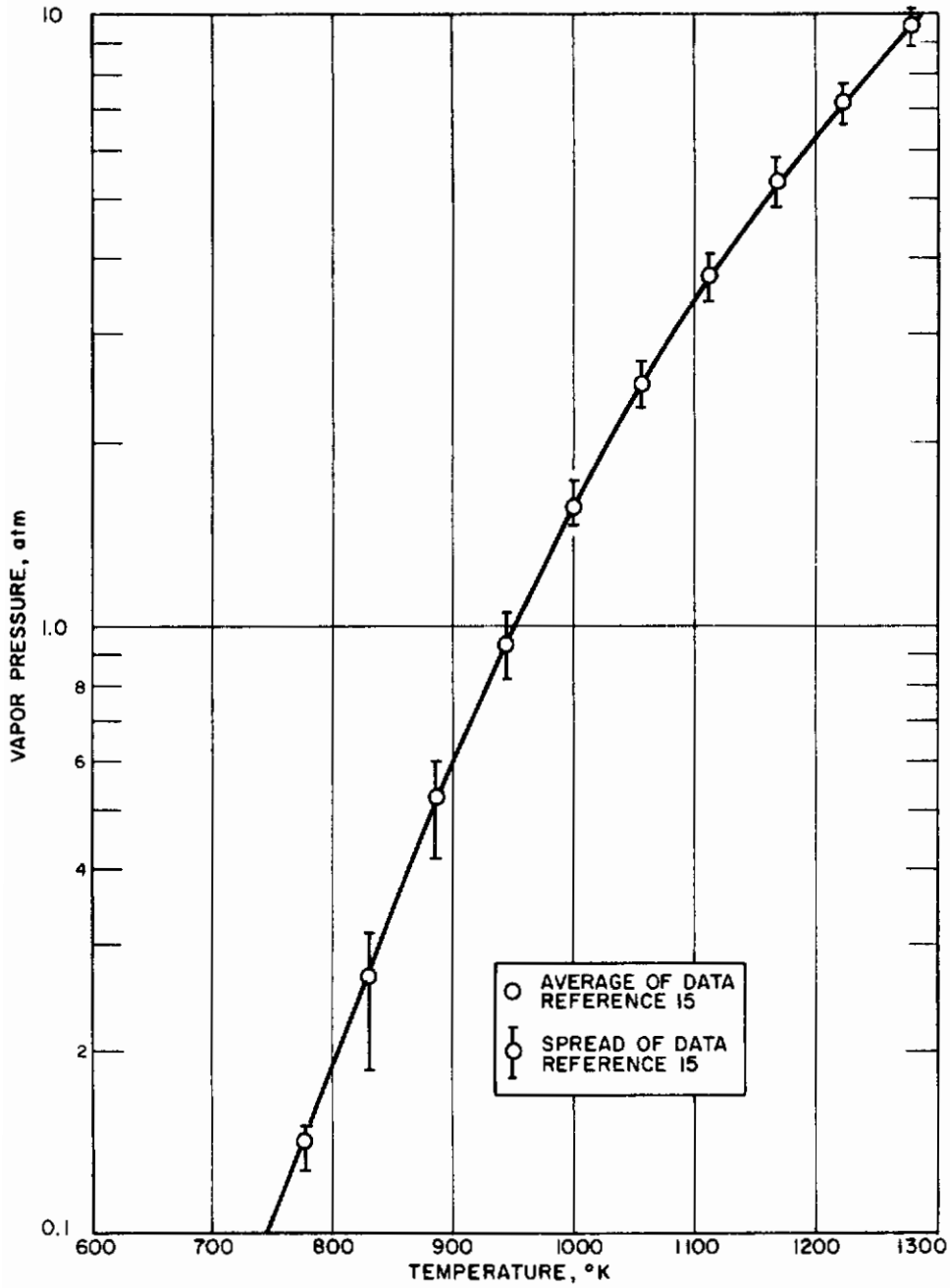

Figure 32 VAPOR PRESSURE VERSUS TEMPERATURE FOR CESIUM

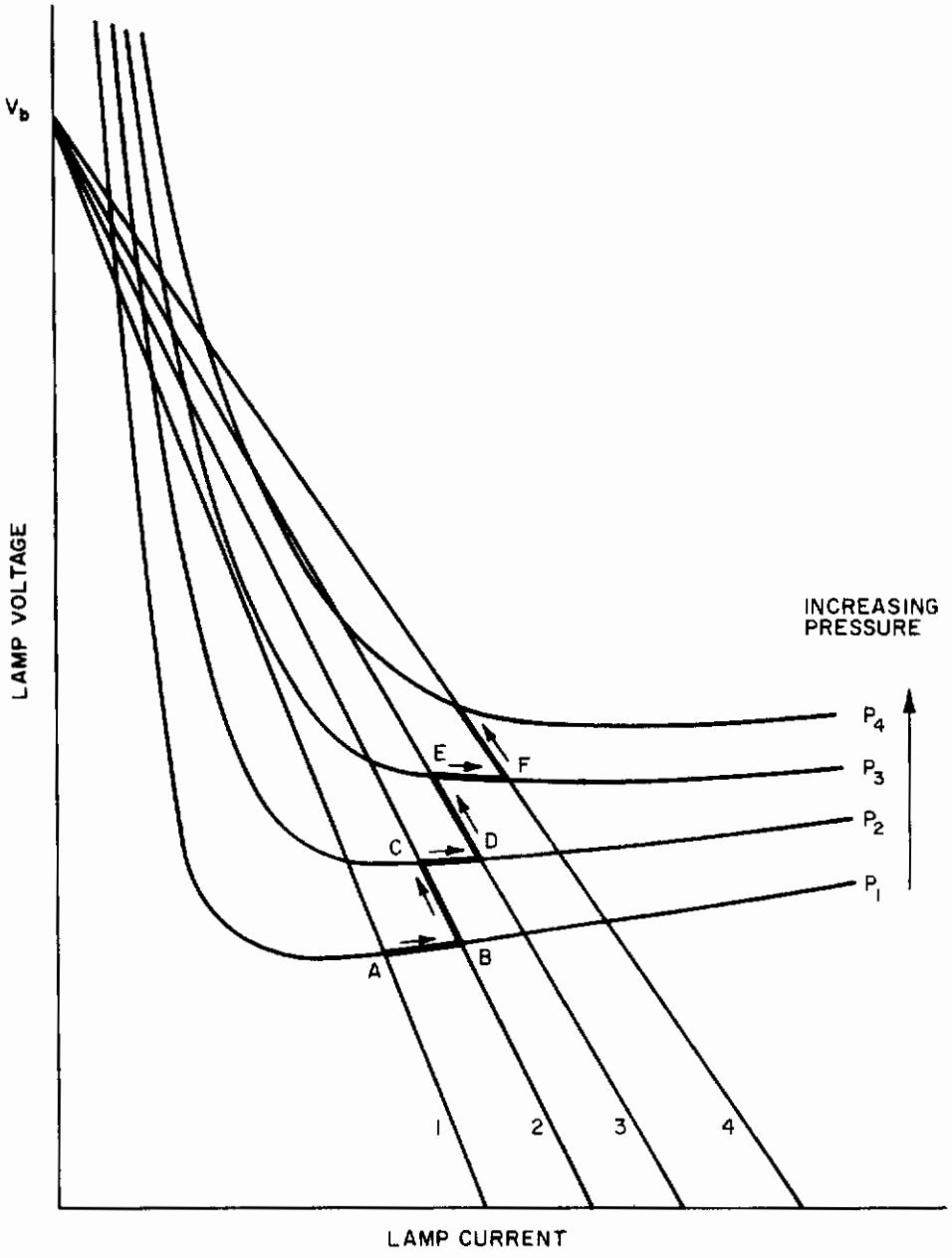

Figure 33 INTERSECTING VOLTAGE-CURRENT CHARACTERISTICS AND RESISTANCE LINES

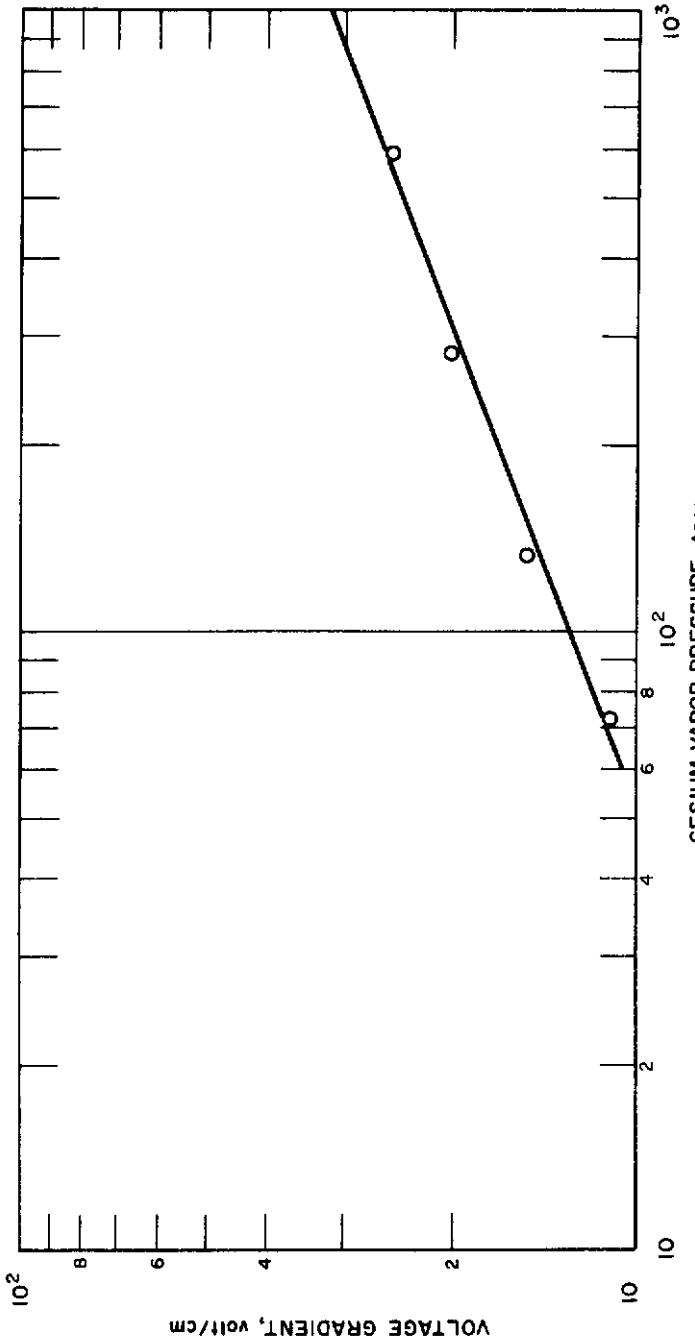

Figure 34 RELATION BETWEEN VOLTAGE GRADIENT AND VAPOR PRESSURE FOR CESIUM VAPOR LAMP

Since the pressure, which has a significant effect on the voltage, is not directly controllable, there is no unique voltage-current characteristic for the cesium vapor lamp as there is for lamps with conventional resistive elements. The cesium vapor lamp has been operated at voltages as high as 520 volts, which correspond to a voltage gradient of about 29 volt/cm. From Figures 32 and 34, this corresponds to a vapor pressure of about one atm and a cesium liquid-vapor interface temperature of 950° K. The highest input power has been 280 watt/cm, achieved at 10.7 amperes and 475 volts.

Of the total radiation emitted by the plasma-envelope system, a portion is due to the plasma and the rest is due to emission by the hot Lucalox. One can distinguish between the two by running a "shut-down" experiment. This consists of turning the lamp off while the radiation detector is being monitored on a continuous strip recorder. The plasma extinguishes very quickly so that the remaining signal is the radiation due to the Lucalox envelope. By employing this method, one will find that at a low voltage gradient (low vapor pressure) the Lucalox contributes as much as 50 percent of the total radiation. At low plasma pressures, the plasma column radiating efficiency, η, is low. There is a significant amount of heat conducted to the envelope which is finally lost to the outside by radiation. However, at high power, i.e., high voltage gradient, the Lucalox contributes only 20 to 25 percent of the radiated power.

An investigation of the spectral distribution of the radiation output of the cesium vapor lamp (cesium plasma plus Lucalox envelope) has been carried out using broad-band infrared filters which cover the range 0.5 to 5.5 μ in six steps. All filters are blocked outside of their range of transmission. The transmission curves have sharply rising edges with a slightly oscillatory top. The bandpass is taken to be the width of the transmission curve at 50 percent of peak transmission. The average transmission, $\bar{\tau}$, is determined so that the area of the rectangle of width equal to the bandpass and height $\bar{\tau}$ has the same area as that under the transmission curve. In general, the use of such filters gives reliable results if the spectral radiation is roughly constant over the bandpass, especially near the edges of the bandpass. At low pressure, the spectrum of cesium shows strong lines near 0.8, 1.2 and 4.5 μ. However, at higher pressures (~1 atm), a strong continuum makes the spectrum more uniform.

The spectral measurements were obtained with an input power in the range 52-185 watt/cm. The lamp voltage varied from 200 to 515 volts. The results are shown in Figure 35. The radiation within the six bandpasses ranges from 82 percent (at the lowest voltage gradient) to 89 percent (at the highest voltage gradient) of the total radiated power. As the voltage gradient, and hence vapor pressure, increases, one will see that the radiation in the 0.8 to 1.2 μ region decreases rapidly while the radiation in the 1.2 to 4.5 μ range increases. At large voltage gradients, about 85 percent of the radiated power is in the bandpass 1-4 μ.

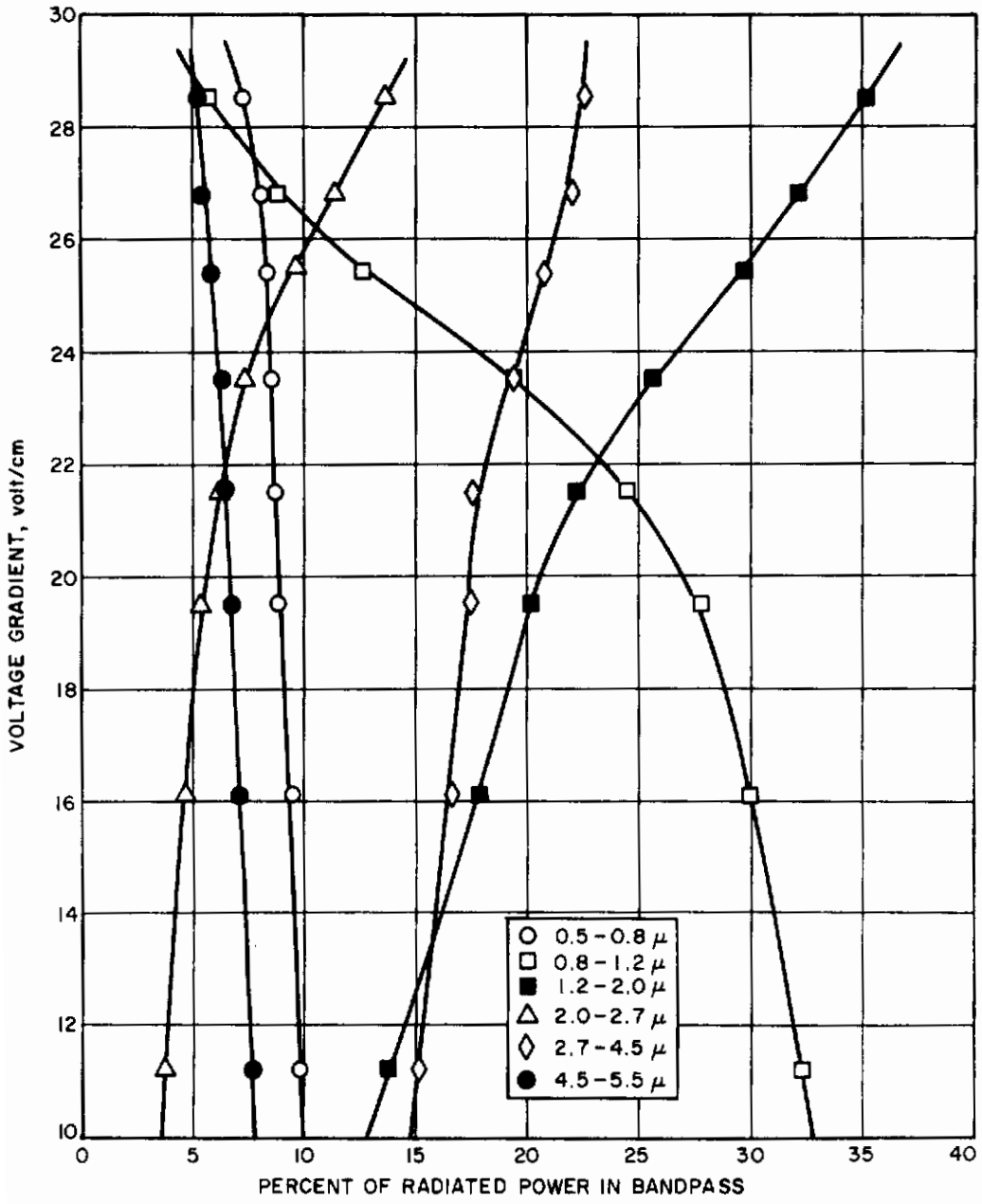

Figure 35 SPECTRAL DISTRIBUTION OF RADIATION FROM CESIUM VAPOR LAMP AS A FUNCTION OF VOLTAGE GRADIENT

F. ALTERNATING CURRENT OPERATION AND PERFORMANCE

1. Power Supply and Starting Procedure

The ac operation of the lamp was accomplished by using a 440-volt (rms) single-phase power source. The circuit diagram is shown in Figure 36. Note that provision is made to include some inductance in series with the lamp. The starting procedure is essentially the same as for dc operation except for the inclusion of the switch that is used to disconnect the protective capacitor once the lamp is started.

2. Operational Characteristics with Series Resistance

The operational characteristics of the cesium vapor lamp are considered first when the principal current limiter is the series ballast resistance, i.e., the resistance in the circuit is large compared to either the inductive or capacitance impedance.

The ac operation of the lamp gives rise to certain phenomena that are not present in dc operation. These phenomena occur as a result of the change in polarity at every half-cycle. Consider the lamp to be in operation at some plasma pressure and let the dc voltage-current characteristic for the lamp be represented by the dashed line in Figure 37. Pick the time $t=0$ to correspond to a point in the cycle when the voltage across the lamp is zero. Thus, the lamp current is zero. As time increases, the voltage increases sinusoidally with time until some value is reached where the arc is reignited. This voltage, called the restrike voltage, V_r , is shown to be at a higher value for the same arc current than would be the case if the lamp were operating with a dc power supply. This is due to the deionization and cooling of the plasma that has occurred during the time interval between when the arc extinguished and when it restrikes. The lower degree of ionization means that the plasma effectively has a higher resistance, and a higher voltage is required for reignition. Once the arc reignites, the lamp follows a characteristic curve slightly above the dc characteristic. The consistently higher voltage is due to the ionization lagging behind the current. The voltage drops to some value and stays essentially constant over a wide range of lamp current. A constant voltage across the lamp means that the voltage across the ballast resistor (Figure 36) is varying sinusoidally and hence, the current in the lamp is also varying sinusoidally. Once the current starts to decrease, the lamp voltage-current characteristic starts to fall slightly below the dc characteristic because the ionization, still lagging behind the current, is greater than is required, and the same current flows at a lower voltage gradient. Finally, the arc extinguishes because as the current becomes small, a high voltage is required to maintain the discharge. The above description is appropriate for a low-frequency ac source. A more thorough discussion is to be found in Ref. 17.

Figure 38 shows the general voltage and current traces that result. One will note that twice during each cycle there is a time interval during which the lamp is extinguished and the current is essentially zero. The eye does not perceive this discontinuity in light output.

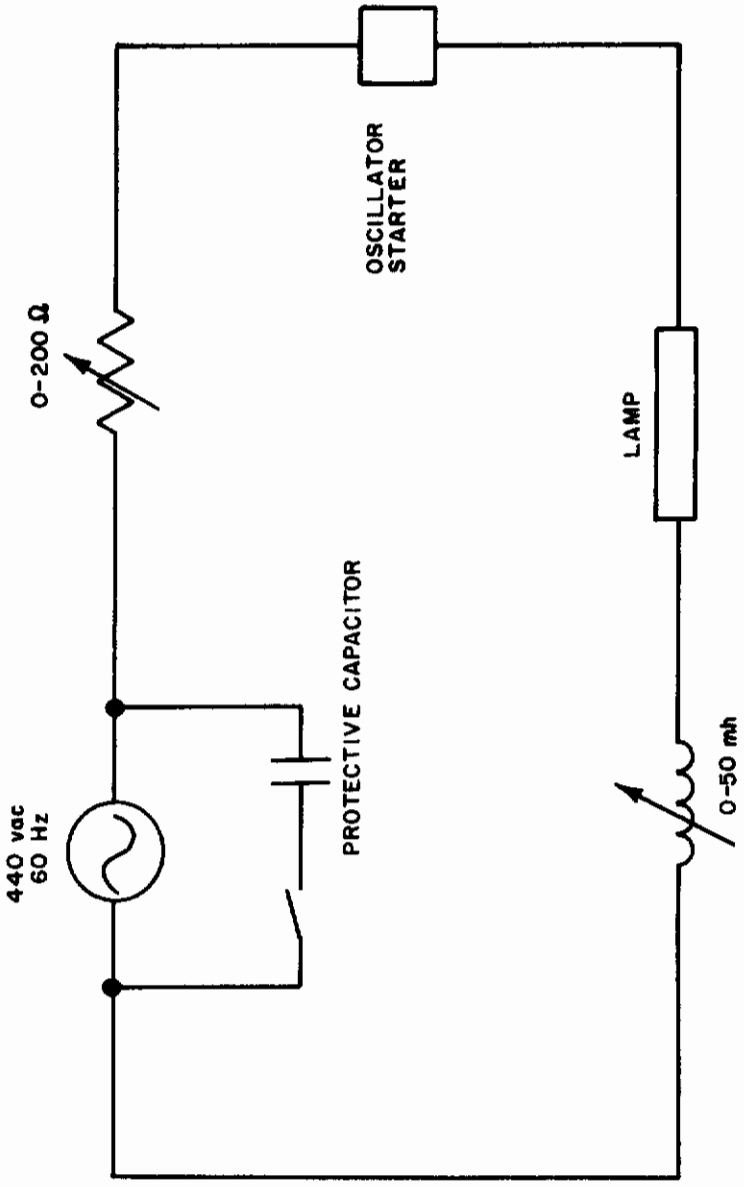

Figure 36 CIRCUIT FOR AC OPERATION OF CESIUM VAPOR LAMP

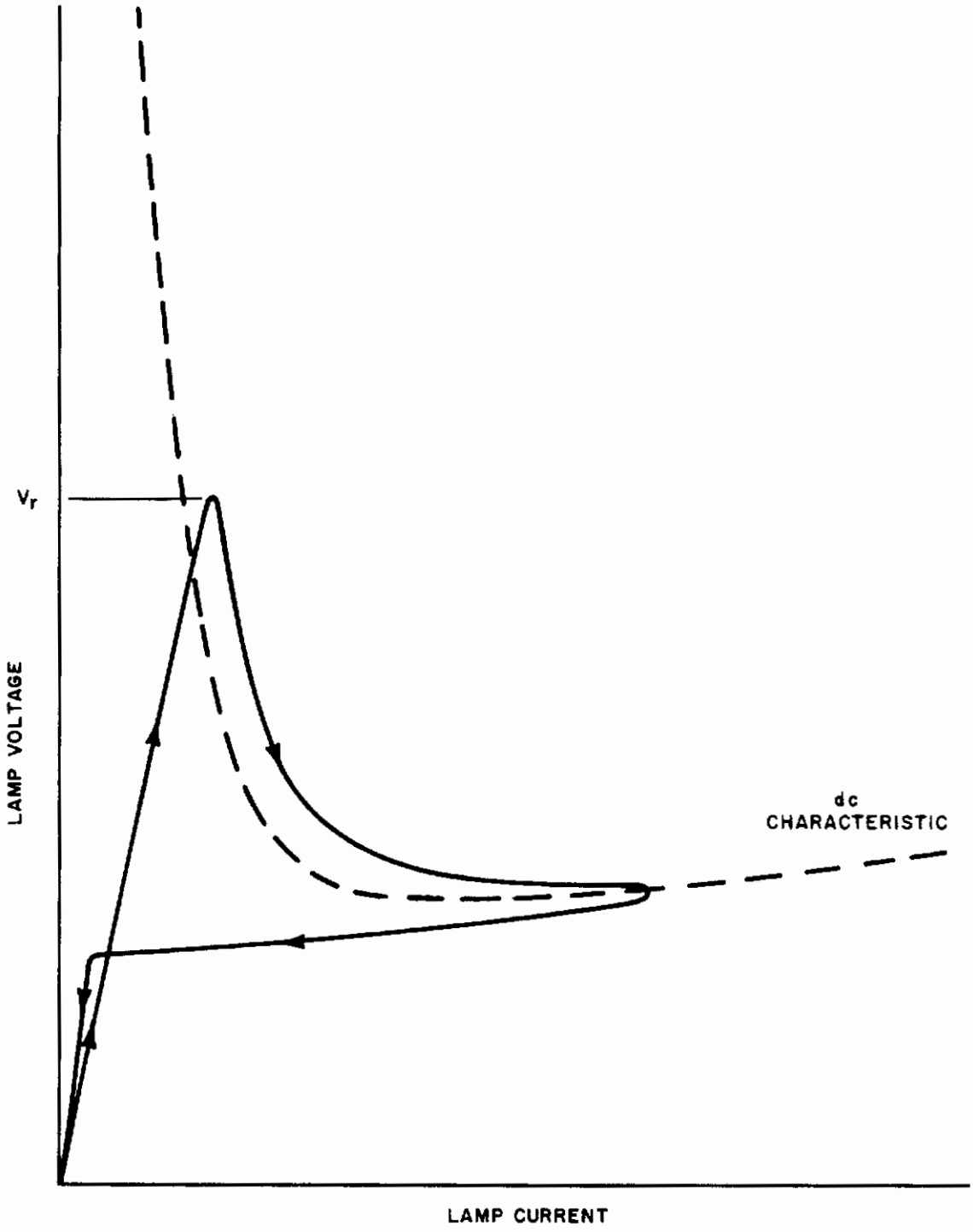

Figure 37 LOW FREQUENCY AC VOLTAGE-CURRENT CHARACTERISTIC FOR A HALF-CYCLE

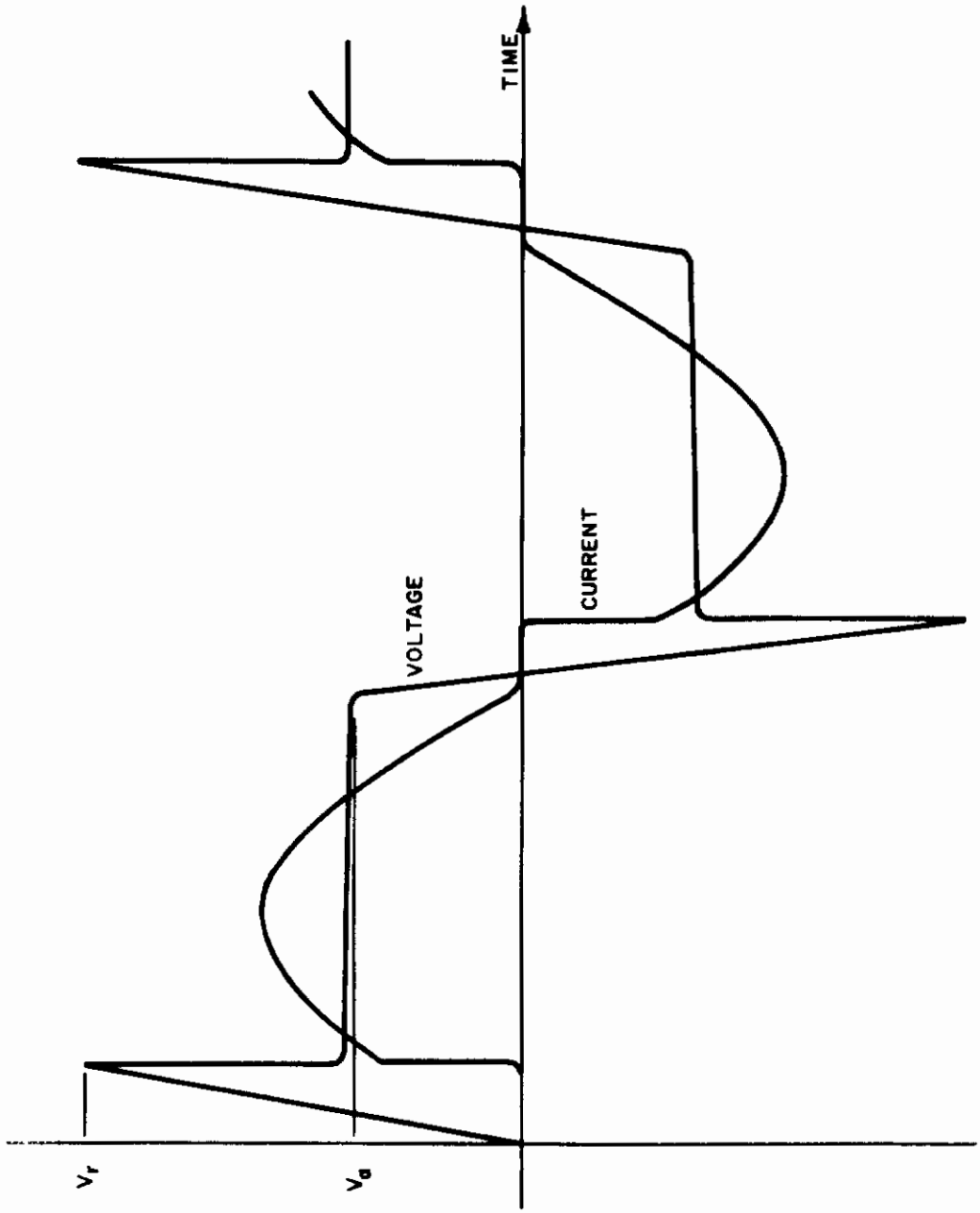

Figure 38 TYPICAL VOLTAGE AND CURRENT TRACES FOR AC OPERATION OF CESIUM LAMP

The restrike voltage required depends on how fast the deionization processes have occurred in the plasma during the time the arc has been extinguished. The greater the vapor pressure, the greater the collision rate of ions and electrons with molecules and atoms and hence, the greater the rate of deionization once the lamp is extinguished. Thus, the restrike voltage increases with vapor pressure. There is also a tendency for the restrike voltage to decrease with current for a given vapor pressure because more plasma has a higher degree of ionization.[17]

Thus, as the input power to the lamp is increased, by decreasing the ballast resistor, the cesium liquid-vapor interface temperature increases, the vapor pressure increases, the restrike voltage increases to the point where it is greater than the peak supply voltage, and the lamp goes out.

Experiments with the cesium lamp, where no attempt is made to control the cesium liquid-vapor interface temperature, indicate that once the rms voltage reaches 140 volts ($I_{rms} \sim 5$ to 6 amperes), a further increase in current leads to an unstable performance, resulting in extinction of the lamp. When the rms voltage is 140 volts, the restrike voltage is about 460 volts. This corresponds to a ratio V_r/V_{rms} slightly greater than 3.

Figure 39 contains oscillograms taken when a cesium lamp is in operation in the circuit of Figure 36 with no inductance. Figure 39a is a voltage-current characteristic. (See Figure 37.) Figure 39b shows a voltage and current trace for an operation point of $V_{rms} = 88$ volts and $I_{rms} = 4.55$ amperes. (See Figure 38.) The restrike voltage is 270 volts and $V_r/V_{rms} = 3.1$. The current is essentially zero for about 1.5 msec or about 20 percent of the time. The input power is about 260 watts. Figure 39c is an oscillogram obtained just before the lamp extinguished. V_r is $\sim$600 volts and the current is zero almost 50 percent of the time. (In this oscillogram, the current and voltage are shown 180 deg out of phase for ease of viewing).

3. Operational Characteristics with Series Resistance and Inductance

The previous results were for a circuit where the current is limited by a ballast resistor. If in addition, an inductance is placed in series with the lamp, a marked improvement is made. This improvement is associated with the voltage across the lamp electrodes after the arc is extinguished, called the recovery voltage, and is determined by the external circuitry. Thus, in an inductive circuit, when the current drops to zero, the inductor becomes a significant voltage source and causes the voltage across the electrodes to rise rapidly with time. Hence, the deionization process in the plasma has little time to proceed before the recovery voltage is high enough to cause reignition. Thus, an inductive element in the circuit has the effect of lowering the restrike voltage.

Figure 40a is a voltage and current trace of a cesium lamp operating with a 50-mh inductor in series with the lamp. The operation point is $V_{rms} = 95$ volts and $I_{rms} = 6.6$ amperes. The recovery voltage V_r is 170 volts so that V_r/V_{rms} is about 1.8 rather than the factor of three without the inductor. Figure 40b is an oscillogram for an operation point unobtainable without inductance: $V_{rms} = 198$ volts and $I_{rms} = 8.25$ amperes. The recovery voltage

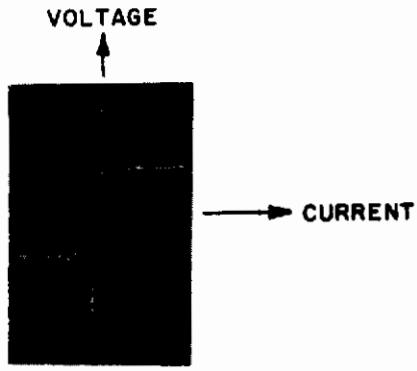

a VOLTAGE-CURRENT CHARACTERISTIC

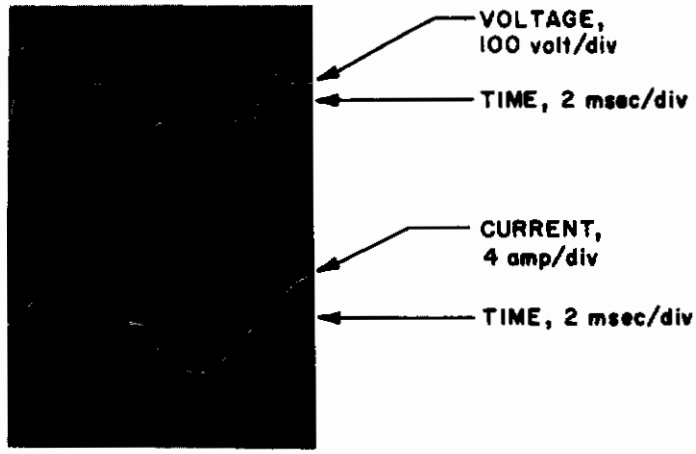

b TRACES WITH V_{rms} = 88 VOLTS AND I_{rms} = 4.55 AMPERES

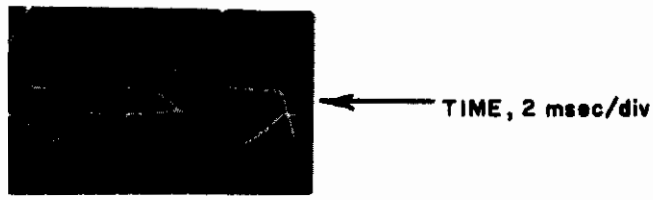

c TRACES PRIOR TO EXTINCTION

Figure 39 VOLTAGE AND CURRENT TRACES FOR AC OPERATION OF CESIUM VAPOR LAMP WITHOUT INDICATOR

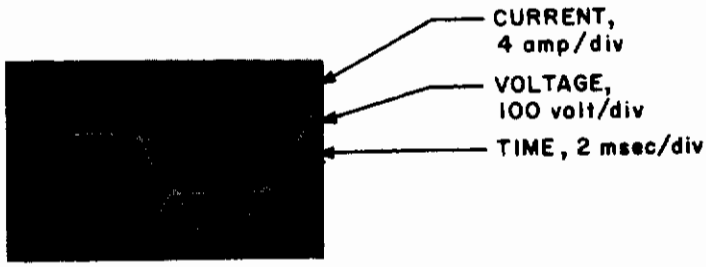

a TRACES WITH V_{rms} = 95 VOLTS AND I_{rms} = 6.6 AMPERES

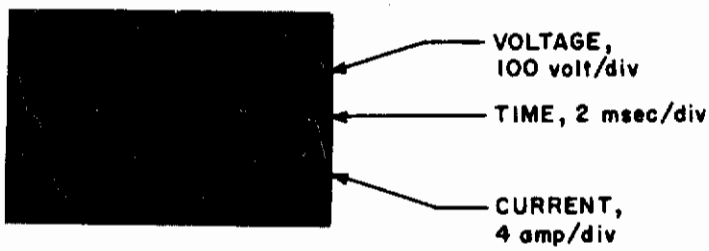

b TRACES WITH V_{rms} = 198 VOLTS AND I_{rms} = 8.25 AMPERES

Figure 40 VOLTAGE AND CURRENT TRACES FOR AC OPERATION OF CESIUM VAPOR LAMP WITH 50-mh INDUCTOR

is 340 volts. The constant voltage part of the voltage trace has a value of about 150 volts. The input power is 1600 watts. With the 50-mh inductor, the lamp can be run at an input power of around 2000 watts or 110 watts per centimeter length of tube ($V_{rms} \sim 200$-210 volts, $V_a \sim 180$ volts $I_{rms} \sim 8.9$ amperes) before the restrike voltage gets too high. The spectral distribution of the radiation output is the same as that found for the dc mode of operation when V_a , the constant voltage portion of the voltage trace, is used to compute the voltage gradient.

4. High Power Operation with Ac Power Supply

The previous sections indicate that to operate the cesium vapor lamp at high power with an ac single-phase supply, a high peak voltage, the use of series inductance or a combination of both is necessary.

There is also another method of restricting the restrike voltage. This involves putting in a reduced amount of cesium, so that at some specified plasma pressure, there is no more liquid cesium. At this point, the vapor pressure is no longer determined by the temperature at the cesium liquid-vapor interface. This means that the power to the lamp can be increased (by increasing the lamp current) while the pressure, and hence the restrike voltage, will increase only slightly.

As indicated previously, the radiating efficiency of the arc column initially increases with pressure. Experiments with the cesium vapor arc discharge suggest that when the voltage gradient reaches 20 to 25 volt/cm, no substantial further increase in radiating efficiency results with a further increase in voltage gradient.

The single-phase power available at AFFDL is 580 volts (rms), which corresponds to a peak voltage of 820 volts. Suppose that the restrike voltage is to be limited to 750 volts, and the lamp contains an amount of cesium such that the liquid phase has vanished for a lamp voltage, V_a , of 400 volts which corresponds to a voltage gradient of 22 volts/cm. Thus, a ratio of $V_r/V_a = \frac{750}{400} = 1.87$ is required. Experiments with a 50-mh inductor showed that $V_r/V_{rms} \sim 1.8$ and $V_{rms}/V_a \sim 1.1$ so that $V_r/V_a \sim 2$. Thus an inductance slightly larger than 50-mh is required and, for example, an imput power of 300 watt/cm and an off-current time of 20 percent requires an rms current of 16 amperes. See Appendix B for the rms current and voltage, and average power in terms of the current and voltage waveforms.

G. FACTORS LIMITING RADIATION OUTPUT

1. Introduction

In previous sections, analyses were presented to show that with suitable forced convective cooling, the cesium vapor lamp with a 1/2-inch o.d. Lucalox tube can be operated at an input power in excess of 1000 watts per centimeter length of tube providing the factors affecting power input are limited to thermal stress and tube temperature. Yet, the highest input power actually achieved with a cesium vapor-Lucalox lamp for any length of

time (approximately half an hour) was 280 watt/cm. In this section, other features of the lamp which limited the input power and hence, the radiation output, are discussed.

2. Plating and Brazes

The two factors which have limited the input power to the cesium vapor-Lucalox lamp have been associated with either the plating (prevents oxidation) or the brazes. The failure mechanisms consist of either a continuing oxidation of the tantalum until a slight hole is created or the deterioration of a braze joint. Either permits air to enter and eventually destroys the lamp. The oxidation occurs most frequently at the braze joint between the electrodes and the endcap and in the vicinity of the joint between the Lucalox and the endcap. (See Figure 25.) The latter oxidation seems to be due to a failure of the plating to adhere to the edge of the endcap. The oxidation at the electrode-endcap joint appears to be due to a lack of adherence of the plating to the nitinol braze material. In the latter stages of the program, an attempt was made to eliminate this problem by replacing the nitinol braze with an electron beam weld. In addition to eliminating the plating problem, a substantially higher temperature joint was obtained. Also, the possibility that the cesium was attacking the braze was eliminated. Although the technique was not completely evaluated, the initial results appeared promising.

The other area susceptible to failure is in the vicinity of the braze joint between the Lucalox and the tantalum endcap. This region is vulnerable in three ways. First, oxidation is always evident after extended operation at high input power levels. This appears to be due to a lack of adherence of the plating to the very edge of the tantalum endcap. This may be due to the associated high curvature to be found at the edge. Second, the braze temperature is lower, having a melting temperature of approximately 1150° C. Finally, there has been some evidence that the Ti-Ni-Ti braze is attacked by cesium.

The plating and braze problems present the most immediate barriers to an increased input power. Though the solution to these problems is not at hand, they certainly are not insurmountable. One partial solution follows from the success of the electron beam weld; the higher melting point (1300° C) nitinol braze can be used for the tantalum-Lucalox joint. This braze is now in the process of being evaluated, particularly with regard to attack by cesium. Other possibilities to be explored include 1) the use of a ceramic coating to prevent oxidation of the tantalum components, and 2) the use of a ceramic braze instead of a metallic braze.

3. Envelope Material

The pertinent physical properties of Lucalox are stability in the presence of the alkali metals, radiation transmission, modulus of rupture, coefficient of thermal expansion and melting point. Its stability in the presence of high temperature cesium vapor is satisfactory. Apparently, no other transmitting material is available. The thermal stress analysis showed that its tensile strength is adequate. The melting point of Lucalox is slightly in excess of 2000° C, which in view of other limitations is also satisfactory.

The coefficient of thermal expansion leads to the specification of the end-cap material. Tantalum provides a good match, but presents the problem of oxidation. A nickel steel could be used, but its melting point is lower, and some problem might occur with the nickel-titanium brazes.

The total transmission of Lucalox is adequate out to 5 to 6μ, if the thickness is not too great. For some applications, the lack of transparency, as indicated by the low in-line transmission, could be a serious disadvantage. If Lucalox were a perfect scatterer, the brightness of the arc column would be reduced by the ratio of the outer diameter of the tube to the diameter of the arc column, a factor of 4 to 5 for cesium vapor in a 1/2-inch tube. Scattering causes the radiation to appear to originate from the envelope and not from the arc column. For applications where many lamps can be used, the important consideration is that of total transmission. However, scattering does adversely affect the total transmission by increasing the optical path and hence, the absorption.

Recently, the General Electric Company has developed a ceramic material called Yttralox. It offers a marked improvement over Lucalox in the property of transparency. Yttralox contains about 90 percent Yttrium and 10 percent thorium in solid solution. A heat treatment process removes the microscopically small pores which cause scattering and account for the opacity associated with ceramics. The in-line transmission for a 0.030-inch sample is 75 percent or better for the wavelength range 0.35 to 7μ. In addition, the absorption is very low, approximately 3 percent for a 2-mm thick sample over the visible range of the spectrum.

The slightly higher transmission and the longer wavelength cut-off gives Yttralox some advantages over Lucalox. However, its modulus of rupture (indicative of tensile stress) is three times smaller than Lucalox and, most importantly, Yttralox apparently darkens upon exposure to the alkali metals at high temperature. At the present, not enough data is available to make a quantitative assessment of this factor.

H. MULTIPLE LAMP OPERATION

Since the cesium vapor-Lucalox lamp could not be operated at power levels any higher than the tungsten-quartz lamps, the problems associated with multiple lamp operation were only incompletely examined. Two potential problem areas will be discussed now.

Since high input power to the lamp corresponds to a lamp voltage of 400 to 500 volts, multiple lamp operation is achievable only by connecting and operating the lamps in parallel. When operating the lamps in parallel, an impedance in series with each lamp must be provided. This requirement arises because each lamp has a somewhat different operating characteristic due to differences in vapor pressure. These differences can be neutralized by series resistors, for then the sum of the voltages across each lamp and its resistor may be the same as across any other pair. An identical situation arises in connection with the operation of neon pilot lights, and the solution to this is also the addition of a series resistor.

When operating with a dc power supply, the impedance would be a resistor, while an inductor could be appropriate with an ac supply. A fixed impedance is desirable; its value is determined by the characteristics of the lamp and the power supply and must be such that the impedance is large enough to limit the startup current while still small enough not to become the principal power dissipator during high current operation.

Operating the cesium vapor lamp at a startup current in excess of 4 to 5 amperes has not been found desirable. During startup, the vapor pressure is low, and excessive currents lead to high heat loads to the electrodes. For dc operation, if the power supply voltage can be regulated to as low as 60 volts, a series resistor of 10 ohms is sufficient to limit the current to below 4 amperes. (See Figure 27.) At a current of 10 amperes or greater, however, a large amount of power (~15 percent of the total power) is dissipated by this resistor.

An attractive feature of ac operation is that inductors, which do not dissipate power, may be utilized to provide the series impedance. In addition, investigation has shown that an inductor decreases the restrike voltage. The value of the inductor that should be used with the cesium vapor lamp operating on the power supply at AFFDL is difficult to predict, because the power supply voltage determination is accomplished by controlling the firing angle on the ignitrons in the current control circuit. Thus, a low rms voltage is accomplished by producing a voltage waveform that is far from sinusoidal.

Some effort was expended in devising circuitry which would permit the use of a single starter for several lamps. A problem situation would otherwise arise if the starter is not isolated from lamps that are already lit. Since the lamps already started have a much lower impedance, the starter current would be shunted away from the unlighted lamps and prevent starting.

One circuit that was studied employed relays to isolate the lamps after starting. The experimental circuit used a dc power supply and is represented in Figure 41. For simplicity, only two lamps are considered. The coil of the relay is connected across the series resistor. Initially, neither lamp is lit. The starter is activated, one of the lamps is ignited and a current of 3 to 4 amperes flows through it. This current is large enough to activate the relay and switch the operating lamp out of the starter circuit. (The switching requires a make-before-break type of relay.) The feasibility of this switching procedure has been demonstrated in the laboratory. Figure 41 shows one lamp in operation and isolated from the starter, while the subsequent lamps are started in a like manner.

In order for the operating lamps to be truly isolated from the starter, the relay gap must be capable of holding off the high starter voltage. A hermetically sealed relay with, for example, air at low pressure can be made to have a higher breakdown voltage than the cesium vapor lamp, and serve the purpose.

On the basis of the few laboratory experiences with multiple-lamp operation, no insurmountable problems are anticipated.

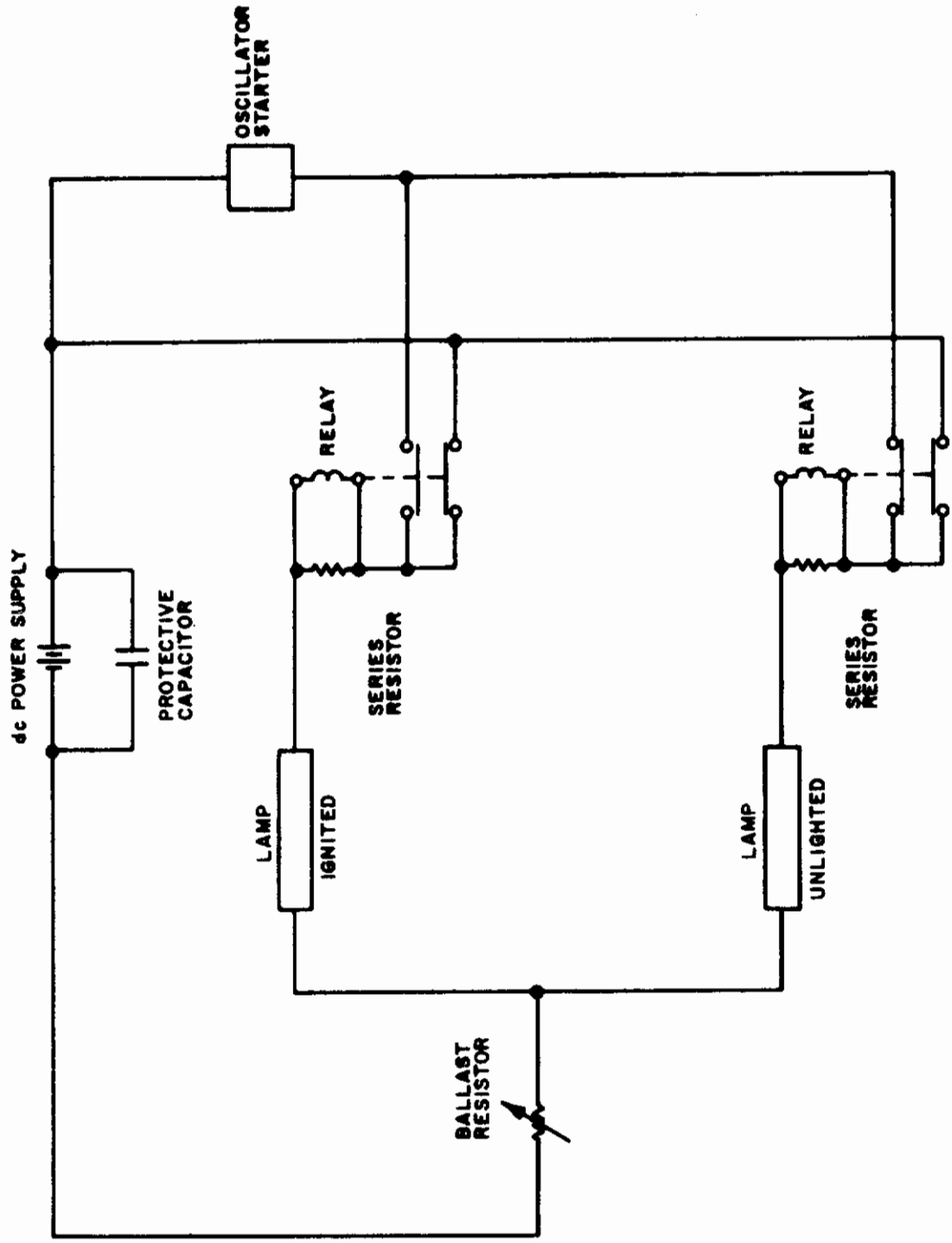

Figure 41 CIRCUIT FOR IGNITING SEVERAL LAMPS WITH A SINGLE STARTER

IV. GRAPHITE ROD HEATER

A. INTRODUCTION AND PRELIMINARY RESULTS

Compared to the tungsten filament heater, another radiant heat source that offers the potential of a higher heat flux is one that uses carbon or graphite as the radiating element. As previously discussed, the increased heat flux is due to the factor of 2.5 to 3 increase in emittance of carbon over that of tungsten. Thus if carbon can be operated at the same temperature (~3000° K), then an increase in radiated power over a comparable tungsten filament of at least a factor of two can be realized.

Well known is the fact that prolonged operation of a carbon material at elevated temperatures in an air environment is impossible due to the accompanying rapid oxidation. Provision of an inert atmosphere does not completely solve this problem because of the high sublimation rate of carbon, a factor of 1000 greater than that of tungsten at 3000° K. Though sublimation leads to a mass loss in the radiating element, and hence, imposes a lifetime limitation, an equally important drawback is the deposition of the sublimation products on nearby colder surfaces such as quartz envelopes or reflecting surfaces. With regard to the quartz envelope, deposition of a carbon film can cause appreciable absorption of the source radiation, thereby reducing its intensity and raising the envelope temperature until failure results. For a reflecting surface, decreased reflectance is the result.

A possible solution consists of providing a flow of inert gas which would carry the sublimation products to some region where they could be harmlessly exhausted to the outside.

As a first step in evaluating the graphite heat source, a series of simple experiments was conducted to measure the sublimation of graphite. The test apparatus consists of an aluminum bell-jar that can be evacuated to a pressure of 100 μ Hg. Inside the bell-jar is a jig which provides a means of making electrical power connections to a graphite rod. The electric current, in passing through the graphite rod, heats it to a temperature which is measured by means of an optical pyrometer, which views the graphite rod through a window provided in the side of the bell-jar.

The test procedure consisted of evacuating the bell-jar to a pressure of 100 μ Hg and filling several times with argon. Finally, a pressure of 7 psig is maintained. The temperature of the rod was inferred from the pyrometer temperature after suitable corrections due to the emittance of the graphite and the presence of the quartz window.

The graphite rod used in this experiment had a diameter of 0.120 inch and a length of 2½ inches. The most important result obtained was that the rod could be operated at a temperature in excess of 2900° K for a time period of 20 minutes with a mass loss of about 5 percent. The deleterious effect of oxygen was demonstrated by evacuating the bell-jar to a pressure of 125 torr and then charging with argon to a pressure of 7 psig. At a surface temperature of 2900° K, failure occurred after 7 minutes of operation with a mass loss of 15 percent.

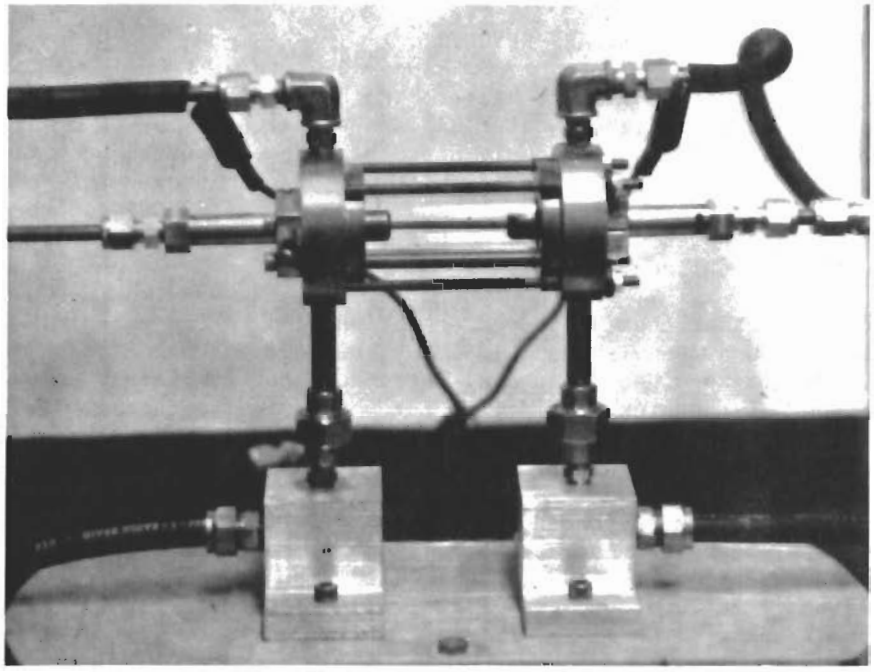

Figure 42 EXPERIMENTAL SINGLE-ROD GRAPHITE HEATER

The preliminary experiments suggested that in the presence of an inert atmosphere, mass loss due to sublimation would not impose a serious restriction on the lifetime of a graphite heat source operating at temperatures as high as 3000° K.

B. DESIGN AND PERFORMANCE OF A SINGLE GRAPHITE ROD HEAT SOURCE

1. Design Consideration

A photograph of the first design of a single graphite heat source is shown in Figure 42. The heat source consists of a graphite rod inside a quartz cylinder which is sealed by means of O-rings against water-cooled end plates. The graphite rod is held by collets contained in the ends of two brass electrodes. The electrodes are inserted through the end plates and sealed by O-rings. Argon flows through one electrode into the quartz cylinder and exhausts into the atmosphere through the other electrode. The quartz tube has an i.d. of 23 mm and a wall thickness of 1 mm.

This design was tested using a graphite rod with a diameter of 0.120 inch. The length of the rod between the collets was 2 inches. Using an argon flow of 0.27 gm/sec through the quartz tube, the test indicated that a surface temperature of 2900-2950° K could be maintained for 40 minutes. At this point, operation was terminated due to a break in the graphite rod near one of the collets. The current required to establish this temperature was in the range of 140 to 150 amperes and the voltage drop was 10 to 11 volts.

The next step in the design was to increase the length of the rod from 2 inches to 7 inches. With the increased length, two modifications were made. One modification was to provide physical support of the rod while at high temperature without seriously interfering with the argon flow. This was accomplished by a piece looking like a three-bladed propeller which fit loosely into the quartz tube. The support, sketched in Figure 43, was made from tantalum, and was 0.010 inches thick.

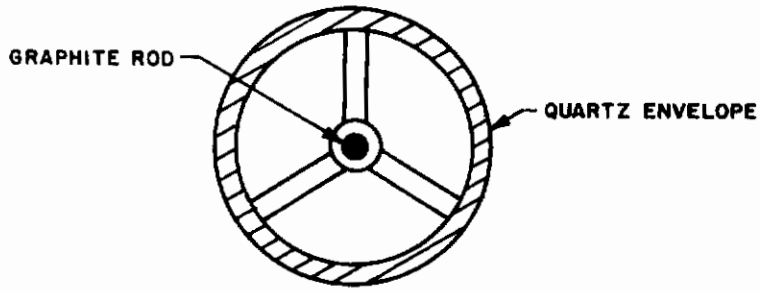

Figure 43 SKETCH OF GRAPHITE ROD HOLDER

The other modification was to provide a means by which the graphite rod could expand upon heating. At this stage in the design, this was accomplished by allowing the electrodes to slip with respect to the end plates. Such could be accomplished with a potential drop across this sliding contact of less than 10 mv even with currents of 150 amperes.

The lamp with the longer graphite rod operated quite satisfactorily. During the course of various measurements the lamp was operated for a total running time of 5 hours, 2 hours at temperatures ranging from 2300-3050° K. The tantalum supports appeared to be unaffected by this exposure though some brittleness was indicated. There was some buildup of graphite on the quartz envelope in the vicinity of the downstream electrode. Temperature measurements along the rod showed that even with water-cooled end plates, the temperature was within 5 percent of the maximum value for over 80 percent of the exposed length of the rod.

The final design modifications were the use of a smaller quartz tube, operation without water-cooling, and improvement of the rod-electrode connection. The quartz tube inner diameter was reduced to 11 mm (0.433 inch), while still maintaining a wall thickness of 1 mm. The rod support piece was increased in thickness. A single support was found to be satisfactory, at least for lengths of 8 inches.

The modifications that were needed for operation without water cooling were concerned with the graphite rod-electrode connection. Operation without water-cooling proved to be unsuccessful with the collet type of rod holder due to excessive temperatures. The collet holder was replaced with a molybdenum cylindrical sleeve into which the rod was placed with a snug fit. One electrode had provision for spring-loading to accommodate expansion upon heating. The final arrangement used provided for expansion by letting the rod slip within the sleeve. Also a conducting paint (e.g., silver) was put on the ends of the rods. This arrangement, where the contact surface between the rod and the sleeve is 5 to 10 times greater than the cross sectional area of the rod, permitted enough relative motion to accommodate expansion without introducing a harmful contact resistance, but allowed operation at rod temperatures only as high as 2700° K. If the full potential of graphite is to be realized, the electrode pieces probably must be cooled.

2. Performance Characteristics

The performance characteristics are summarized in Figures 44 and 45. Figure 44 shows the voltage gradient versus current for rods made of two different graphites and one carbon. The rod diameter was 0.120 inch in all cases. Table II lists some of the properties of these materials which were obtained from the Union Carbide Corporation. The one carbon material has a greater electrical resistivity than the two graphite materials. This is manifested clearly in the operating characteristics (Figures 44 and 45). The principal difference between the two graphites is that of cost -- the AGKS is less pure than the AGKSP and costs about one-fifth as much.

One of the drawbacks of using carbon or graphite as a heater element is that its electrical resistance is low compared to tungsten. This means that associated power supplies must be capable of supplying large currents. Some relief to this problem is indicated by the use of carbon, which has a higher resistance than that of graphite due to its disordered crystal structure. Figure 45 shows that for an element temperature of 2800° K, a current of 100 amperes is sufficient for the L113SP carbon material, while

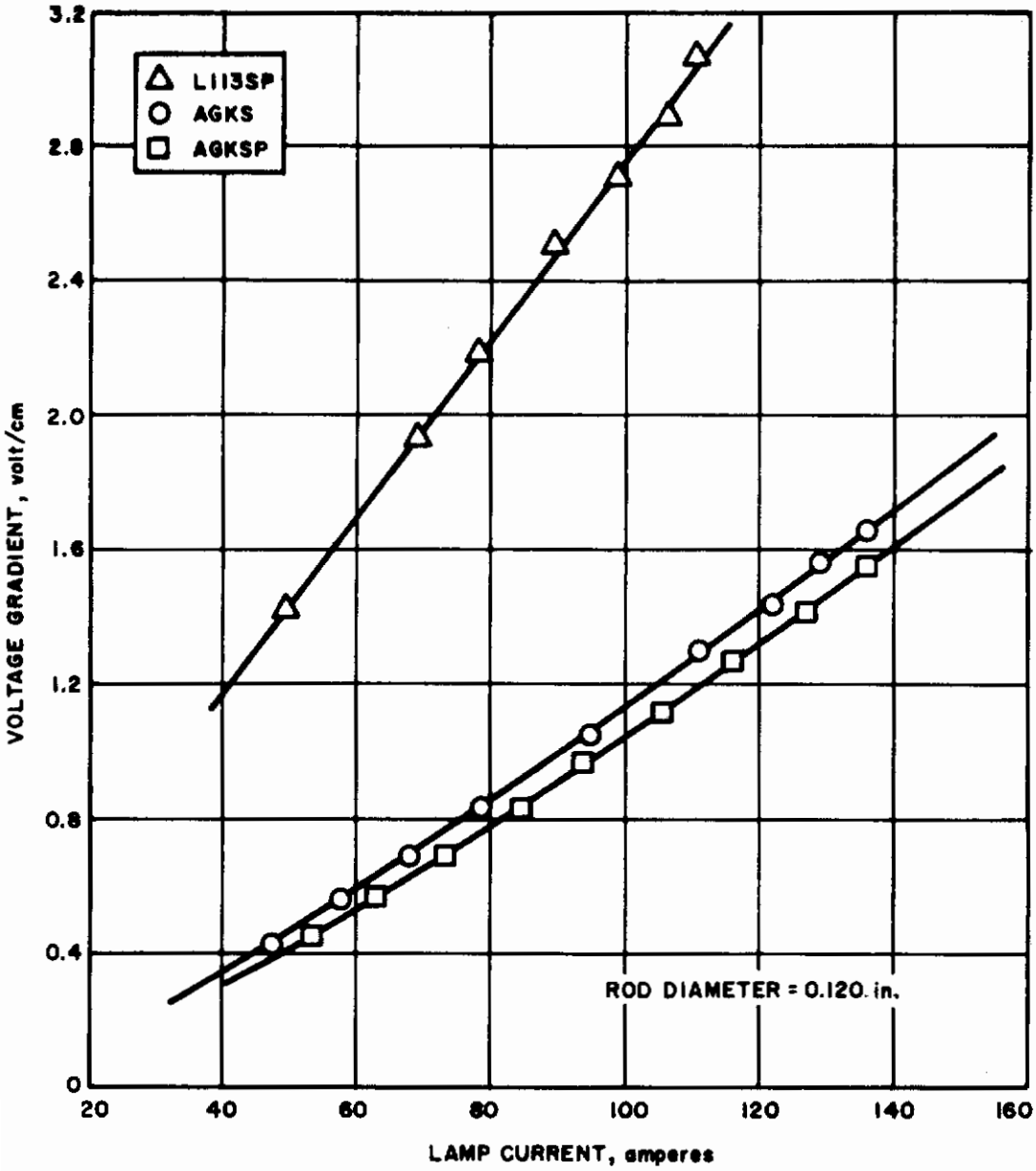

Figure 44 VOLTAGE–CURRENT CHARACTERISTICS FOR GRAPHITE AND CARBON RODS

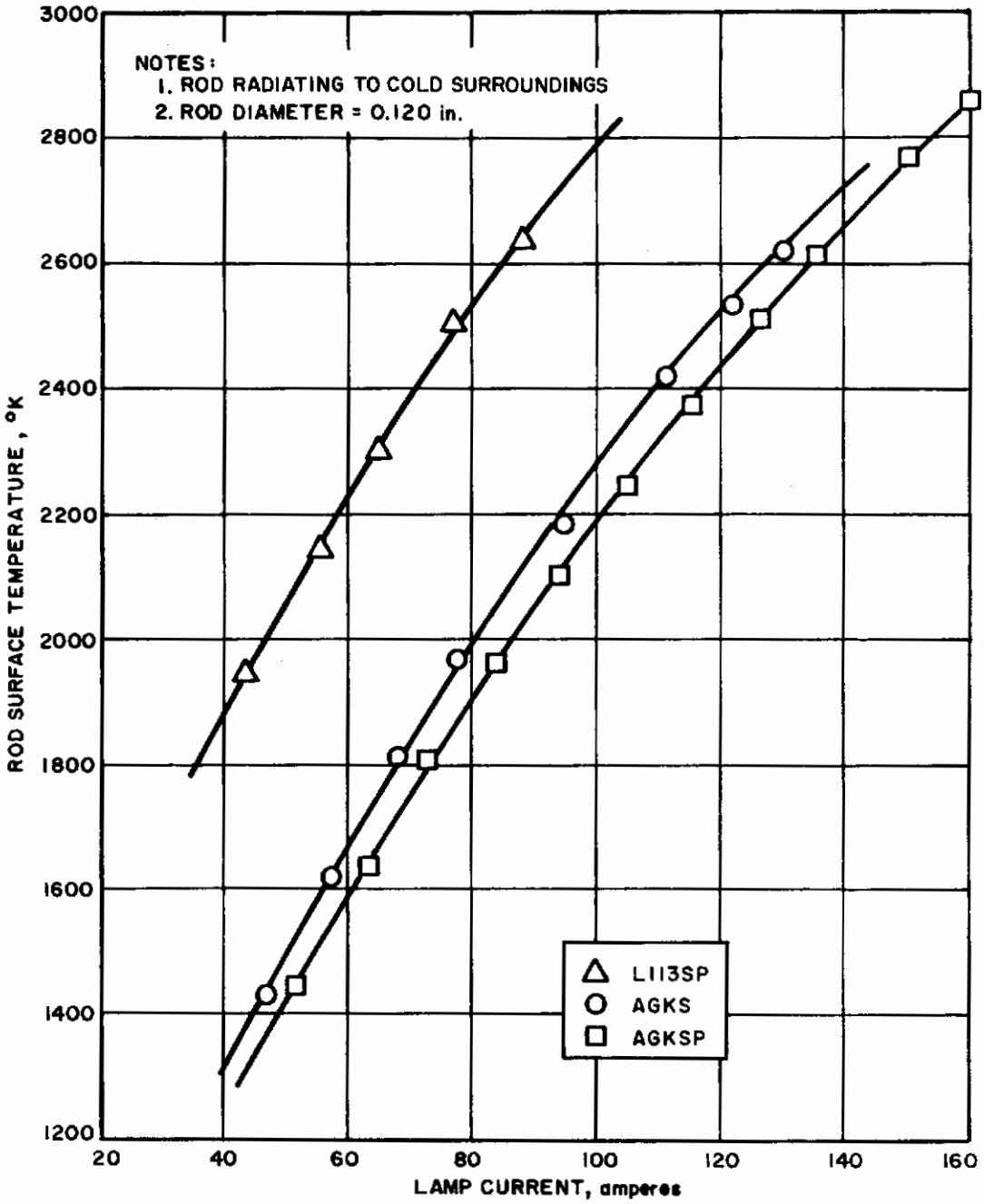

Figure 45 ROD SURFACE TEMPERATURE AS A FUNCTION OF CURRENT

150 amperes is needed for the two graphite materials. However, the L113SP carbon material seems to sublime more readily than the two graphite materials. Whether or not this is an inherent drawback to carbon is not clear.

TABLE II

SOME PHYSICAL PROPERTIES OF VARIOUS HEATER ELEMENT MATERIALS

Union Carbide Grade Designation	L113SP	AGKSP	AGKS
Type of material	Carbon	Graphite	Graphite
Bulk density (gm/cm^3)	1.45	1.61	1.60
Electrical resistivity (ohm-in)	2.0×10^{-3}	2.5×10^{-4}	2.5×10^{-4}
Coefficient of thermal expansion ($10^{-6}/^{o}C$) (1000-2000°C)	8.4	2.6	2.7
Flexural strength (lbs/in^2) (½-inch rods)	2600	3500	3500

The results in Figure 45 were obtained for a lamp with a nominal ½-inch quartz envelope. Temperature was measured by means of an optical pyrometer and then corrected for the emittance of the heater element material and the presence of the envelope. One should note that the relation between the input power (lamp current) and radiated power (rod temperature) depends upon whether or not the rod absorbs any radiation from the surrounding environment. The results shown in Figure 45 are for a lamp radiating into "cold" surroundings, although there is some reflection due to the quartz envelope. The next section will show that a rod temperature of ~ 3000° K is accomplished with a current of ~ 130 amperes. This results because of a significant amount of re-radiation to the heater element.

C. CONSTRUCTION AND EVALUATION OF A MODULAR GRAPHITE HEATER

1. Introduction

During the later stages of the program, the fact became clear that the potential of the cesium vapor arc discharge could not be immediately realized because of the materials limitations discussed above. In conference with the technical staff of AFFDL, the decision was made to devote the remaining

effort toward extending the graphite development work from the single rod graphite heater concept to the design, construction and evaluation of a modular, multi-element graphite heater. This decision was made because the graphite heater appears to offer the most immediate improvement in heat flux capability over the existing tungsten-quartz modular units.

2. Design Considerations

The main task was to incorporate the findings, from the development work on the single rod graphite heater inside a cylindrical quartz tube, into a design of a multi-rod lamp which is modular in concept. These findings are: an inert gas flow must be provided to minimize oxidation and to prevent the deposition of the sublimation products on any reflector and glass surfaces, and a satisfactory joint between the graphite rod and the metal electrode can be obtained using a slip fit. The design considerations in Section I indicate that the spacing of the rods should be as close as possible and that a reflector should be used.

The decision was made to use water-cooling since it permitted maximum radiated power from the lamp, and finally, to connect the rods in parallel. This decision resulted because of two factors: it greatly simplified the construction of the electrode assembly, and the failure of one rod is not as disrupting as in the series connection.

3. Description of Heater

The heater consists of two sections, each containing 16 rods, 0.120 inch in diameter. Within each section, the rods are connected in parallel -- the two sections are connected in series. One electrode assembly is shown in Figure 46. The end of each graphite rod is slipped into a copper sleeve, 0.6 inch long with a ¼-inch outside diameter. (See also Figure 47.) The rod and sleeve are then placed into the electrode assembly which consists of two brass bars sandwiched together to hold the rods secure. Inside the brass bars are passages for water-cooling and for gas. The holes above and below the rods are for gas injection. Figure 47 is a photograph of the lamp with the rods in place. Only one-half of the sandwich is shown.

A photograph of the electrode assembly showing the gas injection holes and copper sleeves is provided in Figure 48. The other electrode assembly is identical, except for the gas outlet slots which are shown in Figure 48. The gas exhausts through the back of the lamp.

The other two sides and the back (which serves as a reflector) are made out of brass plate, ½ inch thick. Holes are drilled to provide water-cooling passages. All of the interior surfaces were made reflective by brush-plating with silver.

Each section is a 5-3/4-inch square. The rods are 6-3/4 inches long with each rod inserted ½ inch into the copper sleeve. The sides and back are insulated by means of boron nitride strips, 1/8 inch thick. The front cover consists of a quartz plate, 6 inches square and 1/16 inch thick. The plate fits onto a shoulder and is held by a tab. No attempt is made to provide a gas-tight seal. In this design, the rods are placed 5/16 inch apart on centers. The distance between adjacent copper sleeves is 1/16 inch. The rods are placed 1 inch (along a centerline) above the back reflector, and the inside surface of the quartz plate is 7/8 inch above the rods.

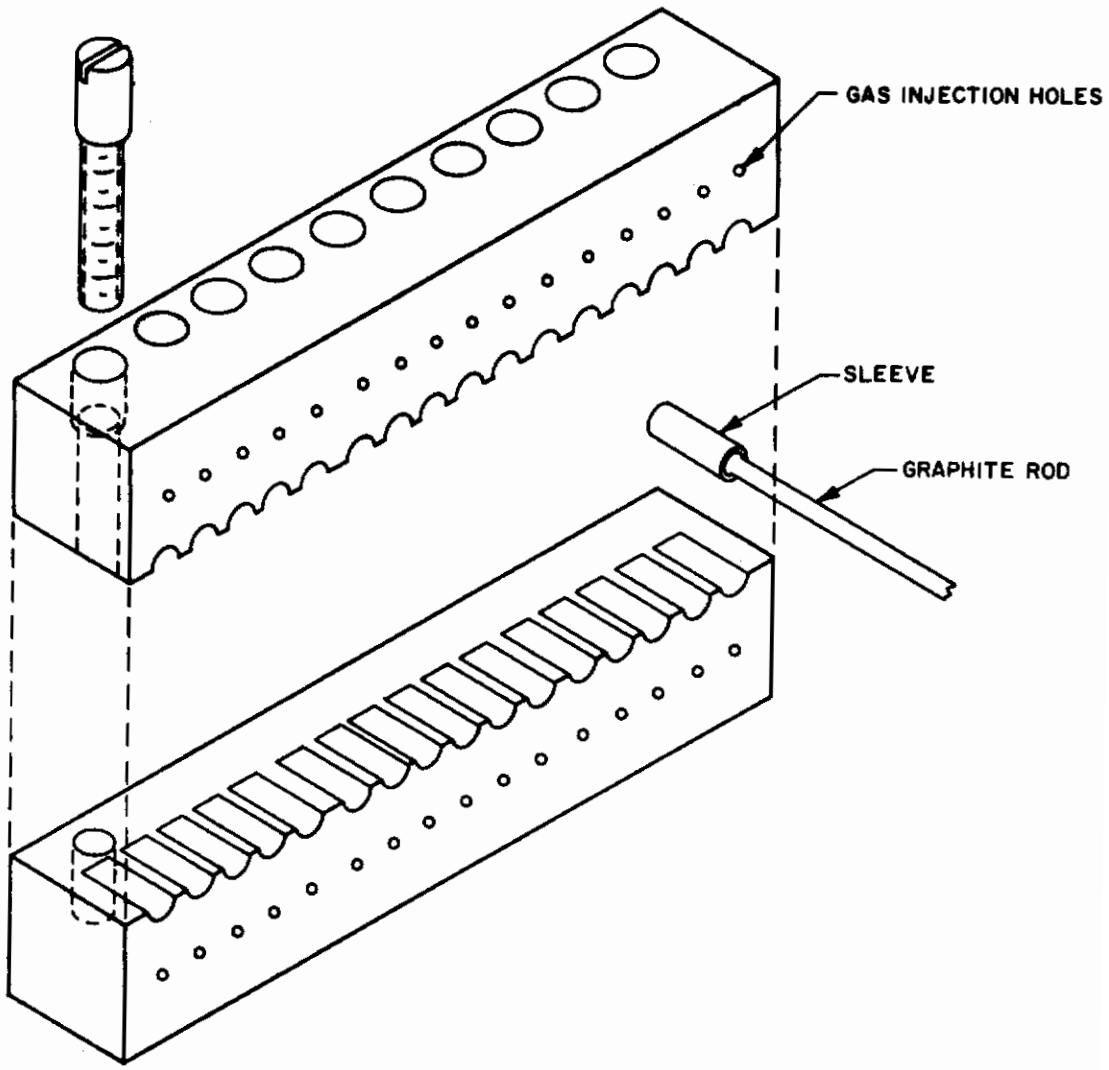

Figure 46 SKETCH SHOWING SANDWICH CONSTRUCTION OF ELECTRODE ASSEMBLY FOR MODULAR GRAPHITE HEATER

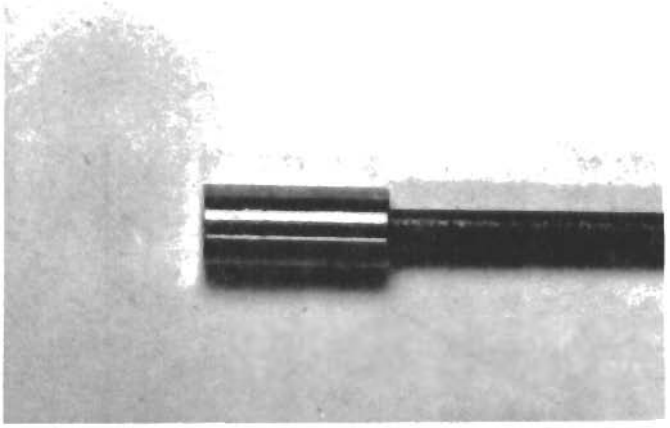

a END OF GRAPHITE ROD IN COPPER SLEEVE

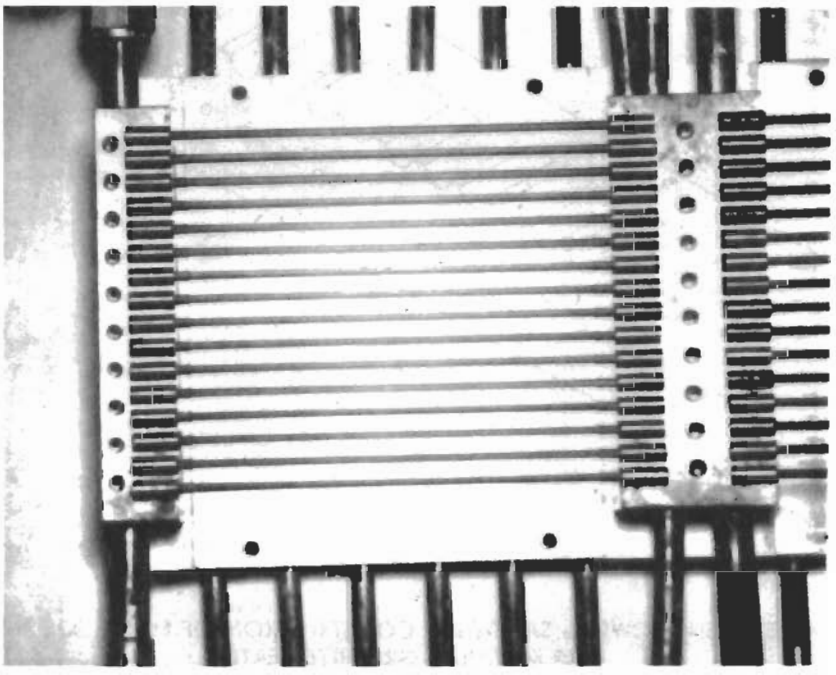

b RODS PLACED IN ELECTRODE ASSEMBLY

Figure 47 ELECTRODE ASSEMBLY FOR MODULAR GRAPHITE HEATER

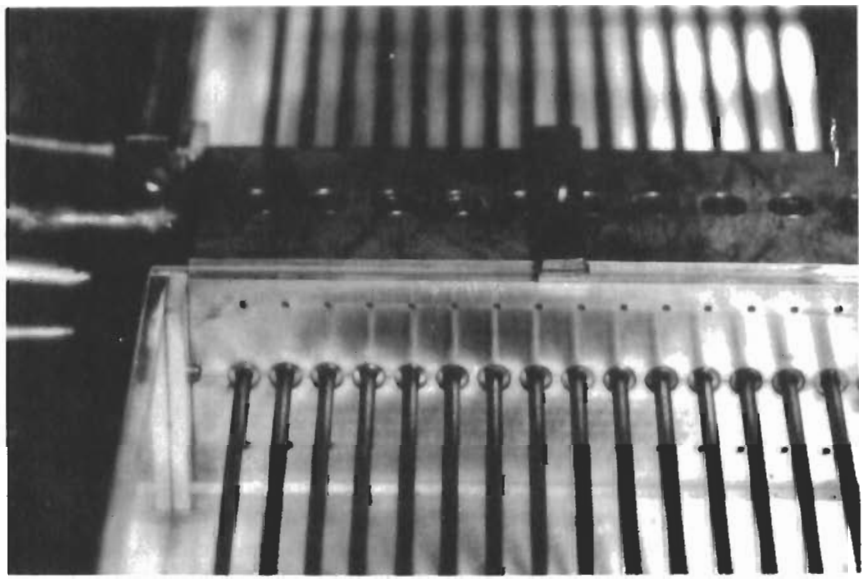

a ELECTRODE WITH GAS INJECTION HOLES

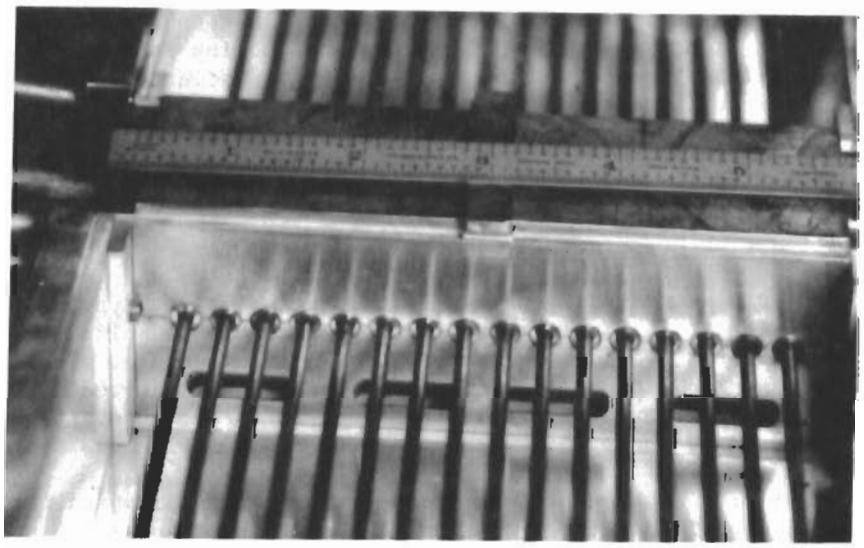

b ELECTRODE WITH GAS EXHAUST HOLES

Figure 48 SIDE VIEWS OF ELECTRODE ASSEMBLY FOR MODULAR GRAPHITE HEATER

The entire lamp is shown in Figure 49. Figure 49a shows the lamp complete with water-cooling hoses and the probe used to measure heat flux profiles. The power connections are made to the two outside electrodes by means of two ½-inch copper tubes, which are cooled with water. With this arrangement, each tube can carry at least 2000 amperes. Figure 49b is a photograph of the lamp in operation.

4. Operational Characteristics

The heater operated on dc power from a ½-Mw rectifier. The rectifier is capable of supplying 2000 amperes at 250 volts. The current is controlled by a saturable core reactor so that the load sets the voltage.

Figure 50 shows the voltage drop across the lamp (both panels) as a function of the current through the 16 graphite rods (AGKS-grade). Also shown is the rod temperature near the center of one panel as inferred from an optical pyrometer. The argon flow rate was about 2/3 gm/sec. At an input power of 95 kw, the rod temperature reached 2900° K when the current was 1950 amperes, or 122 amperes per rod. Figure 44 shows that for a simple rod radiating into cold surroundings, a current of approximately 160 amperes is needed for a rod temperature of 2900° K. This difference is indicative of the absorption by the rods of the radiation from adjacent rods and that reflected back by the side and back reflectors.

Figure 51 shows the radiating efficiency and input power versus the lamp current. The radiating efficiency, η_R, is defined to be the ratio of the radiated power to the input power. The radiated power was obtained by measuring the power loss in the cooling water. One can see that the radiating efficiency increases with input power, reaching a value of 65 percent at the input power levels of 55 kw. The cooling power losses become proportionately less at the higher power levels because the cooling loss to the electrodes is proportional to the rod temperature, while the radiated power is proportional to the fourth power of the temperature. At an input power of 55 kw, the radiation loss to the back reflector is 7 percent, and the radiation loss to the four sides is approximately 8 percent. Thus, the power lost by conduction at the ends of the rods is 20 percent of the input power.

5. Radiation Flux Measurements

Radiation flux measurements were made with a calorimetric type of probe manufactured by the Hy-Cal Engineering Co. The probe was supplied with a calibration of heat flux versus the mv output of a thermocouple. The sensing surface is circular with a diameter of 1/8 inch, and is coated with a black paint having an emittance of 0.89. This fact is used to convert the heat flux as measured by the probe to the incident radiant flux.

The heat flux probe was mounted on a traversing mechanism which permitted the controlled motion of the probe in all three directions. The probe is seen in position at the center of one panel in Figure 49.

Figure 52 shows the radiation flux measured at the center of one panel, 3/8 inch from the front surface of the 1/16 inch thick quartz plate or 1-5/16 inches from the center line of the graphite rods. Also shown is the ratio

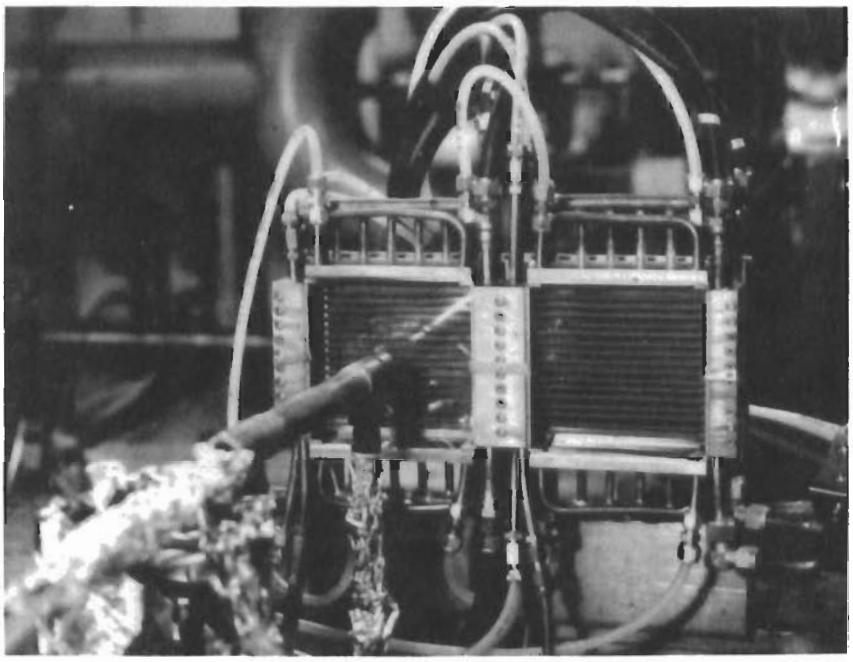

a WITH HEAT FLUX PROBE

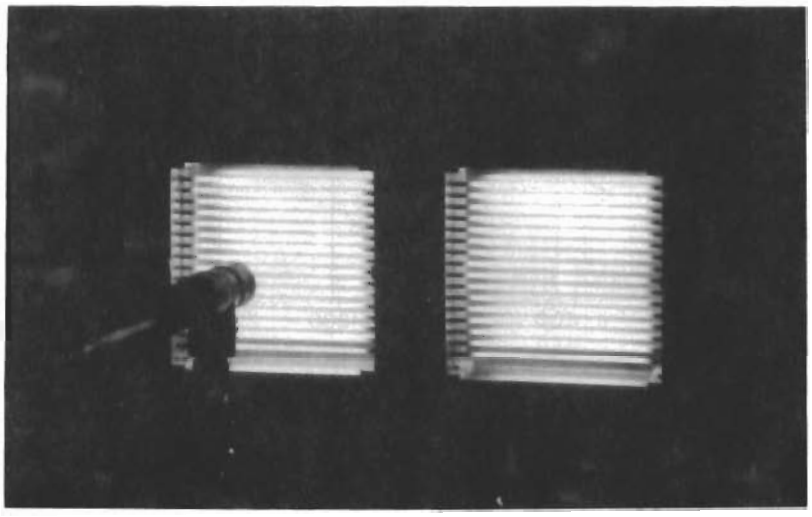

b IN OPERATION

Figure 49 ASSEMBLED MODULAR GRAPHITE HEATER

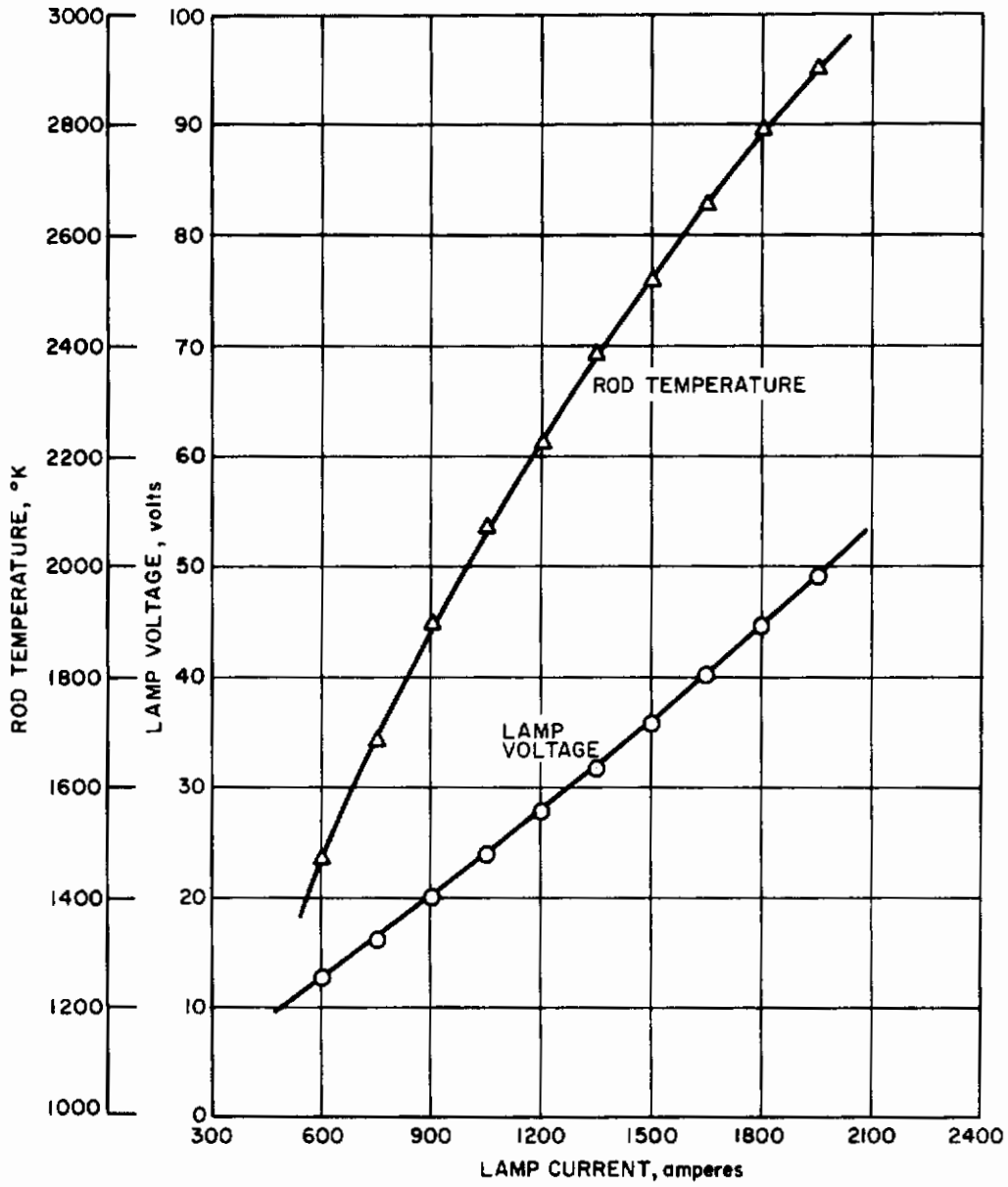

Figure 50 VOLTAGE AND ROD TEMPERATURE VERSUS CURRENT FOR MODULAR GRAPHITE HEATER

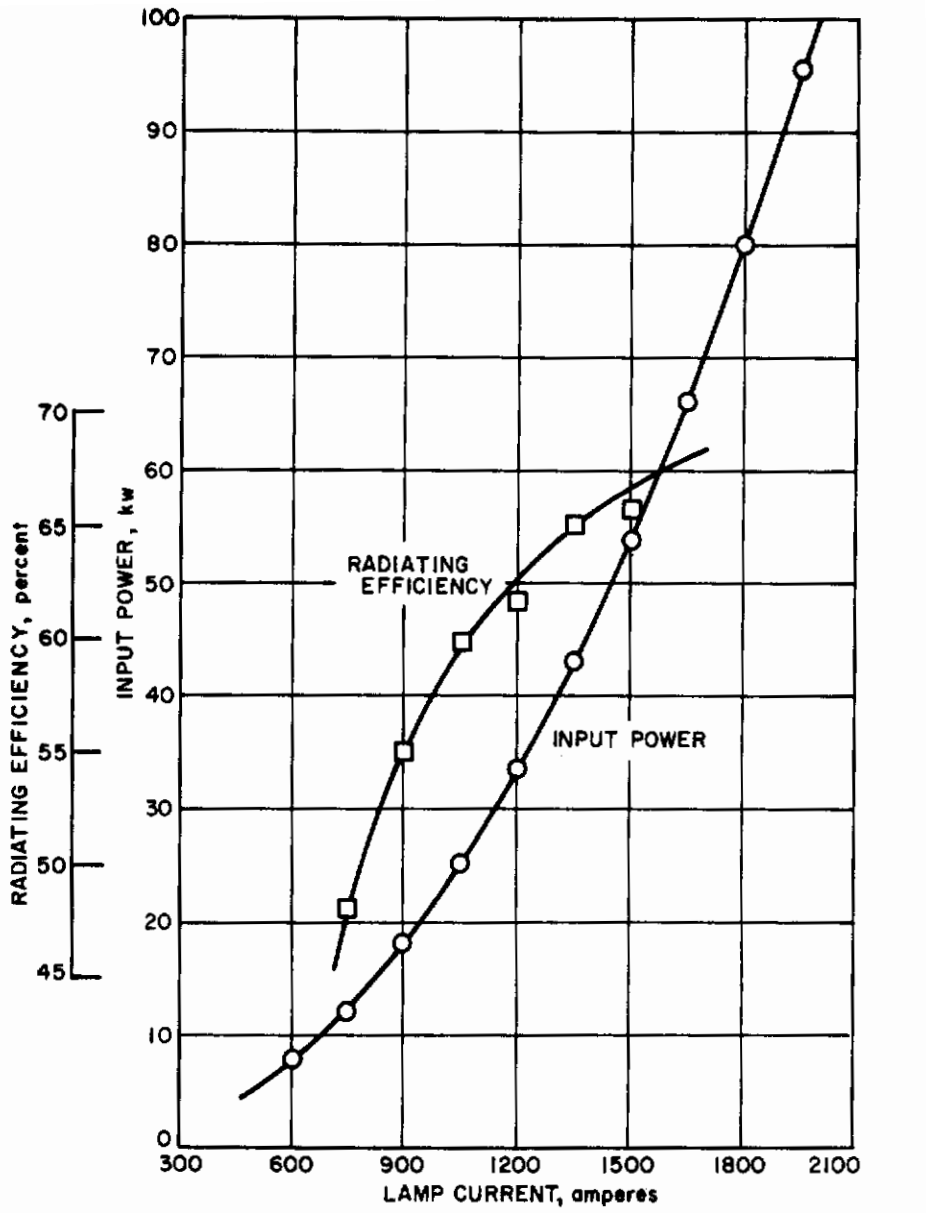

Figure 51 INPUT POWER AND RADIATING EFFICIENCY VERSUS LAMP CURRENT FOR MODULAR GRAPHITE HEATER

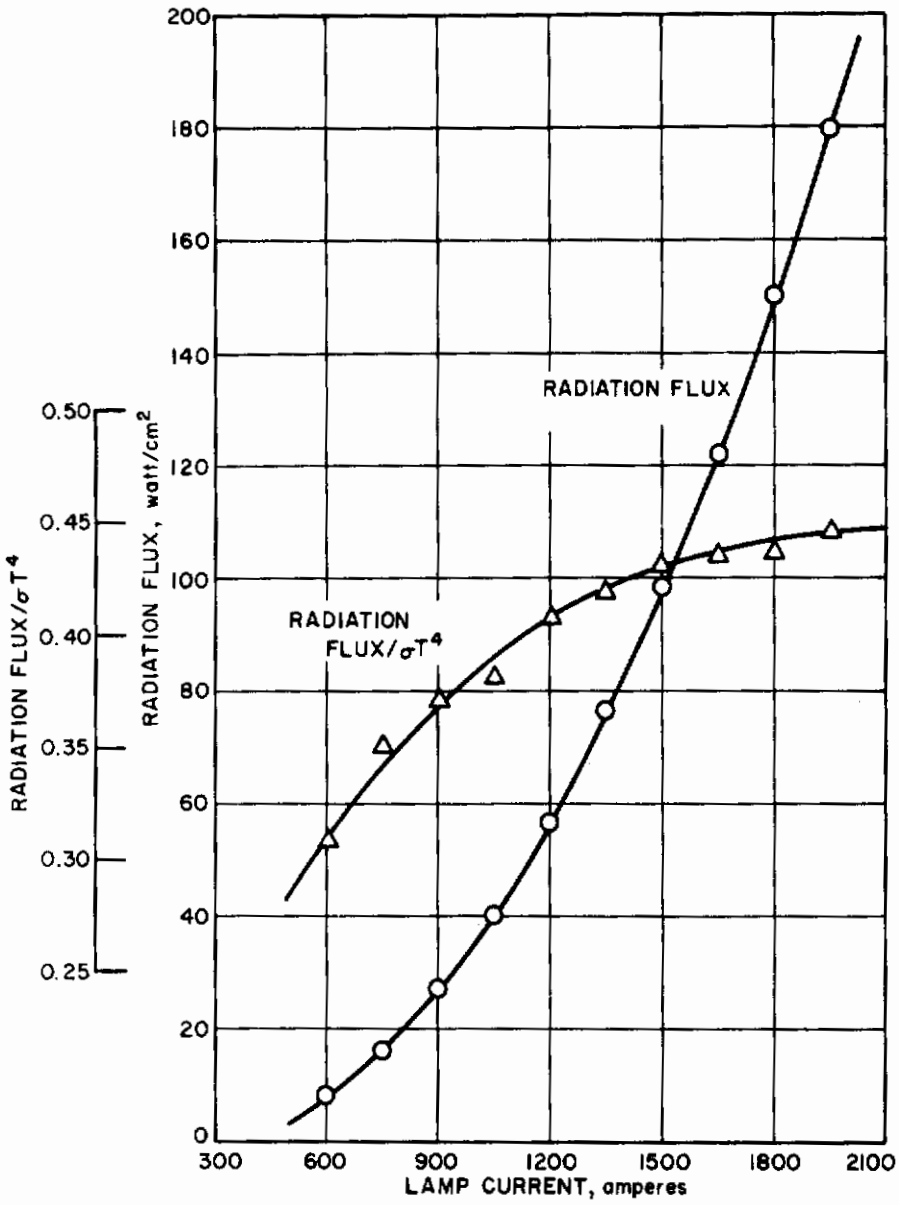

Figure 52 RADIATION FLUX FROM MODULAR GRAPHITE HEATER

of the measured heat flux to the quantity σT^4, which is a measure of the performance of the heater relative to a blackbody source. As the input power increases, the temperature along the rod becomes more uniform, thus increasing the heat flux relative to the blackbody result, which is based on the temperature measured in the middle of the rod.

The above explanation implies that with the detector 1-5/16 inches away, the array of rods still cannot be considered an infinite plane. This is clearly seen in Figure 53, where the radiation flux at the center of one panel is shown as the probe is moved perpendicularly towards the rod array. One can see that at a distance of 1/8 inch from the quartz plate, the radiation flux is still rising uniformly. Figure 54 is plot of the slopes of the curves in Figure 53 near the quartz plate as a function of lamp current.

Figures 55 to 57 show radiation flux profiles in a plane parallel to the quartz plate at various axial distances for a lamp current of 1200 amperes. Figure 55 shows the radiation flux distribution at a plane 1-1/8 inches from the rods. Notice that 40 percent of the inner region has a flux level of 90 percent or better of the peak value. Figures 56 and 57 show the flux profiles at planes 2-3/8 and 3-5/8 inches from the rod array. The elongation of the profile in Figure 57 is due to the influence of the other panel.

The highest graphite rod temperature was 2900° K, corresponding to a lamp current of 1950 amperes. At this temperature, the sublimation products began to deposit on the cooled back reflector plate. As the deposit built up, the radiation flux began to decrease. No deposition, however, was detected on the quartz plate. No attempt has been made to eliminate this problem. One solution would be to put another quartz plate in front of the back reflector, separated by insulators. This would present a hot surface and lessen the deposition rate of the sublimation products. The argon flow would help to insure the integrity of this plate.

From Figures 52 to 54, an estimate can be made of the heat flux that could be delivered from an array of these modular graphite heaters that is large enough in extent that a sample would see an infinite plane. From Figure 53, the assumption that for a single modular heater an infinite plane is obtained at a distance ½ inch from the rods appears reasonable. For a lamp current of 1950 amperes, corresponding to a rod temperature of 2900° K, the slope of the axial profile (Figure 54) is approximately 40 watt/cm^2-inch. From Figure 52, the measured heat flux for a lamp current of 1950 amperes at a distance 1-5/16 inches from the rods is 179 watt/cm^2. Thus, the "infinite plane" heat flux is estimated to be $179+40(1-5/16-\frac{1}{2}) \approx 220$ watt/cm^2. If the rod temperature is 3000° K, the "infinite plane" heat flux is $(3000/2900)^4 \times 220 \approx 250$ watt/cm^2. These values can be further improved by using two rows of rods, one row placed so as to fill the spaces left by the other row. This would increase f by a factor of 2 from the present value of 0.4, and would make the reflector relatively less important.

The above results compare favorably with the highest performance of the tungsten-quartz-iodine heating panels for which a heat flux of 120 to 130 watt/cm^2 at a distance 1 inch from the radiating element is achieved.

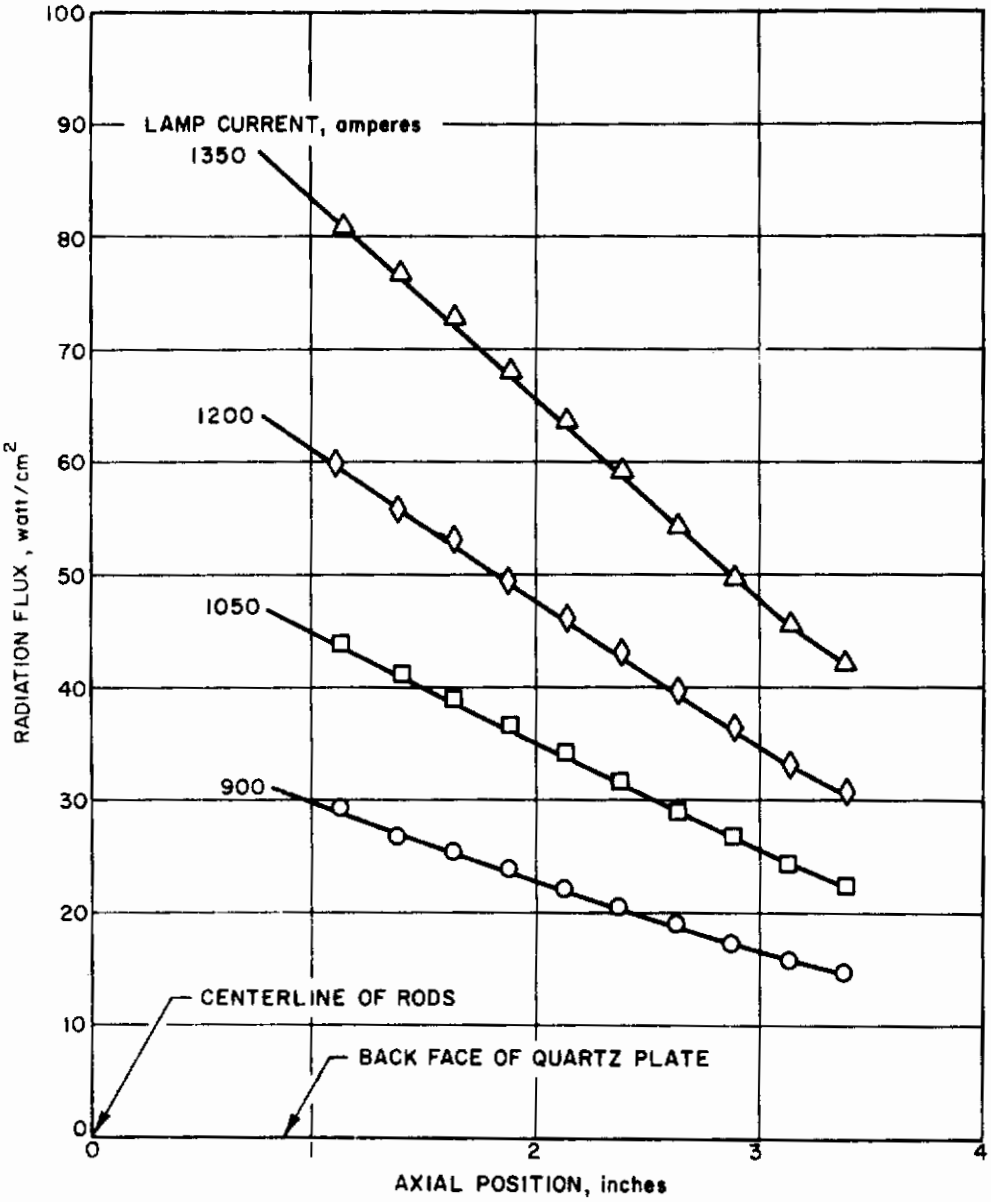

Figure 53 AXIAL PROFILES OF RADIATION FLUX AT CENTER OF PANEL OF MODULAR GRAPHITE HEATER FOR VARIOUS LAMP CURRENTS

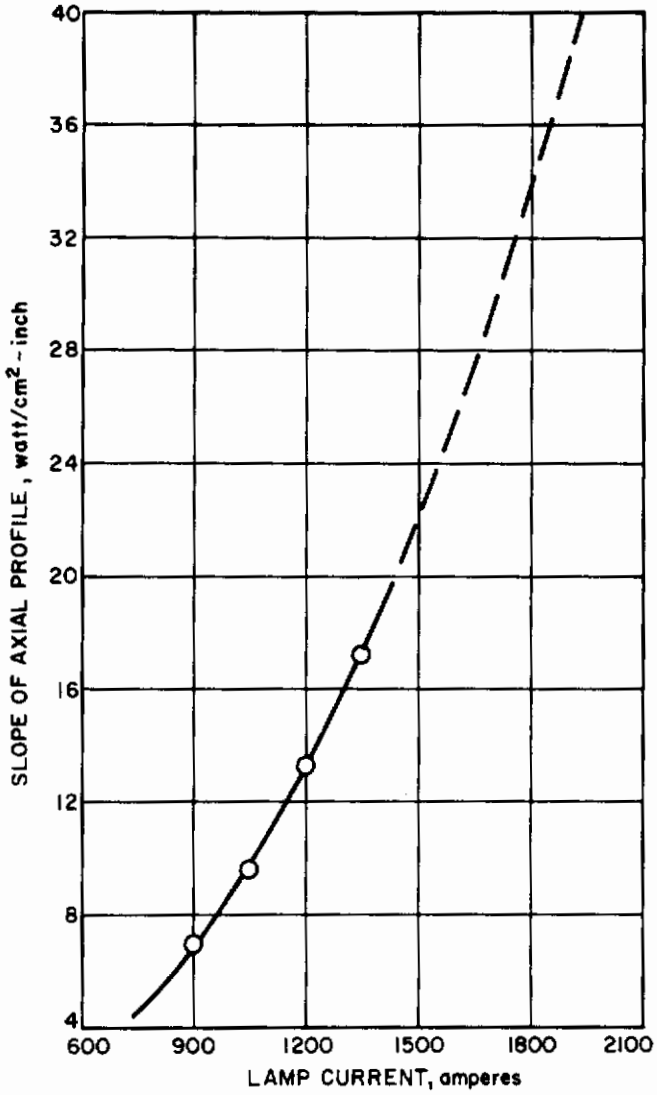

Figure 54 VARIATION OF SLOPE OF AXIAL PROFILE OF RADIATION FLUX AT CENTER OF PANEL WITH LAMP CURRENT

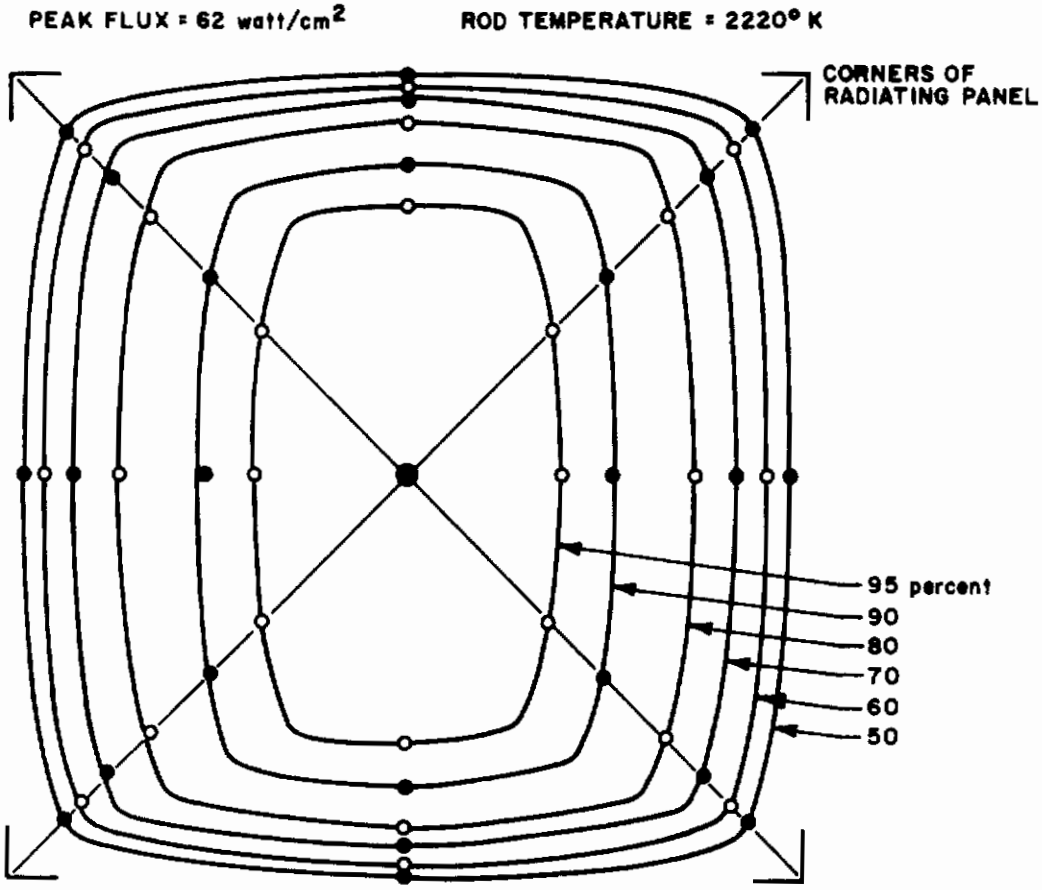

Figure 55 RADIANT FLUX PROFILE 1-1/8 INCHES FROM RODS

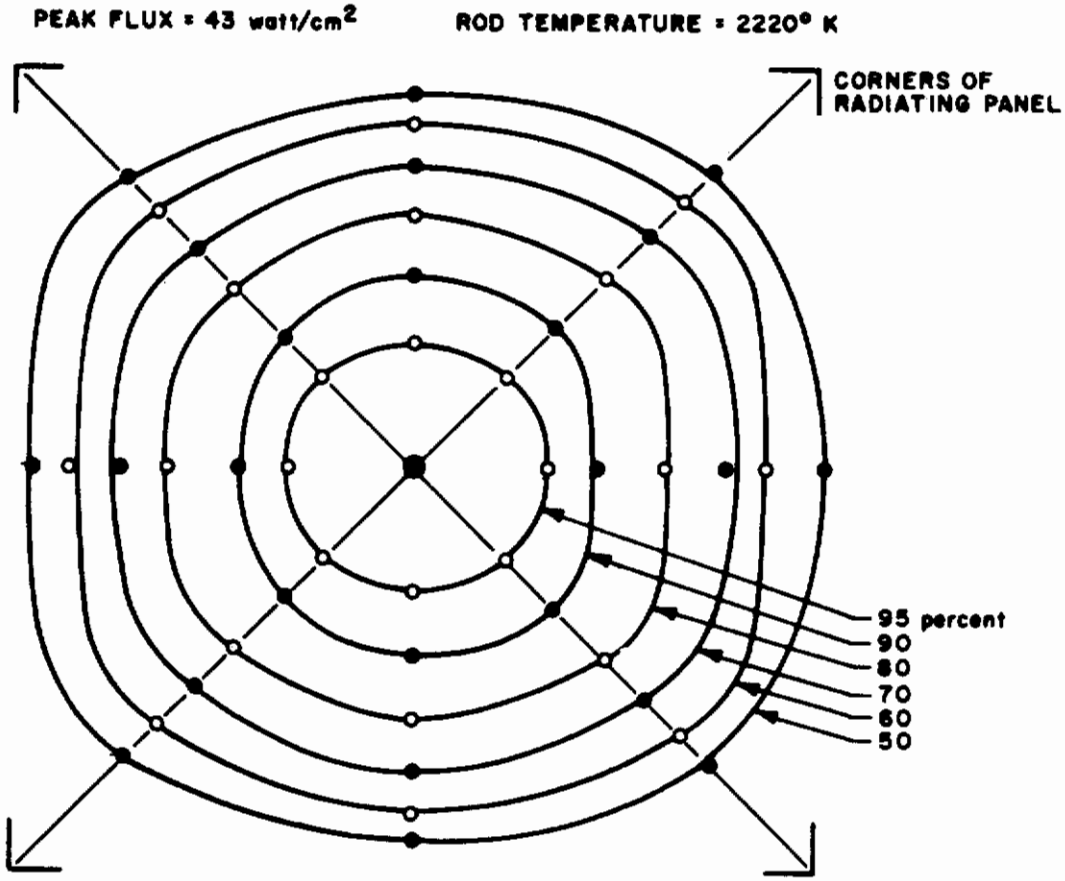

Figure 56 RADIANT FLUX PROFILE 2-3/8 INCHES FROM RODS

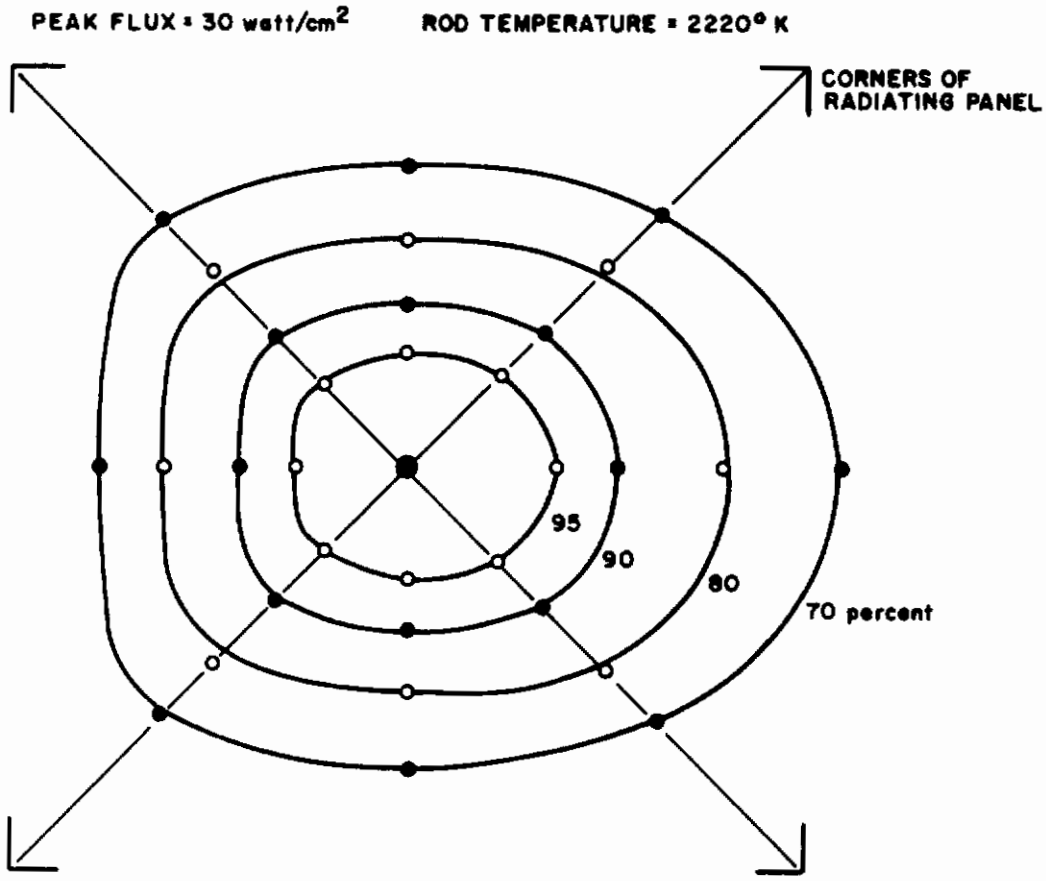

Figure 57 RADIANT FLUX PROFILE 3-5/8 INCHES FROM RODS

V. SUMMARY AND CONCLUSIONS

The radiative heat transfer to a large sample area depends primarily upon the source brightness which depends, in turn, upon two characteristics of the primary radiator material: its emittance and its temperature. Source brightness increases linearly with emittance and with the fourth power of the temperature. The emittance has a blackbody limit of unity, and therefore offers a limited potential for the increase of source radiant heat flux. The operating temperature of solid radiators is limited by their melting point. A source employing a plasma discharge is capable of operating at very high temperatures.

Two radiant heat sources are proposed which are potential improvements over a tungsten filament lamp. The cesium vapor arc discharge offers increased brightness because the radiating plasma can be maintained at a temperature of 4000° K or higher. Graphite offers increased brightness through an increase in emittance by a factor of 2 to 3. The cesium vapor discharge promises the larger potential gain in brightness, and concomitantly, it presents a wider range of development problems. Though graphite is probably the best solid body radiating material, it represents an increase in brightness of only 2 to 3 over that obtainable with tungsten, and this increase is due entirely to its high emittance (~0.9).

The major development effort was directed toward the cesium vapor lamp, which consists of an arc discharge and its containing envelope, along with associated endcaps and electrodes. An analysis of the arc column was carried out for the purpose of developing the various relations between the arc column radius, current, voltage gradient and radiated power for a cesium plasma. Further analyses related the arc column power and radiating efficiency to thermal stress in the envelope and to the envelope temperature for various modes of convective cooling.

Experimental work involved both the dc and ac operation of the lamp. Dc operation was used in the initial stages to develop suitable procedures and to establish the radiant output capability of the lamp. Measurements were made of both the total radiation and the spectral distribution of radiation. The performance of the lamp operating with 60-cycle ac power was investigated, and the determination was made that, with a series inductor, the lamp could, in principle, be operated at high power with the power supply at AFFDL.

The development work proceeded to the point where the radiation output from the cesium vapor lamp with a ½-inch Lucalox envelope was comparable to that from the tungsten-quartz lamp. Though the cesium arc discharge is capable of greatly increased radiant output, this potential cannot be fully realized, at present, because of materials problems associated with the envelope, the integrity of the brazes, and the oxidation of the endcaps at elevated temperatures. These problems are discussed and some solutions are proposed.

Effort was also directed towards the development of a graphite heater. The initial work involved a single graphite rod. The demonstration was made that with an argon gas flow to provide an inert atmosphere and carry away sublimation products, a graphite rod can be operated at surface temperatures of 3000° K for useful periods of time. Much of this development work was concerned with electrode design and the possibility of obtaining high radiant output without water-cooling.

The remaining effort was devoted to extending the graphite development work to the design, construction and evaluation of a modular, multi-element graphite heater. This led to a heater consisting of two radiating panels, each 5-3/4 inches square. Each panel consisted of 16 graphite rods in parallel; the two panels were series connected. Performance data obtained consisted of measurements of voltage-current characteristics, rod temperature, radiating efficiency and radiant flux profiles. The lamp was shown to be capable of delivering a heat flux in excess of 180 watt/cm^2 to a detector located 1 inch from the rod surface. The data indicate that a planar array consisting of many such modular graphite heaters could produce heat fluxes in excess of 250 watt/cm^2. Still higher fluxes would result by increasing the packing fraction of the rods.

Two principal conclusions follow from this development work. First, an immediate improvement in the heat flux capability of the AFFDL thermostructural test facility can be accomplished by using a graphite heater, which represents a potential radiant flux of 250 to 300 watt/cm^2. Second, a facility capable of a factor of 2 improvement over the above figure would require a lamp with a radiating element that is not a solid body. A lamp consisting of a cesium vapor discharge has the potential for such an improvement, although materials problems associated with the containment of the arc discharge prevent the realization of this potential at this time.

REFERENCES

1. Technical Exhibit, RTD PR Nr. (6) 20790.

2. Schiff, E., Study of Heating Methods for Structural Testing Above 3000° F. Technical Report AFFDL-TR-65-B (April 1965).

3. Beck, Clark E., Handbook for Test Engineers (Radiant Heating), TM-64-50, Research and Technology Division, AFSC, USAF, Wright-Patterson Air Force Base (December 1964).

4. Edgerton, Germeshausen & Grier Data Sheet Number 1002 (January 1965).

5. O'Neill, J.H., O.G. Koppius and M.A. Miller, High Temperature (1500° C) Ceramic-to-Metal Seals for Cesium Application, 67th Annual Conference of the American Ceramic Society.

6. Technical Documentary Report No. RTD-TDR-63-4109, AFSC, WPAFB, Ohio.

7. Reed, L., and R.C. McRae, The American Ceramic Soc. Bull., 44, No. 1 (1965), p. 12.

8. Cobine, J.D., Gaseous Conductors (Dover Publications, New York, 1958), pp. 162-168.

9. General Electric, Lamp Glass Department, Bulletin L-3-R (September 1964).

10. Charles, R.J., and R.R. Shaw, General Electric Research Laboratory Report No. 62-RL-3081M (July 1962).

11. McAdams, W.H., Heat Transmission (McGraw-Hill, New York, Third Edition, 1954).

12. Knudsen, J.G., and D.L. Kate, Fluid Dynamics and Heat Transfer (McGraw-Hill, New York, 1958).

13. Von Engel, A., Ionized Gases (Oxford, London, Second Edition, 1965).

14. Reference 8, p. 207.

15. Thermophysical Properties of Rubidium and Cesium, Technical Documentary Report, No. RTD-TDR-63-4018 (DDC No. 441992) (November 1963).

16. Reference 8, p. 339.

17. Reference 8, p. 348.

APPENDIXES

APPENDIX A

THERMAL STRESS ANALYSIS

1. MATHEMATICAL FORMULATION OF PROBLEM

The condition for static equilibrium requires that the displacement vector $\vec{u}$ satisfy the equation

$$\vec{\nabla}(\vec{\nabla}\cdot\vec{u}) + (1-2\nu)\nabla^2\vec{u} - 2\alpha(1+\nu)\vec{\nabla}T = 0 \tag{1}$$

where ν is Poisson's ratio, δ is the (constant) coefficient of linear expansion and T is the temperature. Using the relation

$$\nabla^2\vec{u} = \vec{\nabla}(\vec{\nabla}\cdot u) - \vec{\nabla}\times\vec{\nabla}\times\vec{u} \tag{2}$$

equation (1) becomes

$$2(1-\nu)\vec{\nabla}(\vec{\nabla}\cdot\vec{u}) - (1-2\nu)\vec{\nabla}\times\vec{\nabla}\times\vec{u} - 2\alpha(1+\nu)\vec{\nabla}T = 0 \tag{3}$$

In cylindrical coordinates, the strain components are given by

$$\epsilon_r = \frac{\partial u_r}{\partial r} \qquad \epsilon_{rz} = 1/2\left(\frac{\partial u_z}{\partial r} + \frac{\partial u_r}{\partial z}\right)$$

$$\epsilon = \frac{1}{r}\frac{\partial u_\theta}{\partial\theta} + \frac{u_r}{r} \qquad \epsilon_{ro} = 1/2\left(\frac{1}{r}\frac{\partial u_r}{\partial\theta} + \frac{\partial u_\theta}{\partial r} - \frac{U_o}{r}\right)$$

$$\epsilon_z = \frac{\partial u_z}{\partial z} \qquad \epsilon_{oz} = 1/2\left(\frac{1}{r}\frac{\partial u_z}{\partial\theta} + \frac{\partial u_\theta}{\partial z}\right) \tag{4}$$

The normal stress components are given by

$$\sigma_r = \lambda\epsilon + 2\mu\epsilon_r - mT$$

$$\sigma_\theta = \lambda\epsilon + 2\mu\epsilon_\theta - mT$$

$$\sigma_z = \lambda\epsilon + 2\mu\epsilon_z - mT \tag{5}$$

and the shear stress components by

$$\tau_{rz} = 2\mu\epsilon_{rz}$$

$$\tau_{r\theta} = 2\mu\epsilon_{r\theta}$$

$$\tau_{\theta z} = 2\mu\epsilon_{\theta z} \tag{6}$$

where

$$\epsilon \equiv \epsilon_r + \epsilon_\theta + \epsilon_z \tag{7}$$

and

$$m \equiv \alpha (3\lambda + 2\mu). \tag{8}$$

The Lame' coefficients λ and μ are related to ν and E, Young's Modulus, by the relations

$$\lambda = \frac{E\,\nu}{(1+\nu)(1-2\nu)} \tag{9}$$

$$\mu = \frac{E}{2(1+\nu)} \tag{10}$$

We now specialize to the case that

$$T(r, z) = T_1(r) + T_2(z) \tag{11}$$

$$\frac{\partial}{\partial \theta} \equiv 0 \tag{12}$$

and the displacement vector $\vec{u} = (u_r, u_\theta, u_z)$ is such that

$$u_r = u_r(r, z)$$

$$u_z = u_z(r, z)$$

$$u_\theta = 0. \tag{13}$$

The separation of radial and axial dependencies in (11) is valid for both cases of interest here.

Then equations (4) become

$$\epsilon_r = \frac{\partial u_r}{\partial r} \qquad \epsilon_{rz} = 1/2 \left(\frac{\partial u_z}{\partial r} + \frac{\partial u_r}{\partial z} \right)$$

$$\epsilon_\theta = \frac{u_r}{r} \qquad \epsilon_{r\theta} = 0$$

$$\epsilon_z = \frac{\partial u_z}{\partial z} \qquad \epsilon_{\theta z} = 0 \tag{14}$$

Hence

$$r_{r\theta} = r_{\theta z} \equiv 0 \tag{15}$$

The term $\vec{\nabla}\left(\vec{\nabla}\cdot\vec{u}\right)$ specializes to

$$\vec{\nabla}\left(\vec{\nabla}\cdot\vec{u}\right) = \hat{r}_o \left\{\frac{\partial}{\partial r}\left(\frac{1}{r}\frac{\partial}{\partial r}\, r u_r\right) + \frac{\partial^2 u_z}{\partial z^2}\right\} + \hat{z}_o \left\{\frac{\partial}{\partial z}\frac{1}{r}\frac{\partial}{\partial r}\, r u_r + \frac{\partial^2 u_z}{\partial z^2}\right\} \tag{16}$$

The term $\vec{\nabla}\times\vec{\nabla}\times\vec{u}$ reduces to

$$\vec{\nabla}\times\vec{\nabla}\times\vec{u} = \hat{r}_o \frac{\partial}{\partial z}\left\{\frac{\partial u_z}{\partial r} - \frac{\partial u_r}{\partial z}\right\} + \hat{z}_o \frac{1}{r}\frac{\partial}{\partial r}\, r\left(\frac{\partial u_r}{\partial z} - \frac{\partial u_z}{\partial r}\right) \tag{17}$$

where $\hat{r}_o$ and $\hat{z}_o$ are unit vectors in the r and z directions.

Substituting equations (16) and (17) into equation (3) gives the result

$$2(1-\nu)\frac{\partial \psi}{\partial r} - (1-2\nu)\frac{1}{r}\frac{\partial \Phi}{\partial z} - 2a(1+\nu)\frac{dT_1}{dr} = 0 \tag{18}$$

$$2(1-\nu)\frac{\partial \psi}{\partial r} + (1-2\nu)\frac{1}{r}\frac{\partial \Phi}{\partial r} - 2a(1+\nu)\frac{dT_2}{dz} = 0 \tag{19}$$

where the functions Φ and ψ are defined by

$$\psi \equiv \frac{1}{r}\frac{\partial}{\partial r}(r u_r) + \frac{\partial u_z}{\partial z} \quad ; \quad \Phi \equiv r\left(\frac{\partial u_z}{\partial r} - \frac{\partial u_r}{\partial z}\right) \tag{20}$$

Uncoupled differential equations for Φ and ψ can be obtained by differentiating equations (18) and (19). The result is

$$\frac{\partial^2 \Phi}{\partial r^2} - \frac{1}{r}\frac{\partial \Phi}{\partial r} + \frac{\partial^2 \Phi}{\partial z^2} = 0 \tag{21}$$

and

$$\frac{\partial^2 \psi}{\partial r^2} + \frac{1}{r}\frac{\partial \psi}{\partial r} + \frac{\partial^2 \psi}{\partial z^2} = \nabla^2 T = 0 \tag{22}$$

Thus the problem reduces to finding solutions of equations (21) and (22) which when combined with equations (20) and (14) yield stress components which satisfy the boundary condition that there is no external force applied to the boundaries of the cylinder. That is,

$$\sigma_r = 0 \qquad r = R, \quad r = r_w \quad -\frac{L}{2} \leq z \leq \frac{L}{2}$$

$$\sigma_z = 0 \qquad z = \pm L/2 \qquad r_w \leq r \leq R$$

$$\tau_{rz} = 0 \qquad \begin{cases} r = r_w, \ r = R & -\dfrac{L}{2} \leq z \leq \dfrac{L}{2} \\ z = \pm L/2 & r_w \leq r \leq R \end{cases} \tag{23}$$

2. SOLUTION

The exact solution of stress problems in finite length cylinders is extremely difficult to accomplish because of the boundary conditions at the ends of the cylinder. The solution that is presented here is in the same spirit as that given by Timoshenko and Goodier[1] for the case of the annular cylinder, freely supported but with only a radial temperature gradient. In that solution, the boundary condition that $\sigma_z = 0$ along the ends of the cylinder is not satisfied. However, it is a solution for which the total axial force acting on the end of the cylinder is zero. Then Saint-Venant's principle is used to confirm that the stress distribution given by the solution differs from the correct one only in the immediate region containing the ends of the cylinder.

Similary, the solution given here satisfies the boundary conditions on σ_r and τ_{rz} on the integral of σ_z. One should note that this solution gives τ_{rz} to be zero everywhere. The exact solution would give τ_{rz} to be appreciably different from zero only near the very ends of the cylinder.

The solution that satisfies the boundary conditions in the manner discussed above is obtained by taking the solution to equations (18) and (19) to be

$$\psi = A_1 r^2 - 2 A_1 z^2 + \delta \frac{1+\nu}{1-\nu} T + A_2 \tag{24}$$

$$\Phi = 4 \frac{1-\nu}{1-2\nu} A_1 r^2 z \tag{25}$$

Combining equations (20) gives

$$\frac{\partial}{\partial r} \frac{1}{r} \frac{\partial}{\partial r} r u_r + \frac{\partial^2 u_r}{\partial z^2} = \frac{\partial \psi}{\partial r} - \frac{\partial}{\partial z} \left(\frac{\Phi}{r} \right) \tag{26}$$

and

$$\frac{\partial^2 u_z}{\partial z^2} + \frac{1}{r} \frac{\partial u_z}{\partial r} + \frac{\partial^2 u_z}{\partial r^2} = \frac{\partial \psi}{\partial z} + \frac{1}{r} \frac{\partial \Phi}{\partial r} \tag{27}$$

The solution of equation (26) is taken to be

$$u_r = B_1 r^3 + B_2 r + \frac{B_3}{r} - 4B_1 rz^2 - \frac{A_1 r^3}{4(1-2\nu)} + \frac{\delta(1+\nu)}{(1-\nu)\, r} \int r T_1 \, dr \qquad (28)$$

and the solution of (27) is taken to be

$$u_z = \frac{2}{3}(4B_1 - A_1) z^3 + (A_2 - 2B_2) z + \left[\frac{2A_1(1-\nu)}{1-2\nu} 4B_1\right] r^2 z + \frac{\delta(1+\nu)}{(1-\nu)} \int T_2 \, dz \qquad (29)$$

These equations are now used to satisfy the boundary conditions on the various stress components.

a. r_{rz} - Substitution of equations (28) and (29) into equation (14) for ϵ_{rz} gives the result that boundary condition (23) is satisfied. Moreover, r_{rz} is zero everywhere.

b. σ_r - Substitution of equations (28), (29), (7), (8), and (9) into the expression for σ_r, equation (6), and satisfying the boundary condition (23) gives the result

$$\sigma_r = \frac{E\alpha}{1-\nu} \left[\frac{r^2 - r_w^2}{R^2 - r_w^2} \frac{1}{r^2} \int_{r_w}^{R} r T_1 \, dr - \frac{1}{r^2} \int_{r_w}^{r} r T_1 \, dr + \frac{\dot{Q}\nu}{4(1+\nu)K} \frac{(r^2 - r_w^2)(r^2 - R^2)}{L r^2} \right] \qquad (30)$$

c. σ_z Performing the corresponding steps for σ_z as for σ_r gives the result

$$\sigma_z = \frac{E\alpha}{1-\nu} \left[\frac{2}{R^2 - r_w^2} \int_{r_w}^{R} r T_1 \, dr - T_1 + \frac{\dot{Q}}{2(1+\nu)KL} (2r^2 - R^2 - r_w^2) \right] \qquad (31)$$

This expression for σ_z satisfies the condition that

$$\int_{r_w}^{R} \sigma_z \, r \, dr = 0 \qquad (32)$$

that is, the total, axial force is zero. Then, according to Saint-Venant's principle the stress distribution given by this solution is not appreciably different from the exact one except in a region near the very ends of the cylinder.

d. σ_θ - Finally, σ_θ is found in the same way as σ_r and σ_z. The result is

$$\sigma_\theta = \frac{E\alpha}{1-\nu}\left[\frac{1}{r^2}\int_{r_w}^{r} rT_1\,dr + \frac{r^2+r_w^2}{R^2-r_w^2}\,\frac{1}{r^2}\int_{r_w}^{R} rT_1\,dr + \frac{\dot{Q}\nu}{4(1+\nu)KL}\cdot\left(3r^2 - \frac{r_w^2R^2}{r^2} - R^2 - r_w^2\right)\right] \tag{33}$$

The solution is completed by evaluating the integrals in equations (30), (31), and (33). The final result is

$$\sigma_r = \frac{-E\alpha\dot{Q}r_w}{2(1-\nu)K}\,\frac{r^2-r_w^2}{R^2-r_w^2}\left[\frac{1-\nu}{4(1+\nu)}\left(1-\left(\frac{R}{r}\right)^2\right) + \frac{R^2}{r^2}\,\frac{R^2}{R^2-r_w^2}\,ln\,\frac{R}{r_w} - \frac{R^2}{r^2-r_w^2}\,ln\,\frac{r}{r_w}\right] \tag{34}$$

$$\sigma_\theta = \frac{E\alpha\dot{Q}r_w}{2(1-\nu)K}\,\frac{r_w^2}{R^2-r_w^2}\left[-\frac{R^2}{r_w^2}\,\frac{R^2}{R^2-r_w^2}\,ln\,\frac{R}{r_w}\left(1+\frac{r_w^2}{r^2}\right) + \frac{1-\nu}{4(1+\nu)} + \left(1+\frac{R^2}{r^2}\right) + \frac{R^2}{r_w^2}\,ln\,\frac{r}{r_w} + \frac{1}{4(1+\nu)}\left\{3\nu\left(\frac{r^2}{r_w^2}+\frac{R^2}{r_w^2}\right) + \frac{5R^2}{r_w^2} - \frac{3r^2}{r_w^2}\right\}\right]$$

$$\sigma_z = \frac{E\alpha\dot{Q}r_w}{2(1-\nu)K}\,\frac{r_w^2}{R^2-r_w^2}\left[\frac{1-\nu}{2(1+\nu)}\left(\frac{2r^2}{r_w^2}-1\right) + \frac{3\nu+1}{2(\nu+1)}\,\frac{R^2}{r_w^2} + \frac{2R^2}{r_w^2}\,ln\,\frac{r}{r_w} - \frac{2R^2}{r_w^2}\,\frac{R^2}{R^2-r_w^2}\,ln\,\frac{R}{r_w}\right] \tag{35, 36}$$

For the case where there is only a radial temperature gradient, the stress distribution is given by equations (30), (31), and (33) minus the $\dot{q}$ term. The case of only a radial temperature gradient is realized when the dominant heat loss is from the surface $r = R$. This can happen, for example, when natural convective cooling is replaced by forced convective cooling.

The solution of that equation is given by equations shown below:

$$\sigma_r = \frac{E\,\alpha\,Q r_w}{2(1-\nu)K}\left[\ln\frac{R}{r} - \frac{r_w^2}{R^2 - r_w^2}\left(1 - \frac{R^2}{r^2}\right)\ln\frac{R}{r_w}\right] \tag{37}$$

$$\sigma_\theta = \frac{E\,\alpha\,Q r_w}{2(1-\nu)K}\left[1 - \ln\frac{R}{r} - \frac{r_w^2}{R^2 - r_w^2}\left(1 + \frac{R^2}{r^2}\right)\ln\frac{R}{r_w}\right] \tag{38}$$

$$\sigma_z = \frac{E\,\alpha\,Q r_w}{2(1-\nu)K}\left[1 - 2\ln\frac{R}{r} - \frac{2r_w^2}{R^2 - r_w^2}\ln\frac{R}{r_w}\right] \tag{39}$$

REFERENCE

1. Timoshenko, S., and J.N. Goodier, Theory of Elasticity, Second Edition, (McGraw-Hill Book Co. Inc., 1951).

APPENDIX B

RELATIONS FOR RMS CURRENT, VOLTAGE AND AVERAGE POWER FOR AC CESIUM VAPOR-LAMP OPERATION

In analyzing the performance of the cesium vapor lamp, operating with ac power, the obtaining of relations between certain features of the voltage and current waveforms and the corresponding rms values is useful. The current and voltage waveforms are essential in determining the average power. In this analysis, waveforms are chosen which are idealizations based on oscillograms. These idealizations are assumed valid for operation with and without inductance in the circuit.

1. RMS VOLTAGE

The voltage waveform is assumed to be given by Figure B-1. Let τ be the half-period. Let f be the fraction of the half-period during which the current is zero. Let V_r be the restrike voltage and V_a be the constant voltage portion of the waveform. From Figure B-1, one can see that $\tau_1 = f\tau/\beta$ V_r/V_a, $\tau_2 = \tau(1-f)$ and $\tau_3 = f\tau - \tau_1$ where $\beta = 1 + V_r/V_a$. The equation of the voltage waveform is given by

$$V(t) = \frac{V_a \beta}{f\tau} t \qquad 0 \leq t \leq \tau_1$$

$$V(t) = V_a \qquad \tau_1 \leq t \leq (\tau_1 + \tau_2)$$

$$V(t) = V_a - \frac{V_a \beta}{f\tau} \tau - \tau_3 \qquad (\tau_1 + \tau_2) \leq t \leq \tau \qquad (1)$$

The rms voltage is defined by

$$V_{rms} = \left\{ \frac{1}{\tau} \int_0^{\tau} V^2(t) \, dt \right\}^{1/2} \qquad (2)$$

After the substitution of equation (1) into (2) and algebraic manipulation, the following result is obtained

$$V_{rms} = V_a \left[1 - f + \frac{1}{3} \frac{f}{\beta} \left\{ (\beta - 1)^3 + 1 \right\} \right]^{1/2} \qquad (3)$$

The validity of this analysis can be checked by comparing with the results from the oscillogram in Figure 39b. $V_r \approx 270$ volts, $V_a \approx 70$ volts, and $f \approx 0.18$. Substituting these values into equation (3) gives a value of 86 volts for V_{rms},

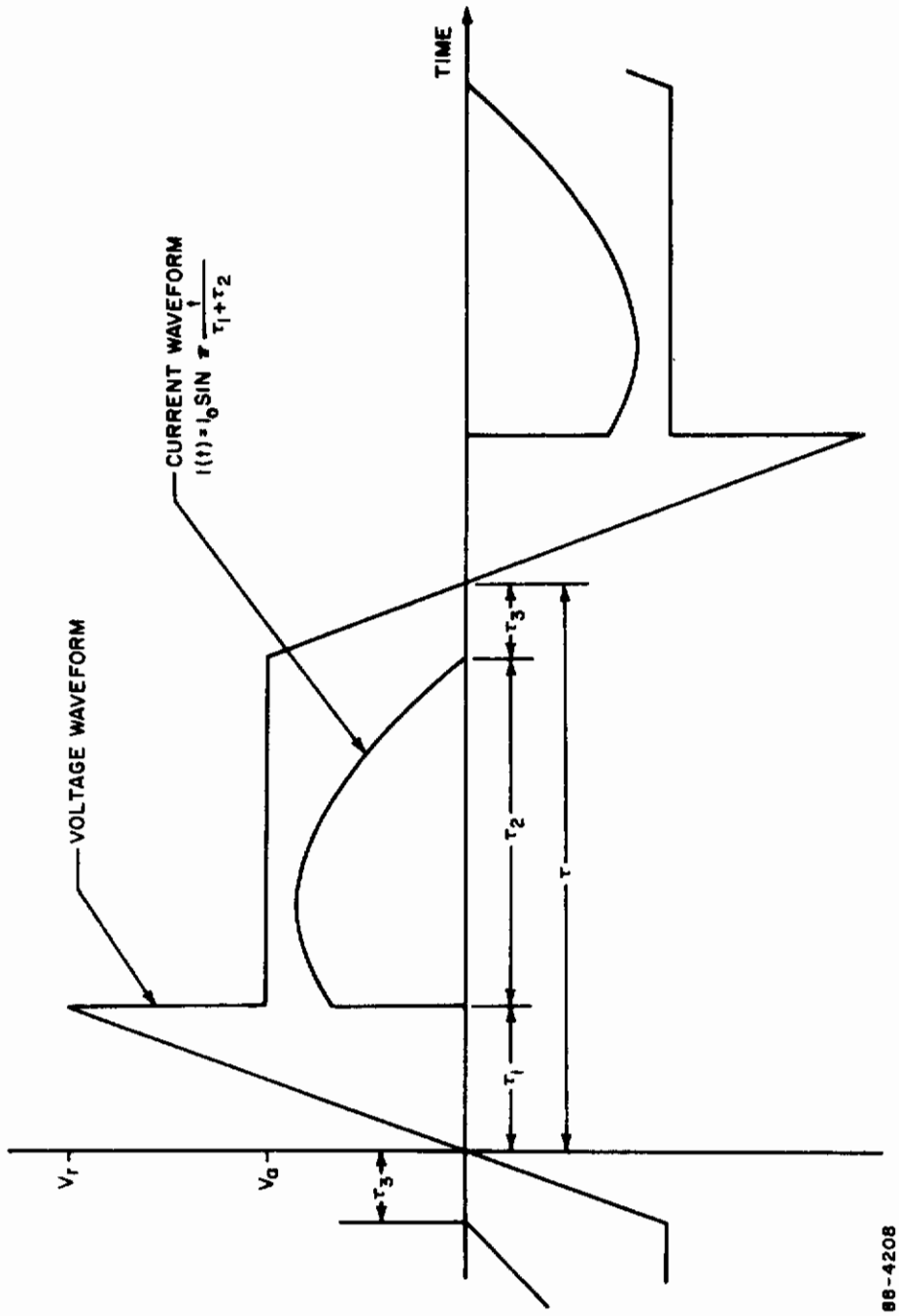

Figure B-1 IDEALIZED CURRENT AND VOLTAGE WAVEFORMS USED TO COMPUTE AVERAGE POWER

which agrees well with the measured value of 88 volts.

2. RMS CURRENT

The current waveform is assumed to be represented by Figure (B-1), i.e., it is part of a sinusoid:

$$I(t) = 0 \qquad 0 \le t \le \tau_1$$

$$I(t) = I_o \sin \pi \frac{t}{\tau_1 + \tau_2} \qquad \tau_1 \le t \le (\tau_1 + \tau_2)$$

$$I(t) = 0 \qquad (\tau_1 + \tau_2) \le t \le \tau \tag{4}$$

The rms current is defined by

$$I_{rms} = \left\{ \frac{1}{\tau} \int_0^{\tau} I^2(t)\, dt \right\}^{1/2} \tag{5}$$

Substituting equation (4) into equation (5) gives the result

$$I_{rms} = \frac{I_o}{\sqrt{2}} \left(1 - \frac{f}{\beta}\right)^{1/2} \left[\frac{\beta(1-f)}{\beta - f} + \frac{1}{2\pi} \sin \frac{2\pi f(\beta - \_)}{\beta - f} \right] \tag{6}$$

Again using Figure 39b, $I_o \approx 6.5$ amperes and equation (6) gives the result I_{rms} =4.45 amperes, which also agrees well with the measured value of 4.55 amperes.

3. AVERAGE POWER

The time average power $\bar{P}_t$ is defined by

$$\bar{P}_t \equiv \frac{1}{\tau} \int_0^{\tau} I(t)\, V(t)\, dt \tag{7}$$

Using equations (1) and (4),

$$\bar{P}_t = \frac{1}{\tau} \int_{\tau_1}^{\tau_1 + \tau_2} I_o V_a \sin \frac{\pi t}{\tau_1 + \tau_2} \, dt$$

$$= \frac{I_o V_a}{\pi} \left(1 - \frac{f}{\beta}\right) \left[1 + \cos \frac{\pi f (\beta - 1)}{\beta - f}\right] \tag{8}$$

Thus for the operating point in Figure 39b, the average input power to the lamp is 260 watts.

Unclassified
Security Classification

DOCUMENT CONTROL DATA - R & D

(Security classification of title, body of abstract and indexing annotation must be entered when the overall report is classified)

1. ORIGINATING ACTIVITY (Corporate author) Avco Government Products Group Space Systems Division 201 Lowell Street, Wilmington, Massachusetts 01887	2a. REPORT SECURITY CLASSIFICATION Unclassified 2b. GROUP --

3. REPORT TITLE

Improved Radiant Heat Source

4. DESCRIPTIVE NOTES (Type of report and inclusive dates)
Technical (September 1966 to March 1968)

5. AUTHOR(S) (First name, middle initial, last name)

Dr. L. A. Cass

6. REPORT DATE November 1968	7a. TOTAL NO. OF PAGES	7b. NO. OF REFS 17
8a. CONTRACT OR GRANT NO. AF33(615)-5384 b. PROJECT NO. c. 1347 d. Task No. 134704	9a. ORIGINATOR'S REPORT NUMBER(S) AVSSD-0133-68-RR 9b. OTHER REPORT NO(S) (Any other numbers that may be assigned this report) AFFDL-TR-68-93	

10. DISTRIBUTION STATEMENT
This document is subject to special export controls and each transmittal to foreign governments or foreign nationals may be made only with prior approval of AF Flight Dynamics Laboratory, Wright-Patterson AFB, Ohio 45433

11. SUPPLEMENTARY NOTES	12. SPONSORING MILITARY ACTIVITY Air Force Flight Dynamics Laboratory Air Force Systems Command Wright-Patterson AFB, Ohio 45433

13. ABSTRACT

The characteristics of the various components of a radiative heat transfer facility are examined to determine how their combination produces a certain heat flux delivered to a sample.

Two radiant heat sources are proposed as potential improvements over the tungsten filament-quartz envelope lamp. The cesium vapor lamp and a graphite rod heater are theoretically detailed and the results of experimental tests are presented.

The conclusions stated are, that an immediate improvement in heat flux capability is possible by use of a graphite heater, and even greater potential for improvement is inherent in the cesium vapor discharge lamp, but materials problems associated with arc containment prevent the present realization of that potential.

This abstract has been approved for public release and sale; its distribution is unlimited.

DD FORM 1 NOV 68 1473

Unclassified
Security Classification

Unclassified
Security Classification

14. KEY WORDS	LINK A		LINK B		LINK C	
	ROLE	WT	ROLE	WT	ROLE	WT
Cesium plasma						
Cesium vapor lamp						
Grapite rod heater						
Modular graphite heater						
Radiant heat sources						
Radiative heat transfer						
Tungsten-quartz lamp						

Unclassified
Security Classification